

# Finite Element Analysis of Laser Forming

by

Yung-Chin Hsiao

B.S., Naval Architecture, National Taiwan University (1990)

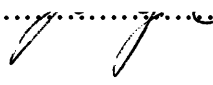
M.E., Naval Architecture and Marine Engineering, University of Michigan (1994)


Submitted to the Department of Ocean Engineering and the Department of Mechanical Engineering in Partial Fulfillment of the Requirements for the Degrees of

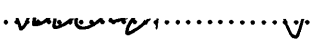
Master of Science in Ocean Engineering  
and  
Master of Science in Mechanical Engineering

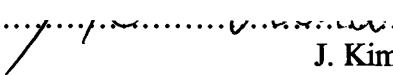
at the  
Massachusetts Institute of Technology  
June 1997

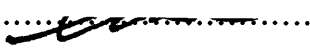
© 1997 Massachusetts Institute of Technology  
All rights reserved

Signature of Author .....  
  
Department of Ocean Engineering  
May 9, 1997

Certified by.....  
  
Koichi Masubuchi  
Professor, Department of Ocean Engineering  
Thesis Supervisor

Certified by.....  
  
David M. Parks  
Professor, Department of Mechanical Engineering  
Thesis Supervisor

Accepted by.....  
  
J. Kim Vandiver  
Chairman, Committee on Graduate Students  
Department of Ocean Engineering

Accepted by.....  
  
Ain A. Sonin  
Chairman, Committee on Graduate Students  
Department of Mechanical Engineering

MASSACHUSETTS INSTITUTE  
OF TECHNOLOGY

Eng.

JUL 15 1997

LIBRARIES

# **Finite Element Analyses of Laser Forming**

by

Yung-Chin Hsiao

Submitted to the Department of Ocean Engineering and  
the Department of Mechanical Engineering  
on May 9, 1997, in partial fulfillment of the  
requirements for the Degrees of Master of Science in  
Ocean Engineering and Mechanical Engineering

## **Abstract**

This thesis is based on the research project "Laser Forming of Flexible Fabrication." The research team consists of Boeing Company (BC), Massachusetts Institute of Technology (MIT), Newport News Shipbuilding Company (NNSC), and Pennsylvania State University (PSU). The MIT research team headed by Professor Koichi Masubuchi has been involved in the following activities: (1) measurement of the transient out-of-plane displacement of plates during laser heating, (2) development of the finite element method (FEM) to predict the metal movement during laser heating and final out-of-plane distortion, (3) development of a model to determine a proper heating pattern to form a metal sheet into a prescribed shape. The investigated materials include low-carbon and high-strength steels (HY-80 and HSLA-80), aluminum alloys, Inconel alloys, and titanium alloys, which are widely used in aerospace, automobile, and shipbuilding industries. This thesis covers the first two activities. A three-dimensional thermal-elastic-plastic FEM is used to investigate the effects of material properties and processing parameters, including power, spot size, and travel speed, on angular distortion of a plate heated by a laser beam. The advantages of FEM approach are (1) the ability of solving the highly nonlinear governing equations of a laser forming process, and (2) the ease of isolating parameters. This thesis presents three achievements: (1) comparisons between the results of FEM analyses and the experimental data, (2) explanations of the mechanisms of the laser forming based on the theory of thermal stresses, experimental observations, and FEM analyses, (3) investigations on the relations between bending angles and processing parameters.

Thesis Supervisor: Koichi Masubuchi  
Title: Professor of Ocean Engineering

Thesis Supervisor: David M. Parks  
Title: Professor of Mechanical Engineering

## **Acknowledgment**

I would like to express my sincere gratitude to Professor Koichi Masubuchi whose guidance, encouragement and support help me study at MIT. I appreciate Professor David M. Parks for his invaluable suggestions on my thesis.

Thank my family for the support. Whenever I have a hard time, they are always with me. Especially, I would like to grant the honor to my father. It is my deepest sorrow that he can not attend my commencement and share my joy of graduate at MIT. Thanks to Li-Chien Hung for her sharing the happiness and the sadness of my life at MIT.

Thanks to Mr. Hideki Shimizu, Mr. Li Lang, Mr. Umekuni, and Mr Yamamoto at the welding lab at MIT. They are good research partners and friends. Thanks to Mr. Wooten, Mr. Waren at Boeing Company, and Mr. Richard at Pennsylvanian State University. They are excellent managers and engineers who worked on the laser forming project. Also thanks to Ms. J. Sucharewicz, Ms. B. Tuths, Ms. C. Brooke, and Ms. Judy Sheitanian for their assistance in department.

I would like to appreciate the friends in the Republic of China Student Associate at MIT for sharing good time together.

Finally, I would like to thank all my friends that I could not mention here for their help.

Table of Contents

# Table of Contents

Abstract .....	2
Acknowledgment .....	3
Table of Contents.....	4
List of Figures.....	9
List of Tables .....	13

## 1. Introduction

1.1 Background.....	15
1.2 Literature Review.....	16
1.3 Characteristics of the Problem .....	18
1.4 Objective of the Thesis .....	20
1.5 Organization of the Thesis .....	20

## 2. Laser Forming Processes

2.1 Laser .....	22
2.2 Laser Forming Processes .....	22
2.3 Energy Transfer of Laser Beam .....	24
2.3.1 Delivery Rate.....	25
2.3.2 Power Profile of Laser Beam .....	26
2.3.3 Absorption Rate .....	26
2.3.4 Cooling Rate .....	28
2.4 Set Up of Measuring System .....	28



## Table of Contents

2.4.1 Overview of Measuring System .....	28
2.4.2 Sensors .....	29
2.4.3 DaqBook 100 and PC/486.....	31

## **3. Experiment**

3.1 Background.....	34
3.2 Experiment 1.....	35
3.2.1 Objective in Experiment 1.....	35
3.2.2 Specimen Definitions and Processing Conditions in Experiment 1 .....	35
3.2.3 Results in Experiment 1 .....	37
3.3 Experiment 2.....	46
3.3.1 Objective in Experiment 2.....	46
3.3.2 Specimen Definitions and Processing Conditions in Experiment 2 .....	46
3.3.3 Results in Experiment 2 .....	46
3.4 Experiment 3.....	49
3.4.1 Objective in Experiment 3.....	49
3.4.2 Measuring Setup in Experiment 3 .....	49
3.4.3 Specimen Definitions and Processing Conditions in Experiment 3 .....	49
3.4.4 Results in Experiment 3 .....	52
3.4.4.1 Comparison of Measurements between Two Set-ups .....	52
3.4.4.2 Neglecting Transducer Sensor Data .....	53
3.4.4.3 Repeatability of Deformation .....	54
3.4.4.4 Comparison of the Final Bending Angles.....	56
3.4.4.5 Effect of Multi-Pass Process .....	56
3.4.4.6 Effects of the Initial Shape and Residual Stresses .....	57
3.5 Experiment 4.....	61
3.5.1 Objective in Experiment 4.....	61

## Table of Contents

3.5.2 Specimen Definitions and Processing Parameters in Experiment 4.....	61
3.5.3 Results in Experiment 4.....	62
3.6 Experiment 5.....	66
3.6.1 Objective in Experiment 5.....	66
3.6.2 Specimen Definitions and Processing Parameters in experiment 5.....	66
3.6.3 Results in Experiment 5.....	67

## **4. Mechanisms of Laser Forming**

4.1 Background.....	70
4.2 Thermal Stresses Theory.....	72
4.3.Mechanisms of Laser Forming.....	86
4.3.1 Angular Bending Mechanism.....	86
4.3.2 Longitudinal Bending Mechanism.....	89
4.3.3 Buckling Mechanism.....	89

## **5. Analytical Solutions**

5.1 Background.....	90
5.2 Heat Transfer Analyses.....	92
5.2.1 Physical Phenomena.....	92
5.2.2 Theoretical Formulations.....	94
5.2.3 Analytical Solution.....	96
5.2.3.1 Rosenthal's Solution.....	96
5.2.3.2 Iwasake's Solution.....	100
5.3 Mechanical Analysis.....	102
5.3.1 Physical Phenomena.....	102

Table of Contents

5.3.2 Theoretical Formulation.....102

**6. Finite Element Method**

6.1 Background.....105

6.2 Procedures of F.E.M. ....105

6.3 Formulations of F.E.M. ....107

    6.3.1 Incremental Equations of Heat Transfer.....107

    6.3.2 Incremental Equations of Mechanical Analyses .....108

6.4 Finite Element Model for Heat Transfer Analyses .....109

    6.4.1 Geometry Model .....109

    6.4.2 Mesh Model .....110

    6.4.3 Element Model .....110

    6.4.4 Heat Input Model .....110

    6.4.5 Material Model.....114

    6.4.6 Boundary Condition Model .....116

    6.4.7 Solution Schemes .....117

6.5 Finite Element Model for Mechanical Analysis.....118

    6.5.1 Mesh Model .....118

    6.5.2 Element Model.....118

    6.5.3 Material Model.....120

        6.5.3.1 Decomposition of Total Strain .....120

        6.5.3.2 Creep Model .....120

        6.5.3.3 Metal Elasticity Model .....121

        6.5.3.4 Metal Plasticity Model .....122

        6.5.3.5 Metal Thermal Expansion Model .....115

    6.5.4 Kinematic Model.....129

Table of Contents

6.5.5 Boundary Condition ..... 130  
6.5.6 Solution Schemes ..... 131

**7. Parametric Study of a Laser Line Heating Process by FEM**

7.1 Introduction ..... 133  
7.2 Mesh Definitions ..... 133  
7.3 Deformation and Parameters ..... 134  
7.4 Parametric Study of A Circular Plate Irradiated by A Laser Beam..... 142  
    7.4.1. Center Irradiation ..... 143  
    7.4.2. Circular Irradiation in 360 Degrees ..... 143  
    7.4.3. Continuous Circular Irradiation in 720 Degrees..... 144  
7.5 Parametric Study of A Rectangular Plate Irradiated by A Laser Beam..... 148

**8. Conclusion and Recommendations**

8.1 Conclusion and Recommendations..... 155

**References** ..... 158

**Appendix A Using ABAQUS for Laser Forming** ..... 162

**Appendix B ABAQUS Input File for Heat Transfer Analysis**..... 178

**Appendix C ABAQUS Input File for Structural Analysis** ..... 181

## List of Figures

Figure 2.2.1	Schematics of laser facility.....	23
Figure 2.2.2	Set-up of the experiment.....	23
Figure 2.3.1	Calibration of Nd:YAG laser .....	25
Figure 2.4.1	Set-up of a measuring system.....	30
Figure 2.4.2	Positions of sensors .....	32
Figure 3.2.2.1	Positions of sensors in the first experiment.....	36
Figure 3.2.3.1	Transient out-of-plane displacement of a mild steel plate heated by the first pass of CO <sub>2</sub> laser .....	38
Figure 3.2.3.2	Transient out-of-plane displacement of a mild steel plate heated by the second pass of CO <sub>2</sub> laser .....	39
Figure 3.2.3.3	Deformation of a mild steel plate heated by the first pass of CO <sub>2</sub> laser ..	40
Figure 3.2.3.4	Deformation of a mild steel plate heated by the second pass of CO <sub>2</sub> laser .....	41
Figure 3.2.3.5	Transient out-of-plane displacement of an HSLA 100 plate heated by The first pass of laser .....	42
Figure 3.2.3.6	Transient out-of-plane displacement of an HSLA 100 plate during second pass heated by CO <sub>2</sub> laser.....	43
Figure 3.2.3.7	Deformation of an HSLA 100 plate heated by the first pass of CO <sub>2</sub> laser .....	44
Figure 3.2.3.8	Deformation of an HSLA 100 plate heated by the second pass of CO <sub>2</sub> laser .....	45
Figure 3.4.2	The set-up of a measuring system .....	50
Figure 3.4.4.1.1	Transient bending angles measured in Set-up A.....	52

Figure 3.4.4.1.2	Transient bending angles measured in Set-up B.....	53
Figure 3.4.4.2	Result of neglecting data measured by transducers .....	54
Figure 3.4.4.3	Comparison of transient angular distortions of seven specimen.....	55
Figure 3.4.4.5	Comparison between transient angular distortions during the first pass and the second pass at the same heating line.....	58
Figure 3.4.4.6.1	Effect of initial shape of an Inconel 625 plate on angular distortion (The second pass is perpendicular to the first pass) .....	59
Figure 3.4.4.6.2	Effect of initial shape and stresses of an HSLA-80 Plate on angular distortion (The second pass is perpendicular to the first pass) .....	60
Figure 3.5.3.1	Temperature distribution of an Inconel 718 plate .....	63
Figure 3.5.3.2	Transient angular distortion of the Inconel 718 #1 plate .....	63
Figure 3.5.3.3	Transient angular distortion of the Inconel 718 #2 plate .....	64
Figure 3.5.3.4	Transient angular distortion of the Inconel HY 80 #1 plate.....	64
Figure 3.5.3.5	Transient angular distortion of the Inconel HY 80 #2 plate.....	65
Figure 3.6.3.1	Transient angular distortion of the HSLA-80 #1 plate .....	67
Figure 3.6.3.2	Transient angular distortion of the HSLA-80 #2 plate .....	68
Figure 3.6.3.3	Transient angular distortion of the Inconel 625#1 plate .....	68
Figure 3.6.3.4	Transient angular distortion of the Inconel 625#2 plate .....	69
Figure 4.1.1	Six types of deformation during a laser forming process.....	71
Figure 4.2.1(a)	Model of thermal stresses due to the uneven temperature distribution during a heating stage.....	73
Figure 4.2.1(b)	Model of thermal stresses due to the uneven temperature distribution during the cooling stage .....	73

Figure 4.2.2	Three-dimensional temperature distribution during laser heating .....	74
Figure 4.2.3	Thermal stress in x direction during laser heating .....	75
Figure 4.2.4	Three-dimensional deformation during laser heating.....	76
Figure 4.2.5	Effective plastic strain during laser heating.....	77
Figure 4.2.6	Three-dimensional transient temperature distribution at the end of laser heating .....	78
Figure 4.2.7	Thermal stress in x direction at the end of laser heating .....	79
Figure 4.2.8	Effective plastic strain at the end of laser heating .....	80
Figure 4.2.9	Transient deformation at the end of laser heating .....	81
Figure 4.2.10	Thermal stress in x direction at the end of laser heating .....	82
Figure 4.2.11	Transient deformation at the end of laser heating .....	83
Figure 4.2.12	Effective Plastic strain at the end of laser heating .....	84
Figure 4.3.1	A simple beam with constant thermal gradient through thickness.....	88
Figure 5.2.3.1	Rosenthal's solution.....	99
Figure 5.2.3.2	Iwasaki's solution.....	101
Figure 6.2.1	A procedure of finite element analysis.....	106
Figure 6.4.4.1	The Gaussian distribution of the heat flux of a laser beam .....	113
Figure 6.4.4.2	Heat flux distribution in the 6×6 mesh .....	113
Figure 6.4.4.3	Heat flux distribution in 12×12 mesh .....	114
Figure 6.5.3.4	The linear strain hardening model in ABAQUS .....	126

Figure 7.3.1	The effects of dimensions of plate on angular distortion .....	136
Figure 7.3.2	The effect of the heating length on the bending angle .....	137
Figure 7.3.3	Deformation of a rectangular plate with elastic pre-strain.....	138
Figure 7.3.4	Effective plastic strains on irradiated and non-irradiated surfaces .....	139
Figure 7.3.5	Angular distortion related to yield stress at room temperature.....	142
Figure 7.4.2	Final deformed shape of circular plate with central irradiation .....	145
Figure 7.4.3	Temperature distribution of a circular plate with circular irradiation in 360 degrees.....	146
Figure 7.4.4	Transient temperature distribution of a circular plate with circular irradiation in 360 degrees .....	147
Figure 7.5.1	Angular distortion related to $p/v$ from experimental study.....	150
Figure 7.5.2	Angular distortion related to $p/v^{1/2}$ from experimental study.....	151
Figure 7.5.3	Angular distortion related to $p/(tv^{1/2})$ from experimental study.....	152
Figure 7.5.4	Angular distortion related to $p/v$ from FEM simulation.....	153
Figure 7.5.5	Angular distortion related to $p/v^{1/2}$ from FEM simulation.....	153
Figure 7.5.6	Angular distortion related to $p/(tv^{1/2})$ from FEM simulation .....	154
Figure 7.5.7	Comparison of angular distortion in Cases 1, 2 and 3.....	154



## **List of Tables**

Table 2.1	Characteristics of lasers.....	22
Table 2.3.3	Penetration temperature of the HSLA-80 plate with various surface coatings .....	27
Table 2.4.2	Standard deviations of various measurement sensors.....	33
Table 3.2.2.1	Processing conditions in the first experiment .....	35
Table 3.2.2.2	Definitions of specimens in the first experiment .....	36
Table 3.2.3	Final angular distortion in the first experiment .....	37
Table 3.3.2.1	Definition of specimen and processing parameters for Taguchi method to determine critical parameters for Nd:YAG laser .....	47
Table 3.3.2.2	Specimen definitions and processing parameters for Taguchi method to determine critical parameters for CO <sub>2</sub> laser.....	48
Table 3.4.3.1	Processing parameters in the third experiment .....	51
Table 3.4.3.2	Processing conditions in the third experiment .....	51
Table 3.4.4.3	Angular distortions of seven specimens in the third experiment.....	55
Table 3.4.4.4	Comparison of final bending angles measured from laser sensors and a three-dimensional coordinate machine.....	56
Table 3.5.2.1	Specimen definition in the fourth experiment .....	61
Table 3.5.2.2	Processing conditions in the fourth experiment.....	62
Table 3.6.2.1	Specimens definition in the fifth experiment.....	66
Table 3.6.2.2	Processing conditions in the fifth experiment .....	66
Table 6.4.4.1	The relation between the spot size and the concentration coefficient .....	112

Table 6.4.5.1	Density and specific heat of Inconel 625 and Inconel 718 .....	115
Table 6.4.5.2	Conductivity of Inconel 625 .....	115
Table 6.4.6	Convection coefficient related to temperature .....	117
Table 6.5.3	Elastic properties of annealed Inconel 625.....	122
Table 6.5.3.4	Plastic properties of DH36.....	127
Table 6.5.3.5	Plastic properties of Inconel 625 and Inconel 718.....	128
Table 6.5.3.6	Thermal expansion coefficient of Inconel 625.....	129
Table 7.2.1	Mesh size definitions.....	134
Table 7.4.1	Processing conditions of center irradiation .....	143
Table 7.4.2	Processing conditions of circular irradiation in 360 degrees.....	143
Table 7.4.3	Processing conditions of continuous circular irradiation.....	144
Table 7.5.	The results of parametric study.....	149

## Chapter 1 Introduction

### 1.1 Background

Laser metal forming is a promising technology in manufacturing industries such as automobile, shipbuilding, and airplane industries. The rapid and low-cost metal forming can improve the competitiveness of the industries. The conventional metal forming methods such as die forming and tooling are expensive and require long development cycles. For example, the conventional fabrication cost of Boeing 777 manifold is \$11.8K while it is estimated at about \$3.2K by laser forming [48]. The other forming method widely used in shipyards is flame line heating method that requires experienced workers. The quality and quantity of the flame line heating method are difficult to control.

The advantages of the laser forming processes over the conventional processes are as follow:

- (1) Laser forming can be incorporated into automatic manufacture processes. Its productivity, flexibility, and repeatability are better than those of the flame line heating method. The cost of productions by laser forming is less expensive and the development cycles of the products is shorter by laser forming than die forming and tooling in a flexible manufacturing system.
- (2) Material degradation is less produced by laser forming than by oxyacetylene flame heating, because a laser beam produces shallower heat affected zone. On the contrary, the use of flame heating with oxyacetylene torch on HY-80 is

## Chapter 1 Introduction

restricted because of possible damage of their excellent fracture toughness [27,30].

- (3) The intensity and the position of the laser beam can be accurately controlled. Therefore, a laser beam can be used in producing high precision and complex parts.
- (4) A laser beam can remotely bend the parts of structures without any contact.

On the other hand, the limitations of laser forming should be considered during the development of this technology. These limitations includes (1) what the maximum bending angle can be achieved (2) what kind of materials can be bent, (3) what kind of shapes can be produced. The new laser-forming processes may lead to more production in the flexible manufacturing systems. The development of laser forming technology will benefit the competitiveness of the industries.

## **1.2 Literature Review**

Laser cutting, laser drilling, and laser surface treatments have been applied to manufacturing in industries since the invention of laser in the late 1960s. However, laser-forming technology began in the 1980s. The delay of the development was due to lack of high-power laser facility to form the plate and inadequate computation power to develop predictive numerical models.

The development of laser forming technology was more concentrated on experimental studies in the 1980s. In the U.S.A., a research program on laser metal

## Chapter 1 Introduction

working started at Massachusetts Institute of Technology (MIT) for the Japan Welding Engineering Society in the 1980. In this program, a limited study was made on feasibility of bending a steel plate by line heating with a high power laser beam. A project on laser forming of steel plates for ship construction line was carried out at MIT from 1984 to 1987. In Phase I, the feasibility of forming steel plate and degradation of materials were studied [27]. The high-strength steels such as HY-80, HSLA 80 and K-TEN80CF were investigated. Various shapes including sine, cone, screw, dish and saddle shapes were formed by CW CO<sub>2</sub> laser. The typical thickness is from 0.25 to 1 inch. The relations between processing parameters and angular distortion were obtained in the experiments. In Phase II, the main objective was an automatic plate bending system. This system needed a bending prediction algorithm to extract a heating pattern and process parameters from a laser forming database [28,41]. In Warsaw Poland, the laser forming technology was initiated by Institute of Fundamental Technological Research of the Polish Academy of Sciences. Researchers studied various laser-forming applications in shaping developable surfaces and spherical cupolas. The details of technical information are only released for payment. In Japan, a series of one-dimensional experiments in various materials was performed with CW CO<sub>2</sub> Laser at Osaka University in 1987 [36]. The thicknesses of the specimens were from 0.5 to 2 mm. The materials included AISI 304 stainless steel, and aluminum alloy. The range of bending angles were 20 to 65 degrees after 10 to 20 passes.

In the 1990s, many research papers have more concentrated on computations. At the University of Erlangen in German, researchers used a supercomputer CRAY YMP-EL to analyze the laser forming process. The bending angle associated with path feed rate and heat conductivity was presented [47]. A good correlation between experimental results and F.E.M. analyses was obtained. At the University of Detroit-Mercy in Michigan, they developed a two-dimensional computer simulator to perform a full-

## Chapter 1 Introduction

factorial experiment. From this simulation of the full-factorial experiment, the most important parameters on deformation were investigated [37].

Many research papers could be found in the related fields of flame line heating and welding. The FEM models in those studies are similar to those in laser forming. The literature survey of the related fields can be referred to the MIT report [29].

### **1.3 Characteristics of the Laser Forming Process**

The major problem of developing the laser-forming technology is that heating-line patterns and process parameters must be determined before using the laser to form metal sheets into the prescribed shapes. Unfortunately, the relations among forming a prescribed shape of particular materials, heating pattern and process parameters are not well established. A database of those relations is needed to be developed, since this database can be adopted in factory to improve effectiveness of the laser forming process.

To bring the laser forming technology into the factory, efforts need to be made towards five directions:

(1) *Non-dimensional analyses of the deformed shape and processing parameters:*

A laser forming process involves many parameters such as materials, thickness, spot size, travel speed and so on. A non-dimensional analysis can identify the relations between deformation and processing conditions. Non-dimensional analyses could be expensive if it only relies on experimental methods due to the need of numerous experiments. The computer analyses can reduce the numbers of trial-and-error experiments.

## Chapter 1 Introduction

### (2) Mechanism analyses:

Mechanism analyses explain why the plate can be bent into various shapes, so the physical phenomenon of a laser forming process can be understood. The mechanism is investigated by performing the experiments and computer simulations.

### (3) Heating pattern and the deformed shape:

A bending algorithm is necessary to find the heating pattern of a laser beam for the defined shapes. The bending algorithm may rely on an experimental database of bending angles to obtain the optimal solutions.

### (4) Experimental study:

The real time measurement of transient displacement is helpful to the study of mechanism and to verify the simulation models. In addition, the experiment can incorporate all the physical aspects that can not be completely considered by computer models.

### (5) Metallurgical analyses:

The degradation of material could be avoided after a laser forming process. The material tests should be conducted to understand the changes of mechanical properties made by the laser forming processes.

## Chapter 1 Introduction

### **1.4. Objectives**

The objectives of the research is as follows:

1. *Development of predictive models:*

1.1 Mechanism study: a finite-element-method (F.E.M.) model has been developed to study the mechanism of laser forming process.

1.2 Parameter study: the relationship between angular change and processing parameters is studied.

2. *Feasibility studies of laser forming on objective materials:*

The experiments were conducted to study the feasibility of laser forming on objective materials. The transient temperature and out-of-plane displacement were measured during a laser forming process. The experimental results were used to verify the FEM models. The final deformed shape was measured by Mr. Hideki using a three-dimensional coordinator at the Design Lab of the Department of Ocean Engineering at MIT.

### **1.5 Organization of the Thesis**

In Chapter 2, The process of forming metal sheets into complex shapes by laser is introduced. The set-ups of the experiments are presented.

In Chapter 3, the experimental results are presented.



## Chapter 1 Introduction

In Chapter 4, the mechanism of laser forming is explained.

In Chapter 5, analytical solutions in heat transfer and mechanical analyses are introduced.

In Chapter 6, finite element method is used to simulate the laser forming processes. The methods of modeling are described.

In Chapter 7, experimental results, analytical solutions and finite-element-analysis are compared. Parametric study is presented.

In Chapter 8, conclusion and recommendations are made.

Appendices A, B, and C provide details of using ABAQUS software for a laser forming process.

## **Chapter 2 Laser Forming Process**

### **2.1. Laser**

Laser is the abbreviation of light amplified stimulated emission radiation. The power intensity of the laser is high, and the position of the laser can be easily controlled. These features make the laser an excellent tool for metal forming. According to the oscillation media of producing the lasers, the lasers can be classified as CO<sub>2</sub> and Nd:YAG lasers. Table 2.1 lists the characteristics of the lasers [31].

**Table 2.1 Characteristics of the lasers**

Name of laser	CO <sub>2</sub>	Nd:YAG
Wave length	10.6 μm	1.06 μm
Power Rate	20KW	5KW
Mode	CW or Impulse	CW or Impulse

### **2.2 Laser Forming Process**

The schematic of a laser facility for a laser forming process is shown in Figure 2.1.1. The laser beam is produced from the laser generator and is amplified to the high power rate by the amplifier. The laser beam is delivered by the reflection mirrors or the fiber optic to the laser beam torch. In Advanced Research Lab (ARL) at Pennsylvania State University (PSU), a 14kW CO<sub>2</sub> laser facility was manufactured by the United Technologies Industrial Lasers Mode 21 and was delivered by the reflection mirrors;

Chapter 2 Laser Forming Process

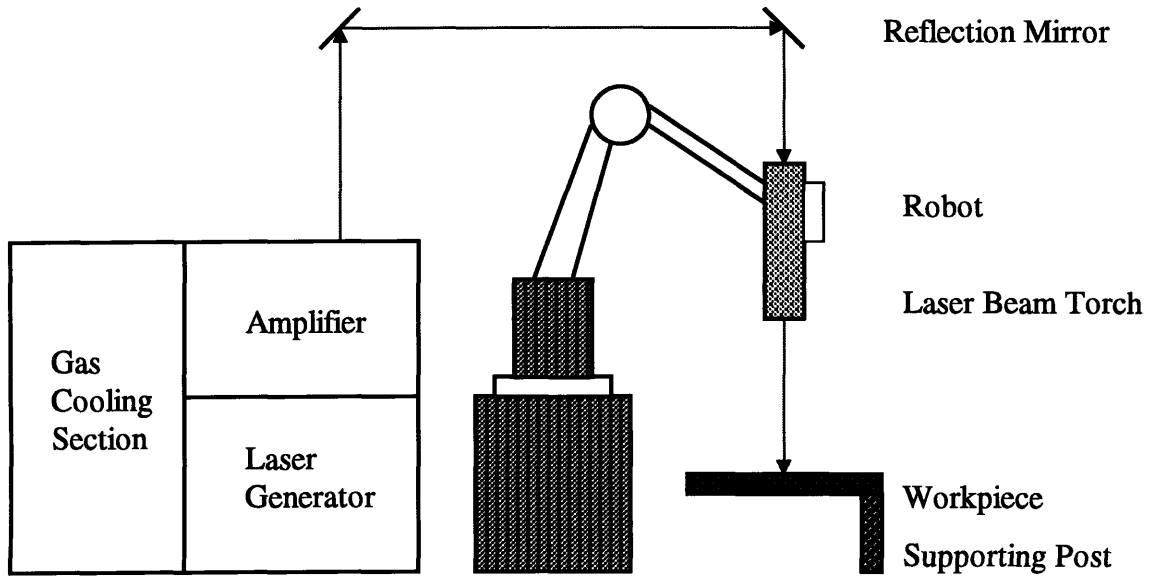


**Figure 2.2.1 Schematic of laser facility**

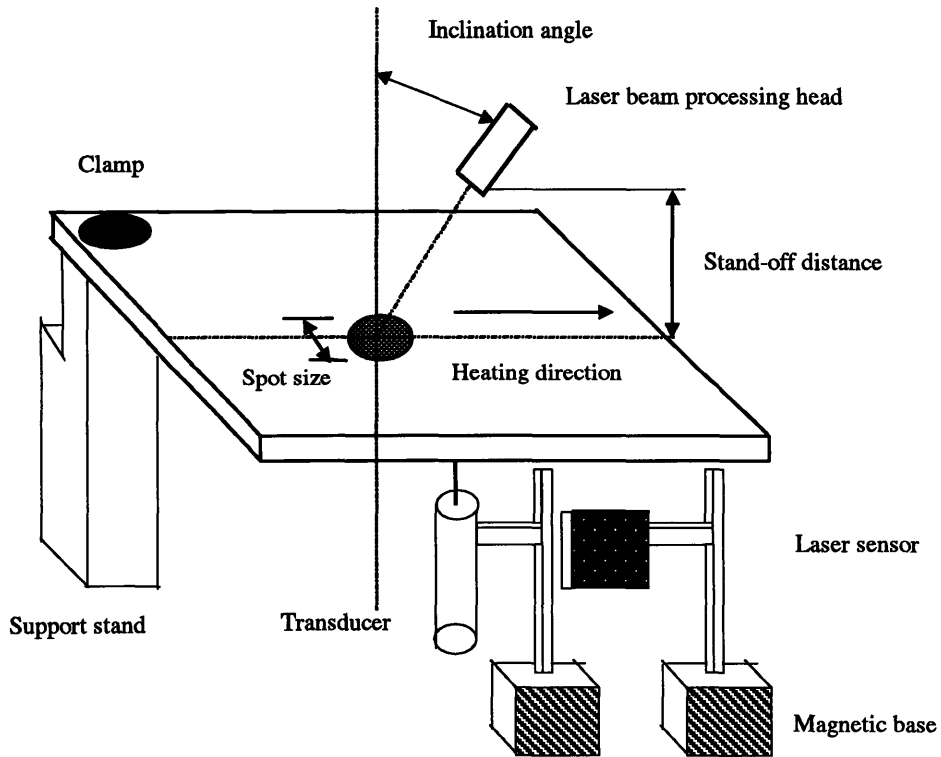


**Figure 2.2.2 Set up of the experiment**

## Chapter 2 Laser Forming Process

A 3kW Nd:YAG laser facility was manufactured by the Hobart TAFA 3000 with fiber optic delivery. The laser beam is defocused in the laser beam-processing head then is delivered to the workpiece. The laser beam is defocused and inclined with an angle to avoid melting the surface of a specimen. An articulated robot moves the laser beam torch while the workpiece is stationary.

Figure 2.2.2 shows the set-up of the experiments. One corner of the workpiece is clamped. The processing head of the laser beam is moving along the centerline of the workpiece. The robot easily controls the heating position. Thermocouples, laser sensors, and transducers are located below the specimen. The details of the positions of measuring sensors are discussed in Chapter 3. The laser beam is inclined with an angle of 10 degrees to the specimen to protect the processing head from the reflective laser beam. The standoff distance is to control the spot size of the defocused laser beam.

### **2.3. Energy Transfer of Laser Beam**

The energy transfer of the laser beam to the workpiece is important to the laser forming processes. This phenomenon of energy transfer is also important in laser surface treatment and laser welding [10,42,43]. Temperature distribution of the workpiece is strongly related to energy transfer. Therefore, various modes of energy transfer may significantly change the deformation of materials. This section discusses the energy transfer in a laser forming process.

### 2.3.1 Delivery Rate

The power loss of the laser beam from a laser generation system to the workpiece is defined as the delivery rate. The delivery rate can be obtained by measuring the power leaving the laser generation system and the power entering the workpiece. Water calorimeter is used to measure the delivery rate. The delivery rate is 87% for Nd:YAG laser and 82% for CO<sub>2</sub> laser. Figure 2.3.1 shows the delivery rate in various power rates [23]. During a laser forming process, no evaporation of metal is assumed.

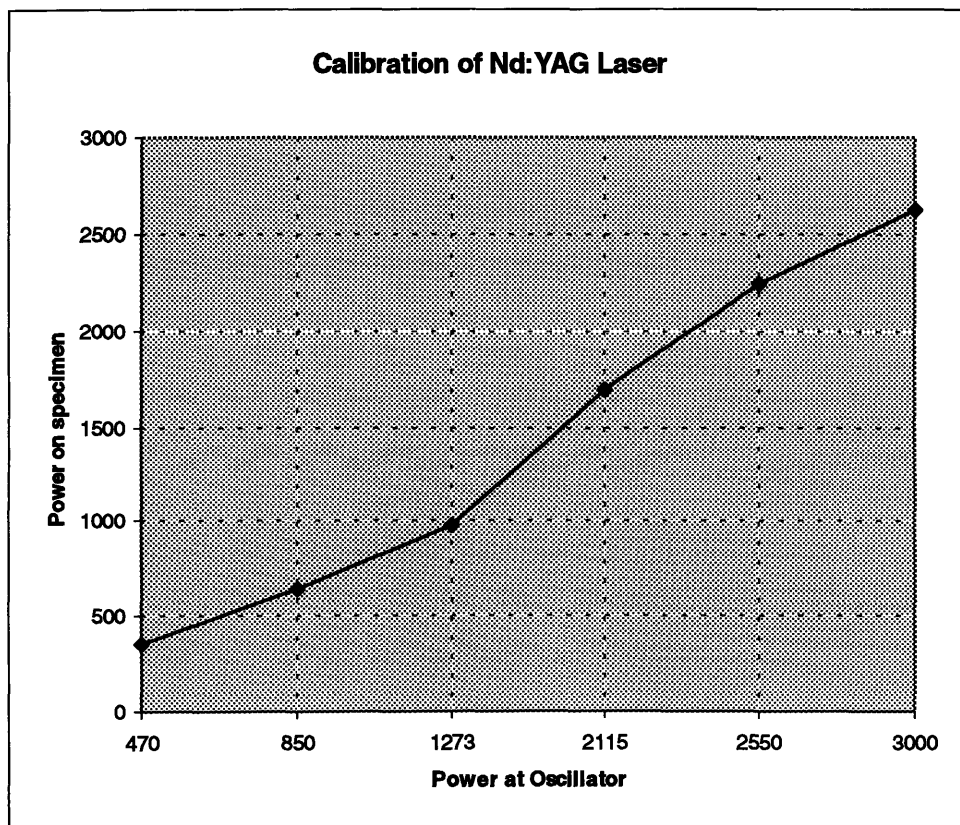


Figure 2.3.1 Calibration of Nd:YAG laser

### **2.3.2 Power Profile of Laser Beam**

The power profile of a laser beam is important in the conduction of the workpiece. Laser facility can produce different power profile of laser beam such as uniform, circular, or Gaussian profiles. PSU used a charged-coupled device (CCD) and a high-resolution infrared-sensitive TV viticon tube respectively to obtain the power profile of the laser beam. The power profile of a laser beam is a Gaussian distribution for the CO<sub>2</sub> and Nd:YAG lasers [23].

### **2.3.3 Absorption Rate**

The surface conditions of the specimen affect the absorption rate. For example, the polished and clean surfaces reflect more the laser beam. The coatings of the surfaces are also changing the absorption rate. PSU performed an experiment to test the sensitivity of coatings of surfaces to the absorption rate. Six surface conditions were evaluated: as-received brown, as-received gray, stove black, ground, boron nitride, and graphite. Table 2.3.3 shows the penetration temperature with respect to various coatings on the surfaces of the HSLA-80 plates [22,23]. The highest penetration temperature was in the as-received brown condition. The other factor affecting the absorption rate is the source of laser. Because the wave length of the Nd:YAG laser is shorter than that of the CO<sub>2</sub> laser, the absorption rate of CO<sub>2</sub> laser is lower than that of the Nd:YAG laser.

**Table 2.3.3 Penetration temperature of an HSLA-80 plate with various surface coatings**

Coatings	Peak Temperature ( °C)
As-Received Brown	243
As-Received Gray	192
Gray, Ground	93
Gray, Stove Black	154
Gray, Boron Nitride	229
Gray, Graphite	221

PSU also performed calorimetry experiments to measure amount of energy absorbed during laser processing. A workpiece of 0.25 inch was placed on the top of calorimeter. The temperature difference of water in the calorimeter before and after laser forming process was measured. The process efficiency is determined by the formula:

$$f = \frac{WC_p \int_{t=0}^{t=\infty} \Delta T dt}{P_p t_p} \quad (2.3.3)$$

where

W = mass flow rate of water (g/s),

C<sub>p</sub> = specific heat of water (cal/g-°C),

ΔT = change of water temperature (°C),

t<sub>p</sub> = total time of the laser process (sec),

P<sub>p</sub> = total power delivered to work piece  
by laser (cal/s),

f = process efficiency.

## Chapter 2 Laser Forming Process

The absorption rate of water calorimetry was around 10% to 20%. The absorption rate of water calorimetry was much lower than that of metal, because the energy of laser was used to evaporate water.

The inclination angle of the processing head also affects the absorption rate. As the inclination angle increases, the shape of the spot will change from a circle to an ellipse. The deformations of the plates during a laser-heating process change the direction of the laser beam. Therefore, the absorption rate is related to the deformation of the plates.

### **2.3.4 Cooling Rate**

Natural or forced convection, and radiation due to lower environmental temperature during a laser forming process cool down the workpiece. However, many methods have been proposed to control the cooling rate. The reason is that deformation may be quite different in different cooling rates. For example, a water jet or a cold air jet follows laser beam. Chill aluminum block, water flow or air flow is placed on the backside of workpiece. Therefore, the transient temperature distribution of the workpiece is dependent on different cooling rates. The deformation of the plate is dependent on the transient temperature distribution.

## **2.4 Set-up of a Measuring System**

### **2.4.1 Overview of Measuring System during Laser Forming**

The set-up of a measuring system is shown in Figure 2.4.1. There are three kinds of sensors: laser displacement sensors, transducers, and thermocouples. These sensors



## Chapter 2 Laser Forming Process

are connected to OMEGA DAQBOOK 100, which has the data acquisition boards to transfer the analog signals from the sensors into digit signals. A PC/486 computer receives the digit signals from the OMEGA DAQBOOK 100 and stores the data in files. The DAQVIEW software in the PC/486 is used to control OMEGA DAQBOOK 100. All the cables connecting the equipment are isolating from the scanning paths of a laser beaming. The PC/486 is located at the controller room of the laser facility.

### **2.4.2 Sensors**

Three kinds of sensors were used in the measuring system. The operation and specifications of sensors are introduced below:

#### *(1) Transducers*

LD300-150 transducers were manufactured by OMEGA. The excitation voltage was 10 V. The voltage difference between yellow and green lines was generated due to the displacement of the measuring points. The signals of the voltage difference were calibrated to the displacement signals.

#### *(2) Thermocouples*

Chromel-alumel K-type thermocouples were attached to the both sides of the plates. The diameter of the thermocouples was 0.5 mm. The K-type thermocouples were used due to the wide range of the temperature measurement.

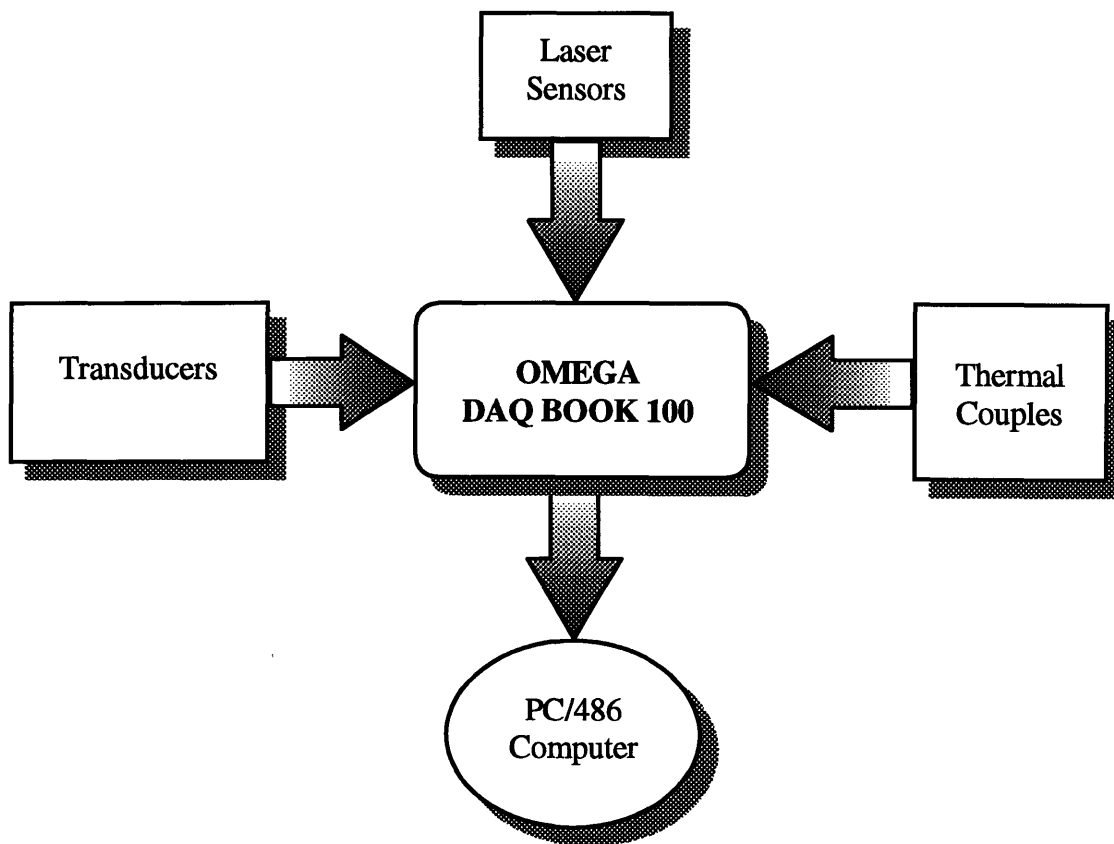


**Figure 2.4.1 Set-up of a measuring system**

## Chapter 2 Laser Forming Process

### (3) *Laser sensors*

A KEYENCE laser-sensor system included the LB-1101 controller and the LB-081 laser sensors. The resolution of measurement was 8  $\mu\text{m}$ . The maximum range of measurement was  $\pm 7.5$  mm. The wavelength of laser sensors was 780  $\mu\text{m}$ . Before measuring, an AUTO-ZERO function was set to make the current positions as zero reference points, which the displacement of the plate referred to.

To avoid cross-talking among the sensors, one channel of the signal lines in each sensor was grounded; the other channels were connected to sensors. The general out-lay of sensors is shown in Figure 2.4.2. The L stands for the laser sensors; The TC stands for the thermocouples; The Tr stands for the transducers. The positions of sensors may be changed in different experiments. The standard deviations of sensors are listed in Table 2.4.2.

### **2.4.3 DAQBOOK-100 and PC/486**

A DAQBOOK-100 included two Analog/Digit transfer boards with sixteen 16-bit I/O channels. The data was passed through a parallel channel by a printer cable to a PC/486. The PC/486 controlled the data acquisition system. The OMEGA Company delivered DAQTEST and DAQVIEW with the DAQBOOK-100. The DAQTEST tested the equipment. The DAQVIEW software in the environments of Microsoft Windows of the PC/486 controlled the operation of the system and acquitted the data. The sampling rate was set from 2 to 8 Hz. The measuring time was from 400 and 600 seconds in the experiments. The data from the sensors were stored in a text file or a binary file. The data can be post-processed by the other software such as Lotus 1.2.3. or Microsoft Excel.

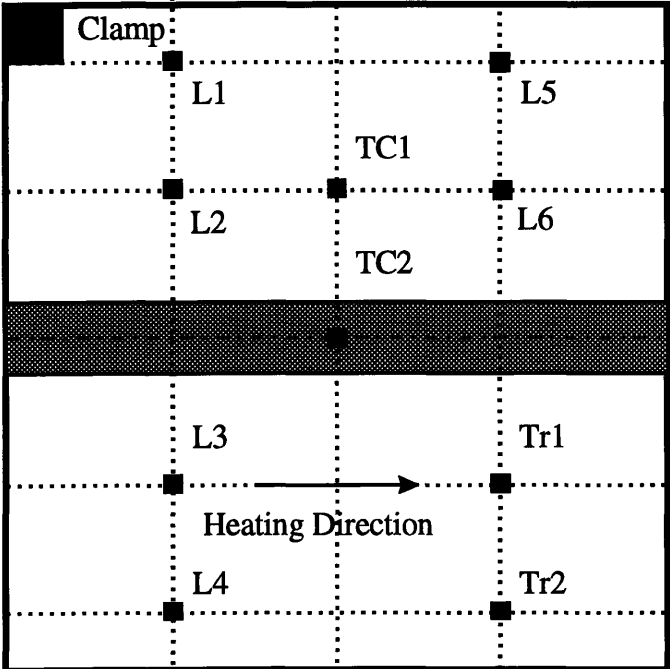


Figure 2.4.2 Positions of sensors

Chapter 2 Laser Forming Process

**Table 2.4.2 Standard deviations of various measurement sensors**

Measurement Sensors	Standard Deviation of Measurement
Laser Sensor 1	0.05 mm
Laser Sensor 2	0.04 mm
Laser Sensor 3	0.29 mm
Laser Sensor 4	0.48 mm
Laser Sensor 5	0.41 mm
Laser Sensor 6	0.48 mm
Transducer 1	0.51 mm
Transducer 2	0.05 mm
Thermocouple 1	19 °C
Thermocouple 2	28 °C
Thermocouple 3	14 °C
Thermocouple 4	6 °C
Thermocouple 5	5 °C

## **Chapter 3 Experiment**

### **3.1 Background**

The experiments were performed at Applied Research Laboratory (ARL) at the Pennsylvania State University. The MIT research teams participated in five experiments:

- (1) The first experiment was performed from December 18 to December 20 in 1994.
- (2) The second one was performed from January 22 to February 16 in 1996.
- (3) The third one was from June 11 to June 13 in 1996.
- (4) The fourth one was from October 28 to Nov 2 in 1996.
- (5) The fifth one was from December 16 to 17 in 1996.

All the experiments were conducted with the cooperation of ARL at PSU except the second one, which also included collaborations of Boeing. The experiment can incorporate the effects on bending distortion that computer simulation may not consider. The transient temperature and the transient out-of-plane displacement were measured to investigate the mechanisms of a laser line heating process. MIT used a real-time non-contact measuring system in the five experiments. In addition, those transient measurements were used to validate the FEM models. The final deformed shapes were accurately measured by a three-dimensional coordinate machine at the Design Lab in the Department of Ocean Engineering at MIT. Mr. Hedeki Shumuzi performed this work. The support of the Design Lab that is lead by Prof. Patrikalakis is appreciated. The objective and results of each experiment are described in each section of this Chapter.

## Chapter 3: Experiment

### **3.2 Experiment 1**

#### **3.2.1 Objective in Experiment 1**

- (1) Studying the feasibility of forming metal sheets into complex shapes by lasers
- (2) Testing the capability of measuring the out-of-plane displacement by non-contact laser sensors.

#### **3.2.2 Specimen Definitions and Processing Conditions in Experiment 1**

Table 3.2.2.1 lists the processing conditions in the first experiment. The definitions of specimens are listed in Table 3.2.2.2.

**Table 3.2.2.1 Processing conditions in the first experiment**

Beam Diameter	0.25 inch
Velocity	20.0 inch/second
Scan speed	13 Hz
Scan width	1.0 inch
Processing time during first pass	36 seconds
Processing time during second pass	27 seconds
Room temperature	73 F

Chapter 3: Experiment

**Table 3.2.2.2 Specimen definitions in the first experiment**

Specimen No.	Laser Source	Dimension (in×in×in)	Power (Kw)
MILDSTEEL1	CO <sub>2</sub> Laser	12×9×3/8	2.6
MILDSTEEL2	CO <sub>2</sub> Laser	12×9×3/8	2.2
HSLA 100 -1	CO <sub>2</sub> Laser	12×9×1/2	2.5
MILDSTEEL3	Nd:YAG Laser	12×9×3/8	1.8
MILDSTEEL4	Nd:YAG Laser	12×9×3/8	1.8
HSLA 100 -2	Nd:YAG Laser	12×9×1/2	1.8

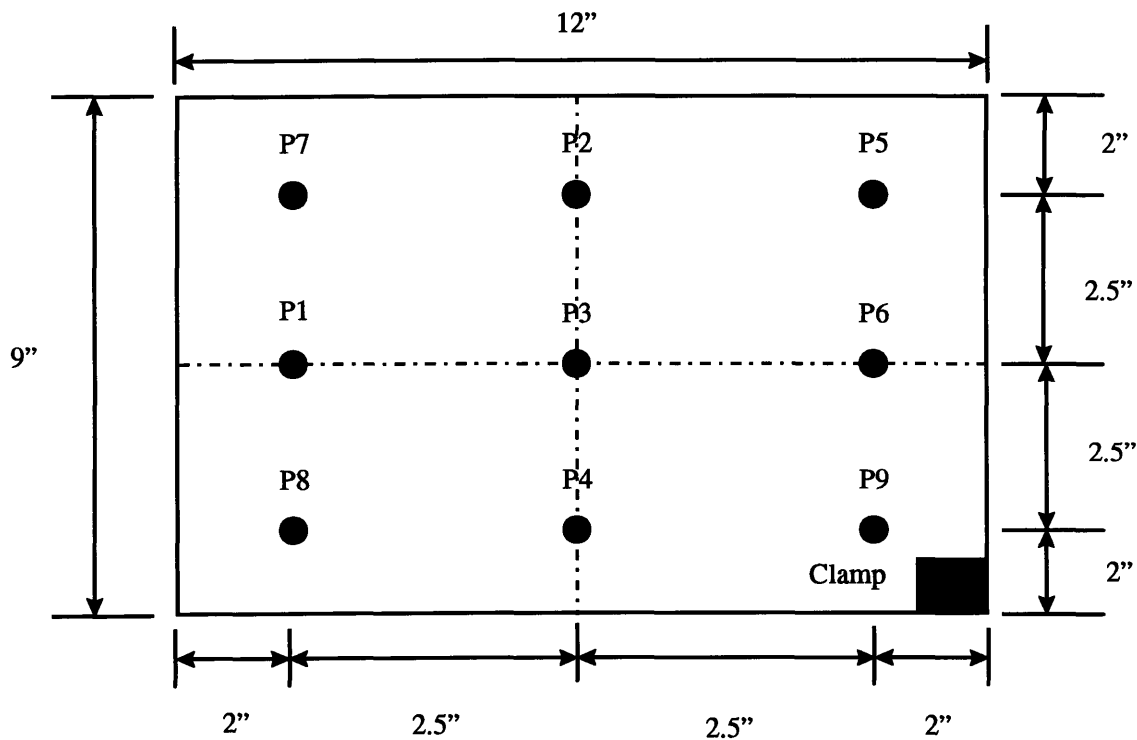


**Figure 3.2.2.1 Positions of sensors**



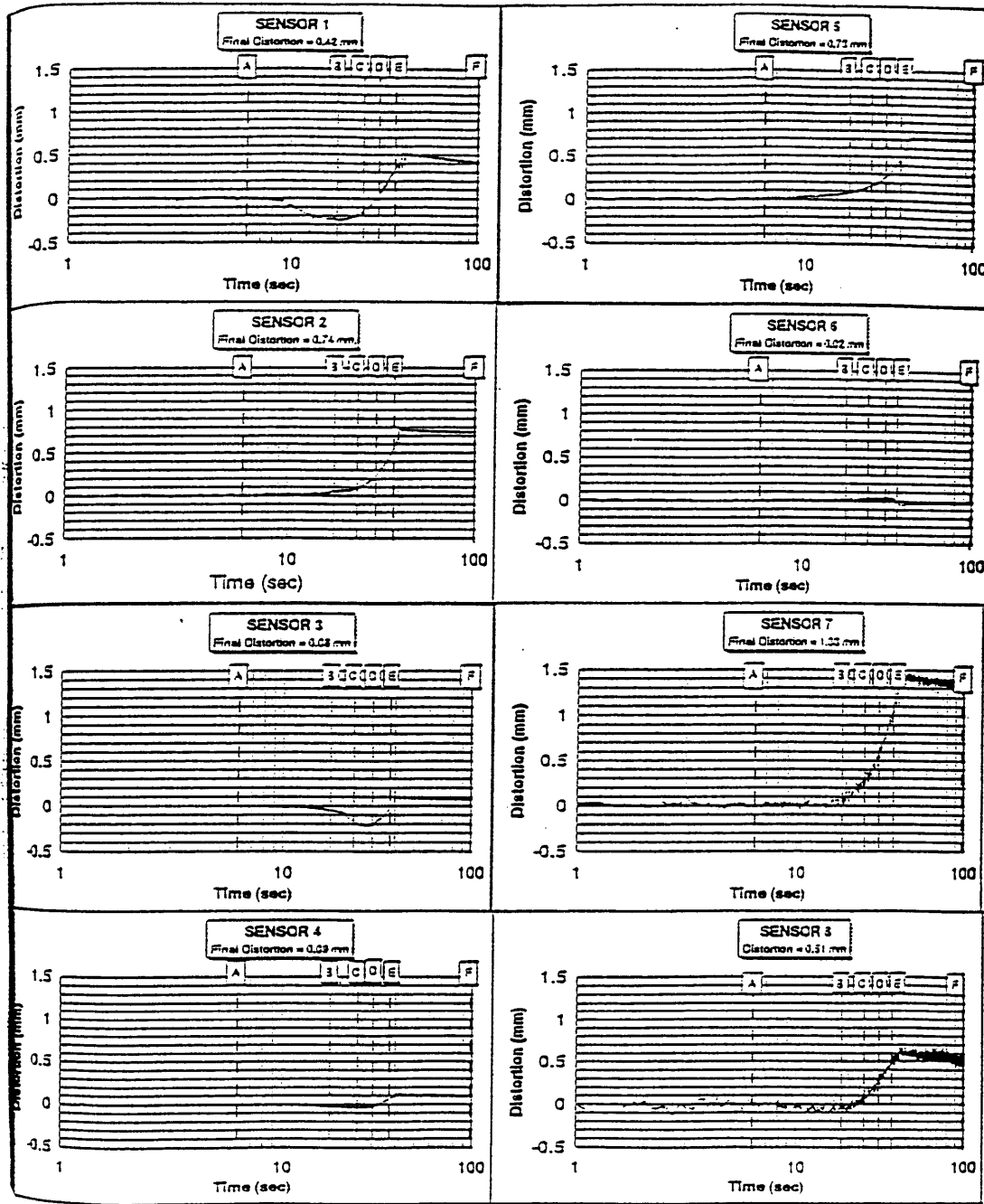
Chapter 3: Experiment

**3.2.3 Results in Experiment 1**

The mild-steel and HSLA-100 plates were irradiated by the CO<sub>2</sub> and Nd:YAG lasers respectively. Two laser heating lines were crossing in the center of the workpiece. The out-of-plane displacements of the mild-steel plate during and after a laser forming process are shown in Figures 3.2.3.1 and 3.2.3.2. Figures 3.2.3.3 and 3.2.3.4. These figures illustrate how the workpiece deforms during and after the laser heating process. The results of the HSLA-100 plates are shown from Figure 3.2.3.5 to Figure 3.2.3.8. The above figures show that a laser beam irradiated the workpiece that deforms into a complex shape. The final angular distortion in the first experiment is listed in Table 3.2.3.

**Table 3.2.3 Final angular distortion in the first experiment**

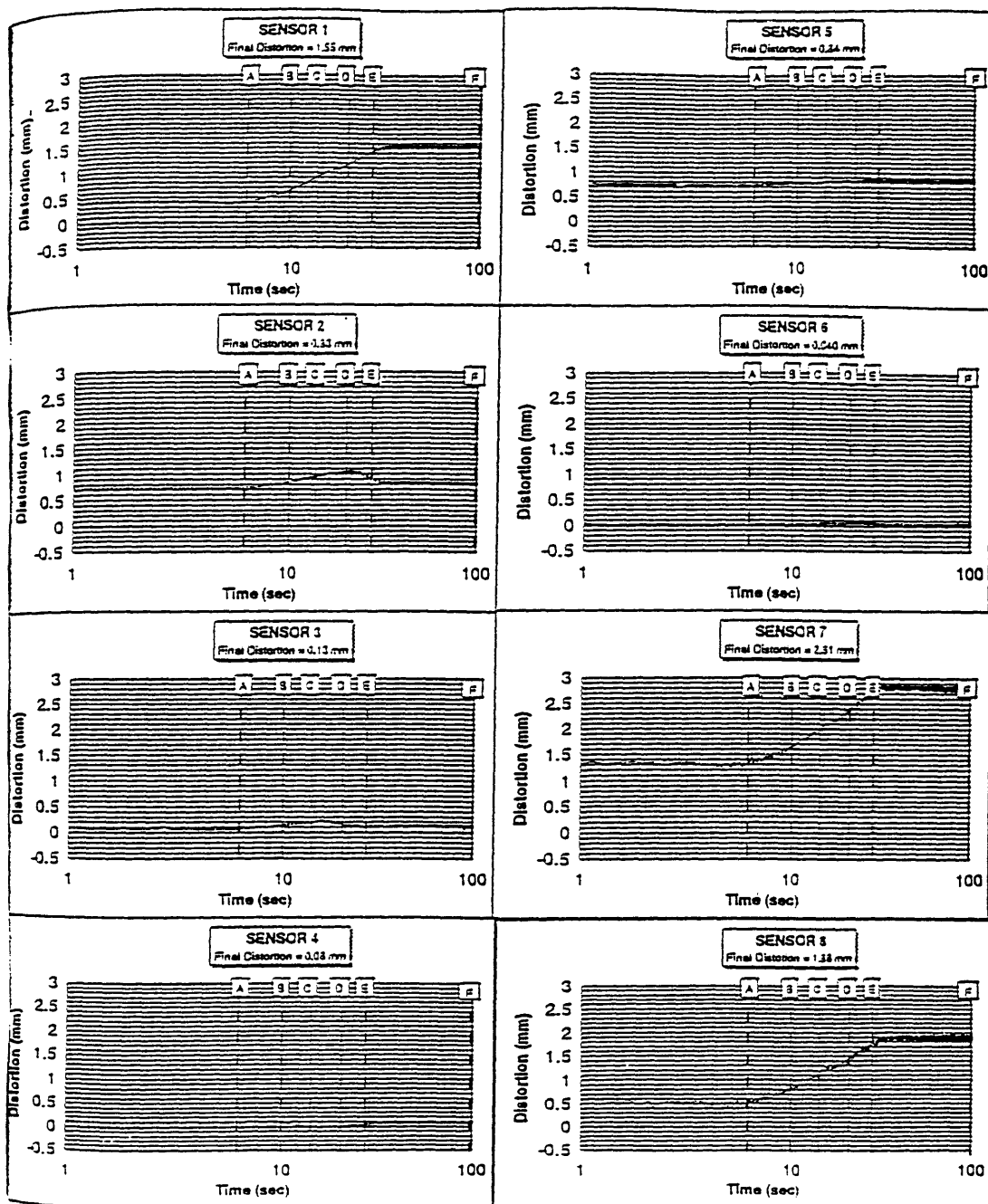
Specimen No.	Descriptions	Angle (degree)
MILDSTEEL2	First pass in the middle of the plate	1.80
MILDSTEEL2	Second pass perpendicular to first one	3.01
HSLA 100-1	First pass in the middle of the plate	0.66
HSLA 100-1	Second pass perpendicular to first one	1.20



MILDSTEEL 2-CO2-FIRST PASS

A: Laser at Sensor 1 (6 sec)      B: Laser at Sensor 3 (18 sec)      C: Laser between Sensor 2 and 6 (23 sec)  
 D: Laser at Sensor 6 (30 sec)      E: Laser Stopped (36 sec)      F: Final Distortion (100 sec)

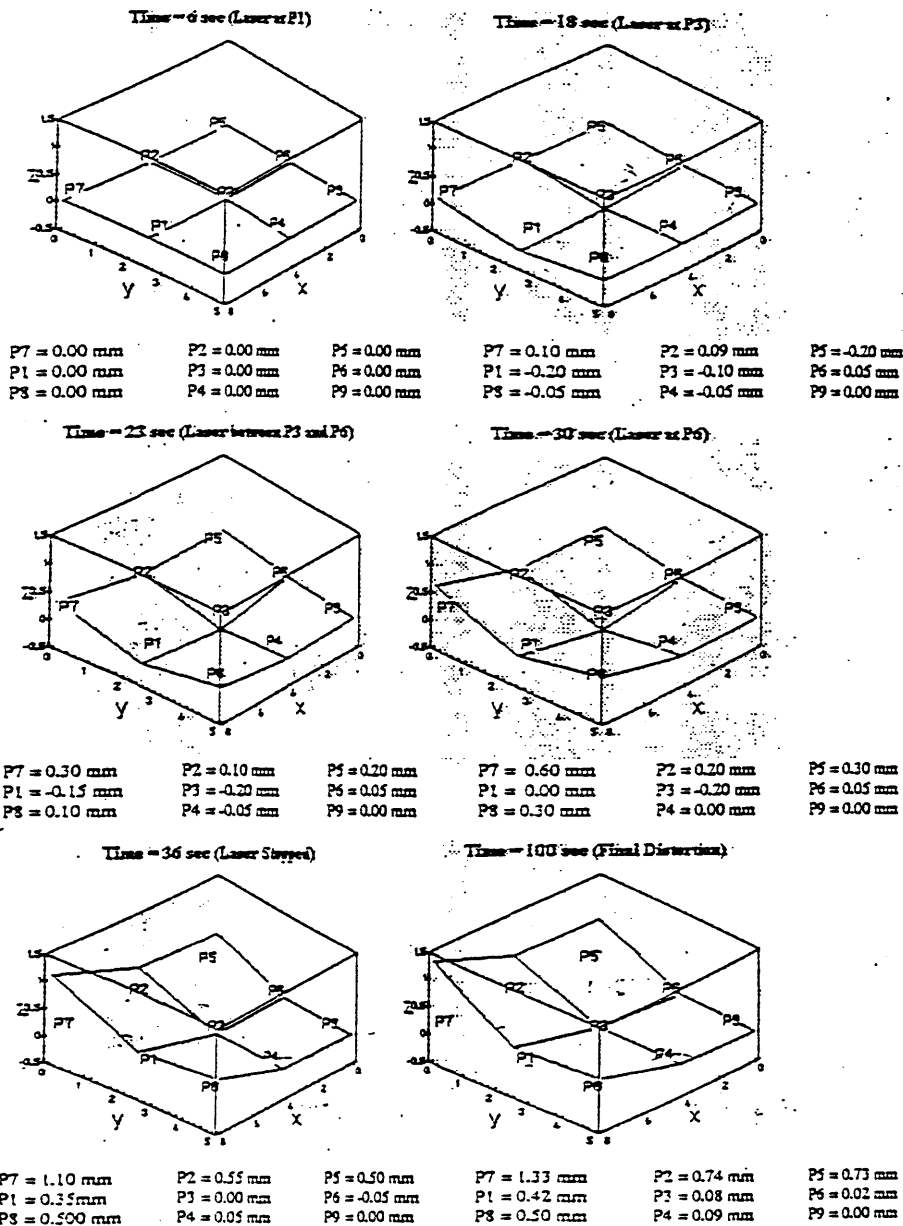
Figure 3.2.3.1 Transient out-of-plane displacement of a mild steel plate heated by the first pass of CO<sub>2</sub> laser



MILDSTEEL2-CO2-SECOND PASS

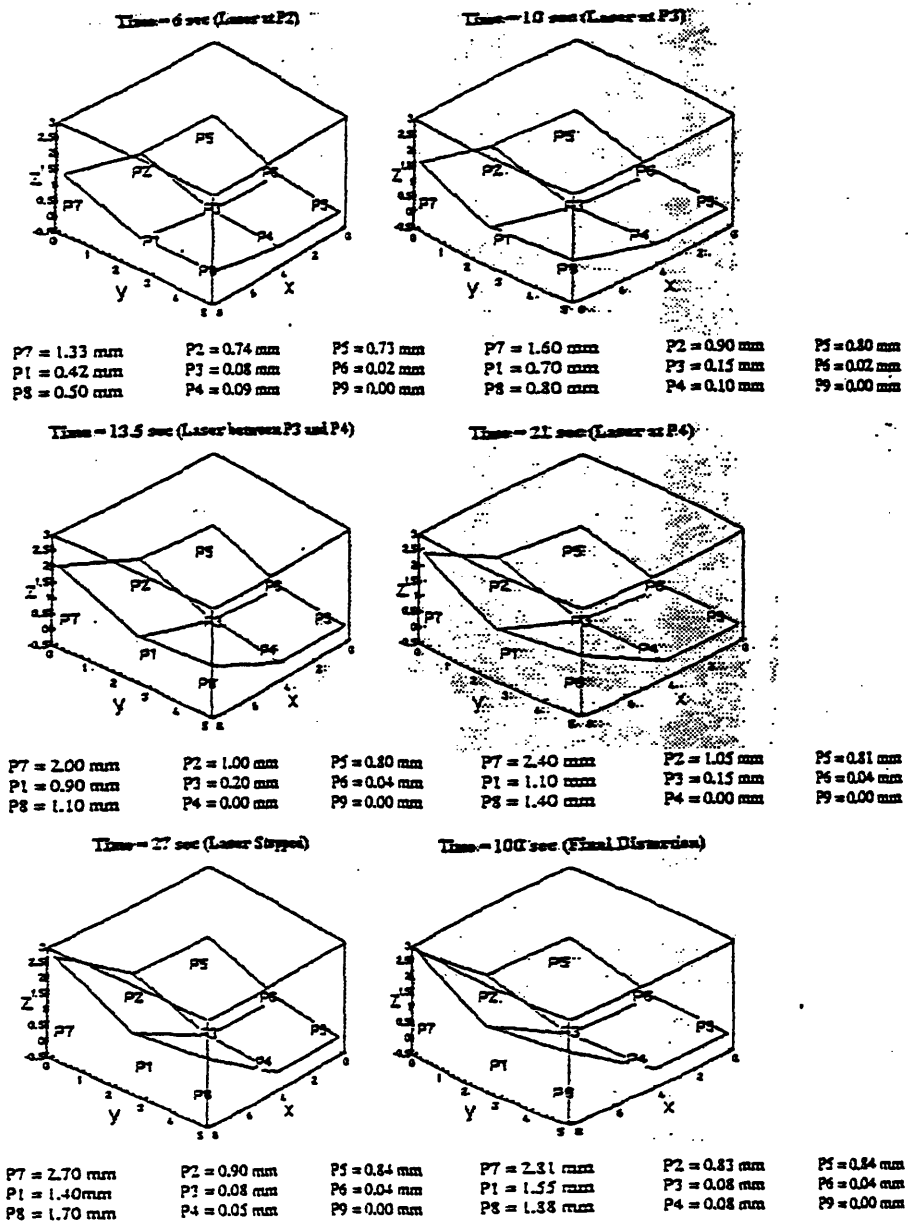
A: Laser at Sensor 2 (6 sec)      B: Laser at Sensor 3 (10 sec)      C: Laser between Sensor 3 and 4 (13.5 sec)  
 D: Laser at Sensor 4 (21 sec)      E: Laser Stopped (27 sec)      F: Final Distortion (100 sec)

Figure 3.2.3.2 Transient out-of-plane displacement of a mild steel plate heated by the second pass of CO<sub>2</sub> laser



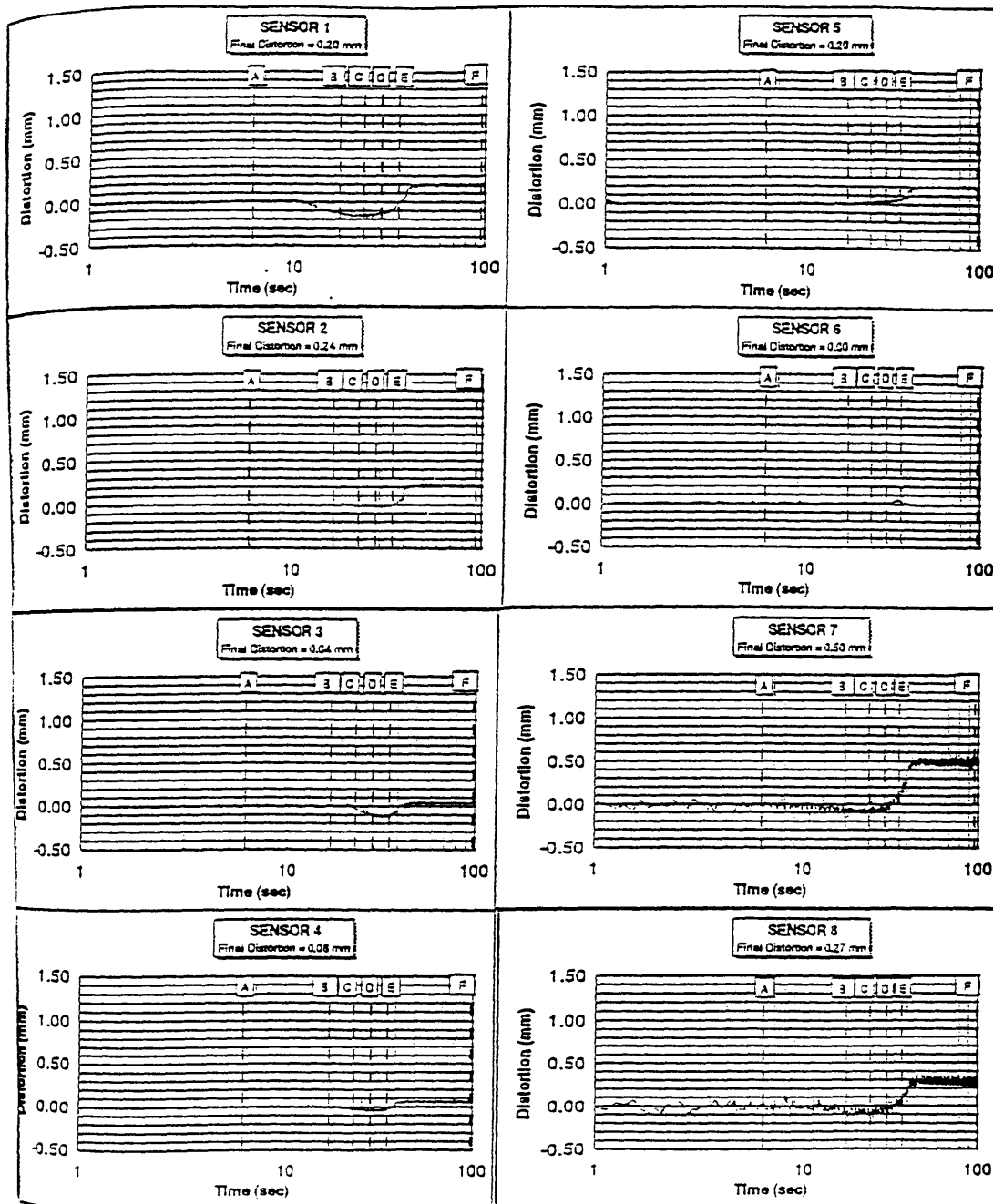
MILDSTEEL2-CO2-FIRST PASS

Figure 3.2.3.3 Deformation of a mild steel plate heated by the first pass of CO<sub>2</sub> laser



**MILDSTEEL-CO2-SECOND PASS**

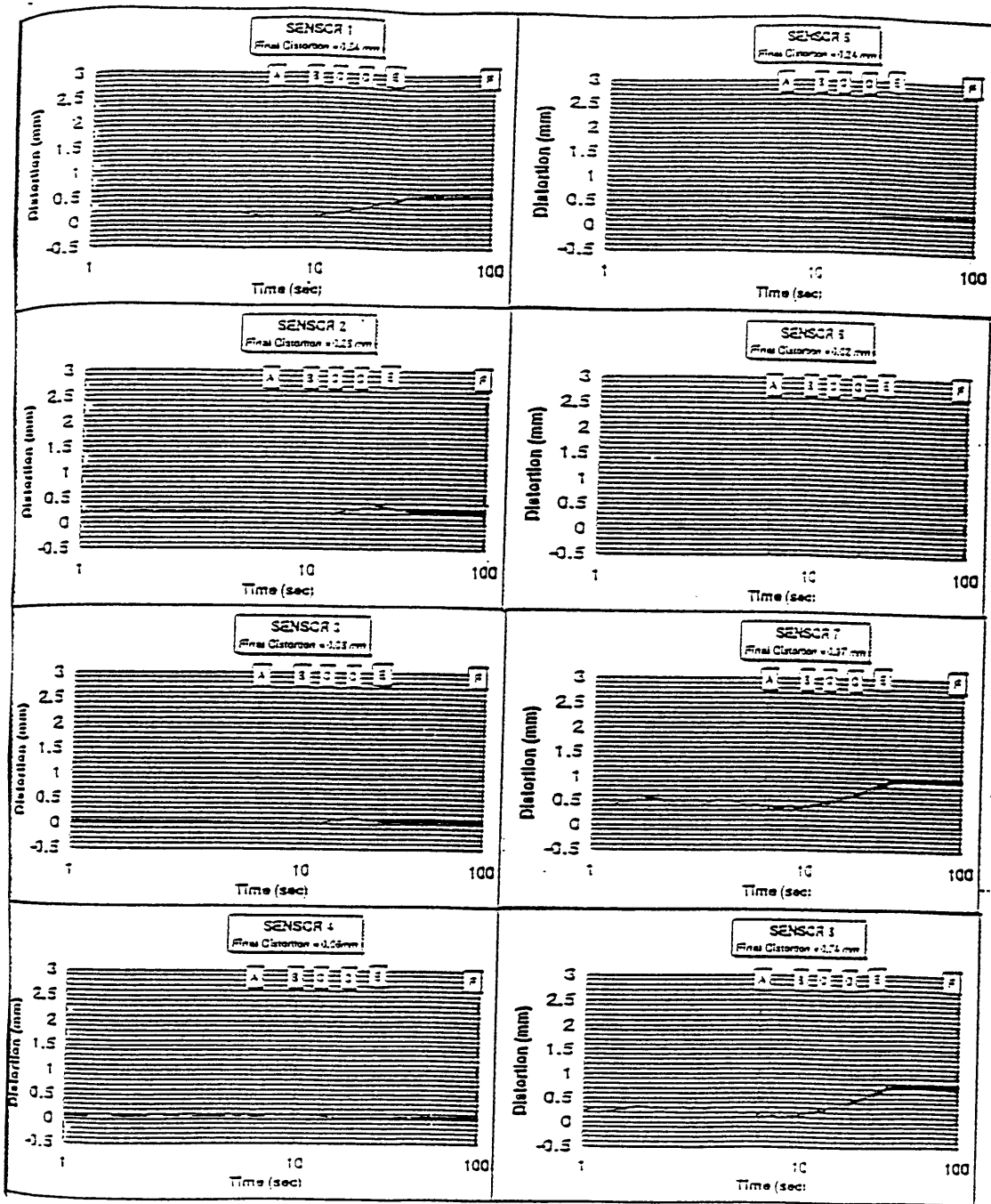
Figure 3.2.3.4 Deformation of a mild steel plate heated by the second pass of CO<sub>2</sub> laser



HSLA1-CO2-FIRST PASS

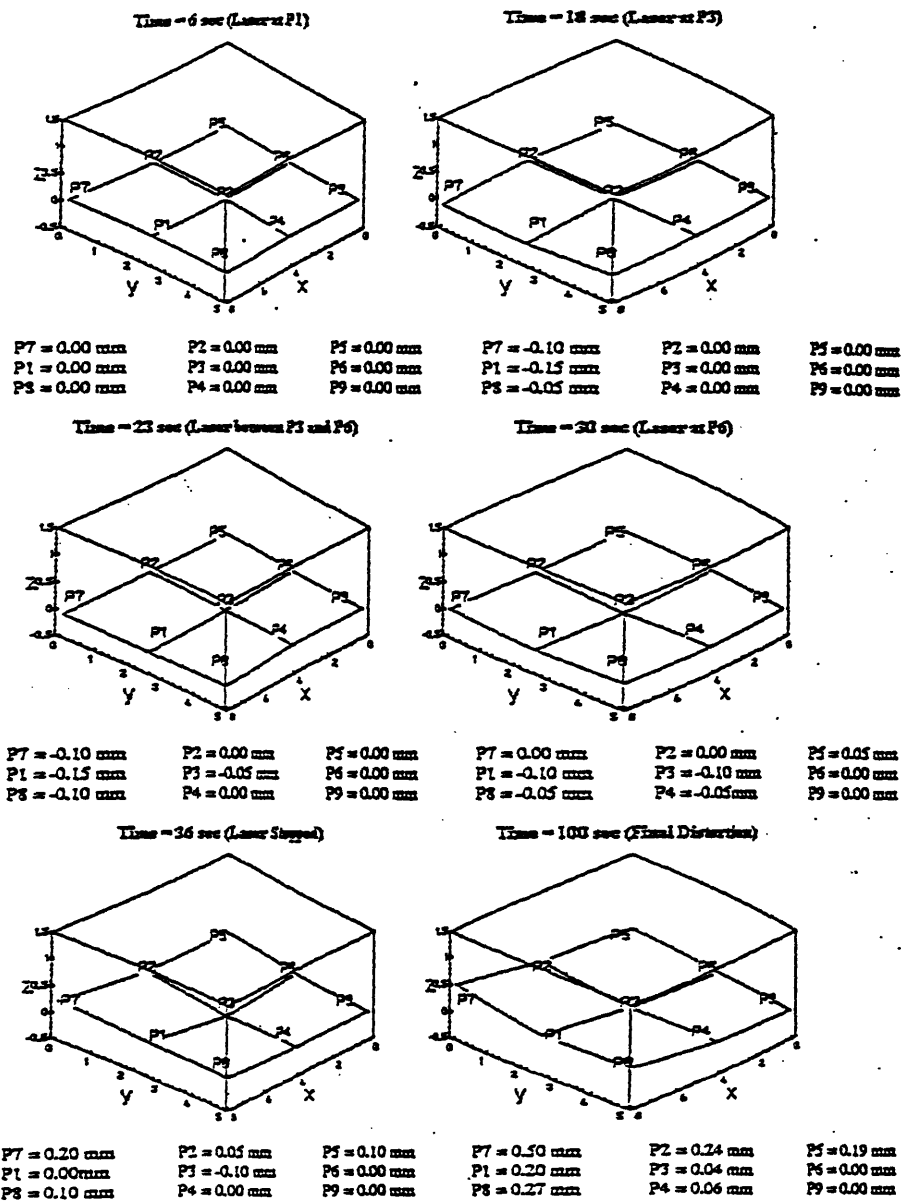
A: Laser at Sensor 1 (6 sec)      B: Laser at Sensor 3 (18 sec)      C: Laser between Sensor 3 and 6 (23 sec)  
 D: Laser at Sensor 6 (30 sec)      E: Laser Stopped (36 sec)      F: Final Distortion (100 sec)

Figure 3.2.3.5 Transient out-of-plane displacement of an HSLA 100 plate heated by The first pass of laser



A: Laser at Sensor 2 (6 sec)      B: Laser at Sensor 3 (10 sec)      C: Laser between Sensor 3 and 4 (10.3 sec)  
 D: Laser at Sensor 4 (21 sec)      E: Laser Stopped (27 sec)      F: Final Distortion (100 sec)

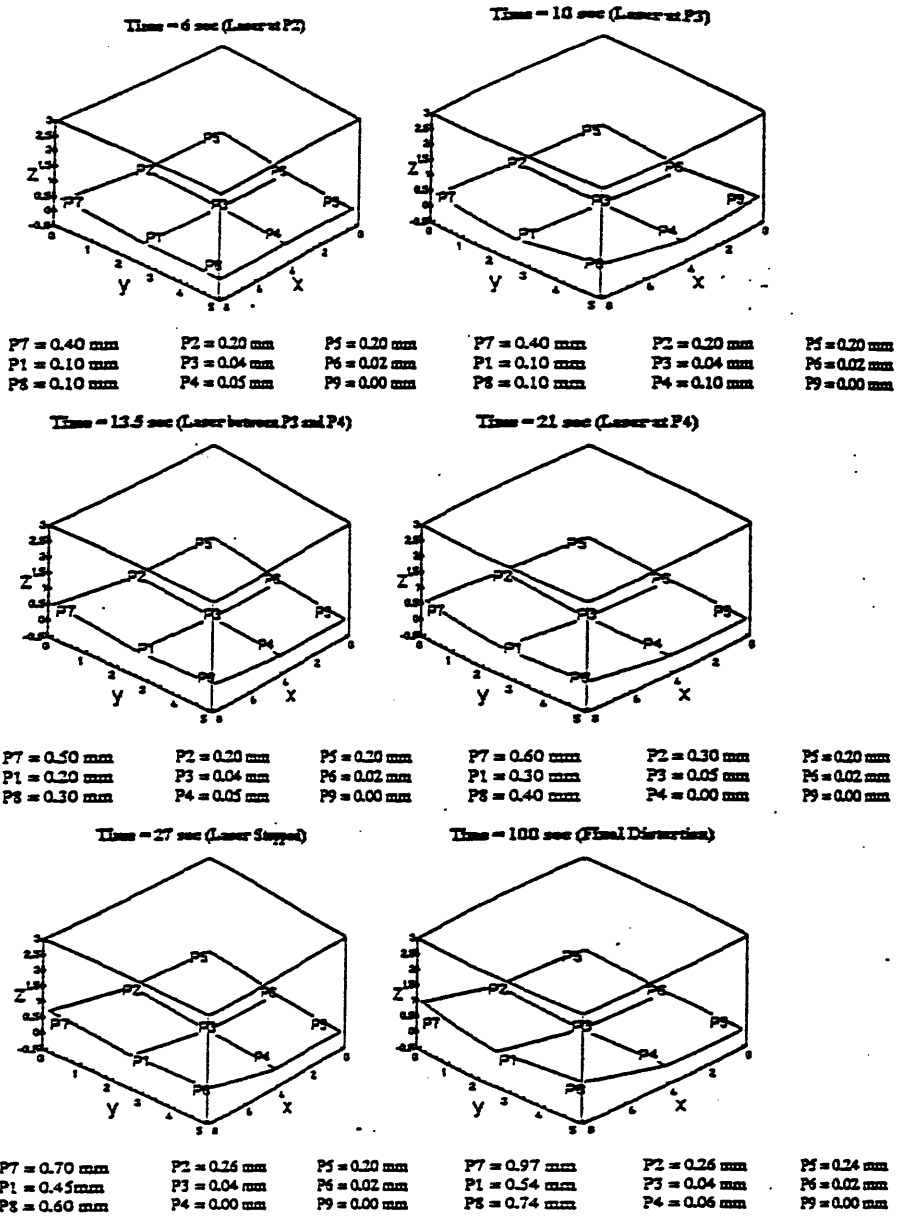
Figure 3.2.3.6 Transient out-of-plane displacement of an HSLA 100 plate during second pass heated by CO<sub>2</sub> laser



HSLA1-CO2-FIRST PASS

Figure 3.2.3.8 Deformation of an HSLA 100 plate heated by the second pass of CO<sub>2</sub> laser





HSLA100-CO2-SECOND PASS

Figure 3.2.3.7 Deformation of an HSLA 100 plate heated by the first pass of CO<sub>2</sub> laser

## Chapter 3: Experiment

### **3.3 Experiment 2**

#### **3.3.1 Objective in Experiment 2**

- (1) Validate previous experiments by Koichi Masubuchi at M.I.T.
- (2) Determine the optimum conditions for laser forming steel plates
- (3) Obtain the real time out-of-plane displacement
- (4) Investigate forming complex shapes

#### **3.3.2 Specimen Definition and Processing Conditions in Experiment 2**

The dimensions of the plates were 12×12×0.25 (inch×inch×inch). The power was 2.6 kW delivered by the Nd:YAG laser facility. Taguchi method was used to determine the influence of the parameters on the bending angle of a laser forming process. Tables 3.3.2.1 and 3.3.2.2 list the processing conditions and the bending angles for the Taguchi method to determine the critical parameters.

#### **3.3.3 Results in Experiment 2**

From Table 3.3.2.1, the maximum angle (3.28 degrees) was produced at specimen 4F with stove-pipe coating and aluminum chill-block which was irradiated by a 2.6 kW Nd:YAG laser beam with 2 cm spot size and 27 cm/min. scan speed. From Table 3.3.2.2, the maximum angle (5.02 degrees) was produced at specimen 1T with aluminum chill-block which was irradiated by a 8.4 kW CO<sub>2</sub> laser beam with 6 cm spot size and 32 cm/min. scan speed.

Chapter 3: Experiment

**Table 3.3.2.1 Specimen definitions and processing parameters for Taguchi method to determine critical parameters for plates heated by Nd:YAG laser.**

Specimen No	Speed (cm/min)	Spot size (cm)	Coating	Cooling	Bending Angle (degrees)
HSLA-80 1F	27	2	As-Received	Aluminum Chill	1.13
HSLA-80 2F	21	2	As-Received	Aluminum Chill	1.90
HSLA-80 3F	32	2	As-Received	Aluminum Chill	0.60
HSLA-80 4F	21	1.6	Stove-pipe	Aluminum Chill	3.28
HSLA-80 5F	32	1.6	Stove-pipe	Aluminum Chill	2.35
HSLA-80 6F	27	1.6	Stove-pipe	Aluminum Chill	2.62
HSLA-80 7F	21	2	As-Received	Natural Convection	1.34
HSLA-80 8F	27	1.6	As-Received	Natural Convection	1.85
HSLA-80 9F	21	1.6	As-Received	Natural Convection	2.57
HSLA-80 10F	21	2	Stove-pipe	Natural Convection	2.54
HSLA-80 11F	32	2	Stove-pipe	Natural Convection	0.56
HSLA-80 12F	32	1.6	Stove-pipe	Natural Convection	1.16
HSLA-80 13F	21	1.6	Stove-pipe	Aluminum Chill	1.71

### Chapter 3: Experiment

**Table 3.3.2.2 Specimen definitions and processing parameters for Taguchi method to determine critical parameters for plates heated by CO<sub>2</sub> laser.**

Specimen No	Speed (cm/min)	Power (kW)	Spot size (cm)	Coating	Cooling	Bending Angle (degrees)
HSLA-80 1T	40	8.4	6	None	Aluminum	5.02
HSLA-80 2T	40	8.4	5	Graphite	Aluminum	2.93
HSLA-80 3T	40	8.4	5	none	none	4.60
HSLA-80 4T	40	8.4	6	graphite	none	1.41
HSLA-80 5T	50	8.4	6	none	Aluminum	4.37
HSLA-80 6T	50	8.4	5	graphite	Aluminum	1.79
HSLA-80 7T	50	8.4	5	none	none	3.89
HSLA-80 8T1	60	8.4	6	graphite	none	1.40
HSLA-80 8T2	60	8.4	6	graphite	none	0.88
HSLA-80 9T	60	8.4	6	none	Aluminum	3.07
HSLA-80 10T	50	8.4	5	graphite	Aluminum	0.80
HSLA-80 11T	50	8.4	5	none	none	4.20
HSLA-80 12T1	60	8.4	6	graphite	none	0.79
HSLA-80 12T2	60	8.4	6	graphite	none	0.44

## **3.4. Experiment 3**

### **3.4.1 Objective in Experiment 3**

- (1) Studying the effects of a multi-pass process on deformation.
- (2) Studying the effects of both initial shapes and stresses on deformation.
- (3) Measuring transient out-of-plane displacements to validate the F.E.M. analyses [25].

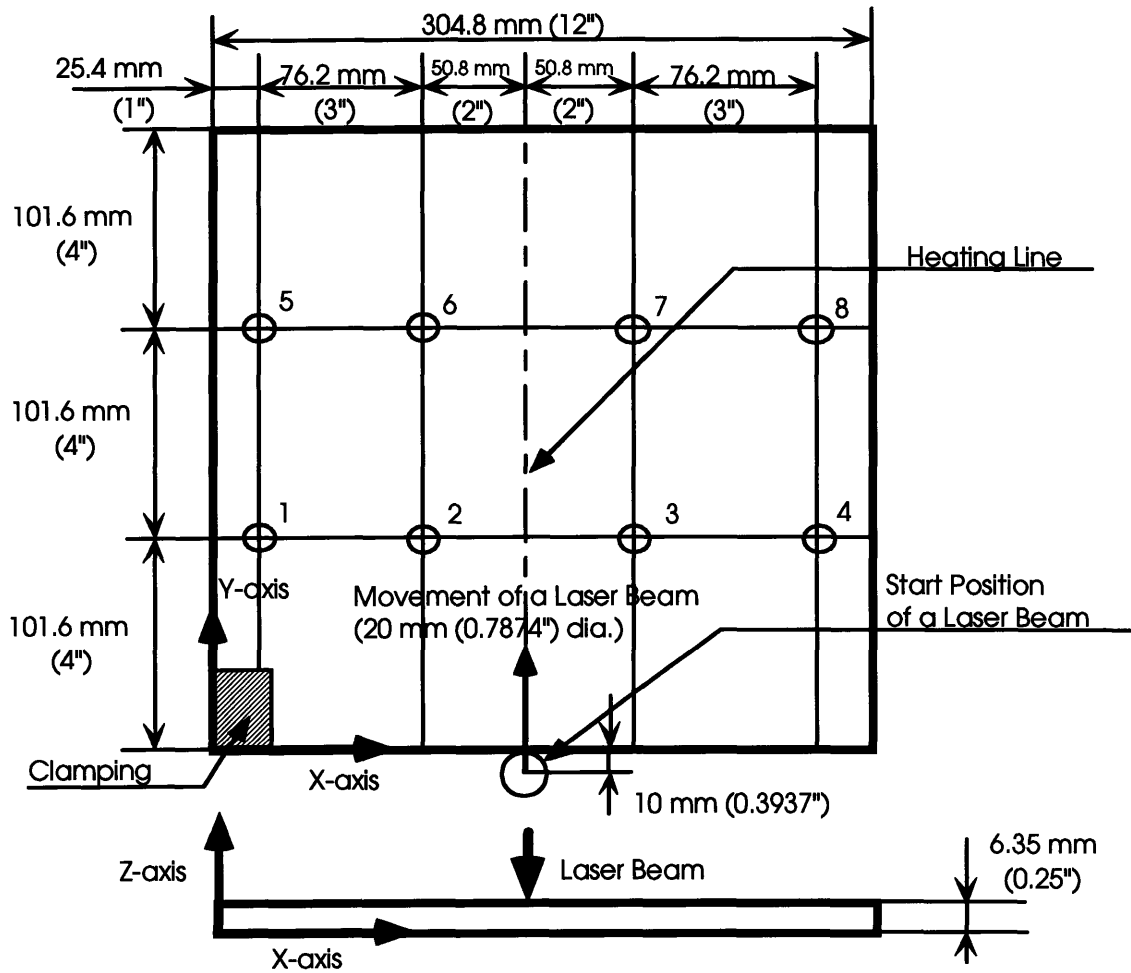
### **3.4.2 Measuring Set-up in Experiment 3**

Set-up A and Set-up B as shown in Figure 3.4.2 were used to measure the transient out-of-plane displacement in the experiments. In Set-up A, the measurements at positions 7 and 8 obtained from displacement transducers contained many noises. Transducers at positions 1 and 2 seldom moved vertically. In Set-up B, displacement transducers were switched with laser sensors from positions 7 and 8 to positions 1 and 2. The measuring data from Set-up B had fewer noises than Set-up A. The coordinate system as shown in Figure 3.4.2 was defined so that X and Y directions are in-plane directions, and Z-axis was in out-of-plane direction.

### **3.4.3 Specimen Definitions and Processing Conditions in Experiment 3**

The processing parameters and conditions are shown in Tables 3.4.3.1 and 3.4.3.2. The processing time was 97.44 seconds. The measuring time was either 300 or 600 seconds. The workpiece cools down naturally during the measuring time.

Chapter 3: Experiment



Position	Setup A	Setup B
1	Laser Sensor (L1)	Displacement Transducer (TR1)
2	Laser Sensor (L2)	Displacement Transducer (TR2)
3	Laser Sensor (L3)	Laser Sensor (L5)
4	Laser Sensor (L4)	Laser Sensor (L6)
5	Laser Sensor (L5)	Laser Sensor (L1)
6	Laser Sensor (L6)	Laser Sensor (L2)
7	Displacement Transducer (TR1)	Laser Sensor (L3)
8	Displacement Transducer (TR2)	Laser Sensor (L4)

Figure 3.4.2 Measuring set-ups

Chapter 3: Experiment

**Table 3.4.3.1 Processing parameters in the third experiment**

Process Parameter	Value
Output at a Laser Oscillator	3.0 kW
Output of a Laser Beam on a Specimen (P)	2.6 kW
Stand-off Distance (h)	190 mm
Laser Spot Size (s)	20 mm (.787 inch)
Inclination Angle ( $\alpha$ )	-10 degree
Traverse Rate (u)	200 mm/min (7.87 ipm)

**Table 3.4.3.2 Processing conditions in the third experiment**

Specimen ID	Material	Process ID	Set-up	Process Description
IN625-1	Inconel 625	IN625-1	A	One pass in the middle
IN625-2	Inconel 625	IN625-2	A	One pass in the middle
IN625-3	Inconel 625	IN625-3	A	One pass in the middle
IN625-4	Inconel 625	IN625-4	A	One pass in the middle
		IN625-4B	B	Second pass perpendicular to the heating line of IN625-4
IN625-5	Inconel 625	IN625-5	A	One pass in the middle
IN625-6	Inconel 625	IN625-6	A	One pass in the middle
		IN625-7	A	Second pass on the heating line of IN625-7
IN625-8	Inconel 625	IN625-8	B	One pass in the middle
H3D	HSLA-80	H3D-1	B	One pass in the middle
		H3D-2	B	Second pass perpendicular to the heating line of H3D-1

### 3.4.4 Results in Experiment 3

#### 3.4.4.1 Comparison of Measurements from Two Set-ups

Figures 3.4.4.1.1 and 3.4.4.1.2 show the typical transient bending angles in Set-ups A and B respectively. Due to the data from transducer displacement with many noises, the transient angular distortions at  $y=203.2$  mm measured in Set-up A can be neglected. In Set-up B, the transient angular distortions from transducers are similar to that from laser sensors.

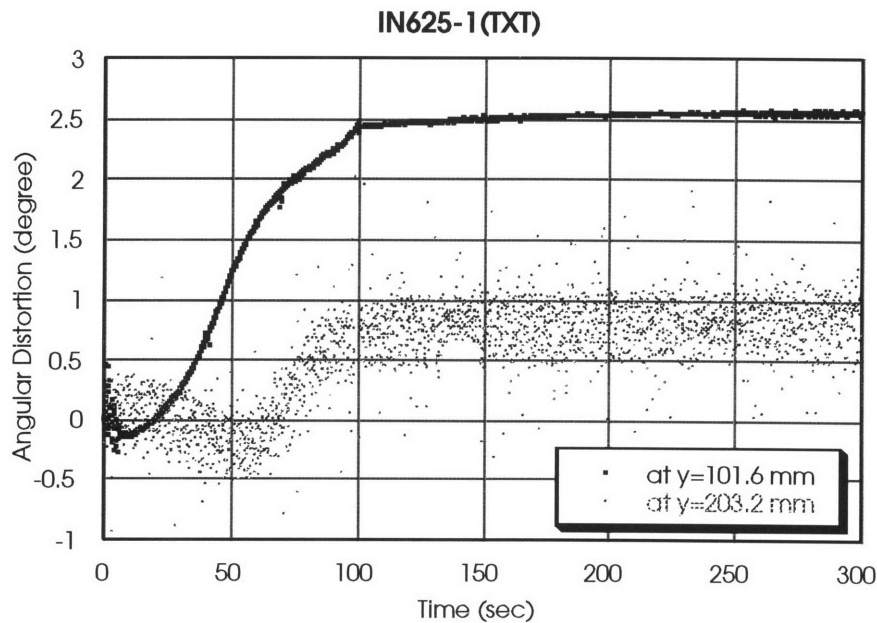
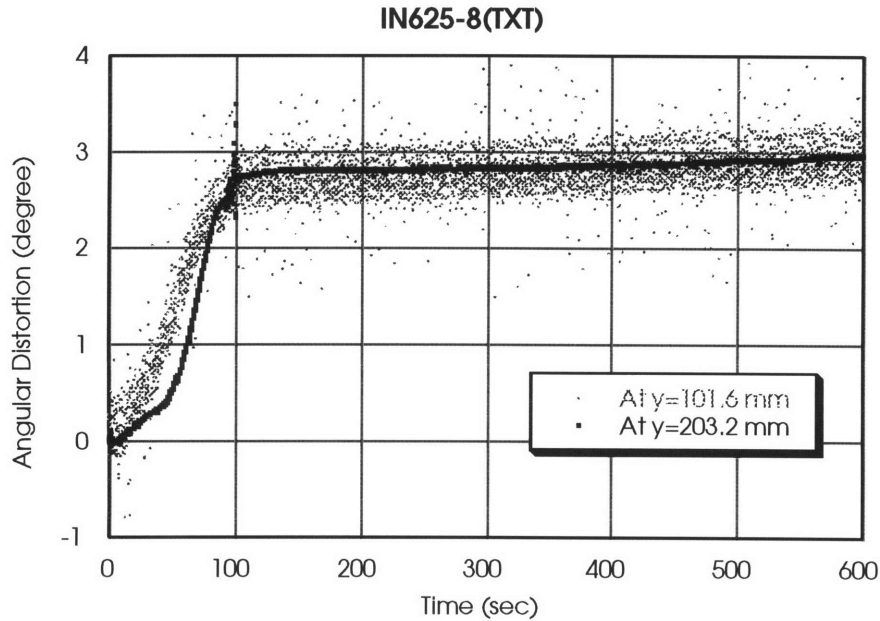


Figure 3.4.4.1.1 Transient bending angles in Set-up A



### Chapter 3: Experiment



**Figure 3.4.4.1.2 Transient bending angles in Set-up B**

#### 3.4.4.2 Neglecting Transducer Sensor Data

The out-of-plane displacement at position 1 and 2 were nearly zero, since these positions were close to the clamps. Therefore, only the data measured at position 3 and 4 by laser sensors were used to calculate the angular distortion at  $y=101.6$  mm as shown in Figure 3.4.4.2. The transient angular distortion at  $y=101.6$  mm went negative at the beginning, started increasing after approximately 10 seconds, and reached to the final distortion at the end of the heating process. The transient angular distortion at  $y=203.2$  mm gradually increased from the beginning up to 50 second after the start of the heating process. When the laser beam approached to the point at  $y=203.2$  mm (it passed there at 60 seconds), the distortion started increasing greatly and finished increasing at the end of the process.

### Chapter 3: Experiment

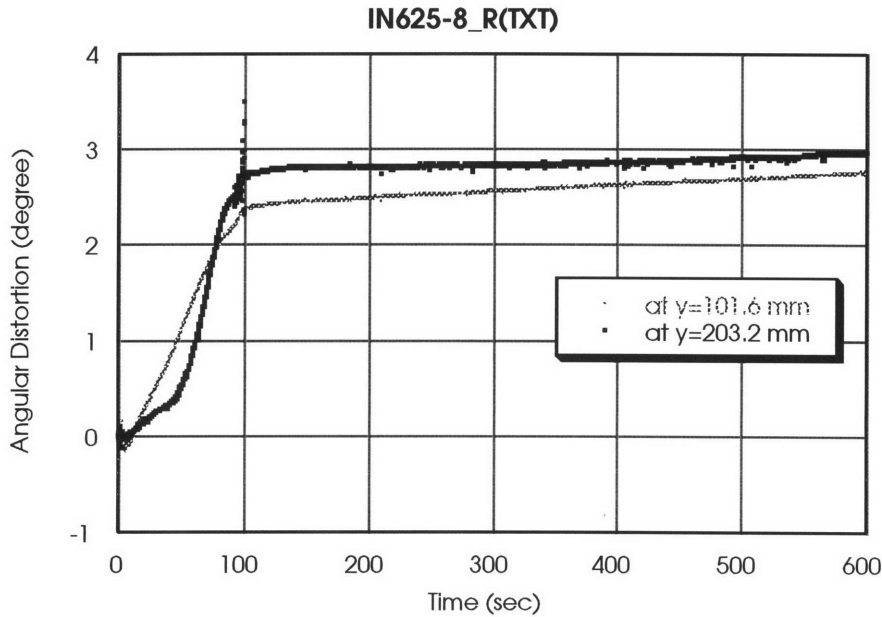


**Figure 3.4.4.2 Results with neglecting data measured by transducers**

#### 3.4.4.3 Repeatability of Deformation

Figure 3.4.4.3 shows the transient angular distortion at  $y=101.6$  mm of seven specimens. The trends and the amounts of transient angular distortions were similar in seven specimens. The results show the good repeatability of a laser forming process on Inconel 625. The actual values, the average value, and the standard deviation of the final angular distortion are as follow:

**Table 3.4.4.3 Angular distortion of seven specimens in the third experiment**

Actual values	2.56, 2.88, 2.87, 2.92, 2.70, 2.64, 2.76
Average value	2.76
Standard deviation	0.1262

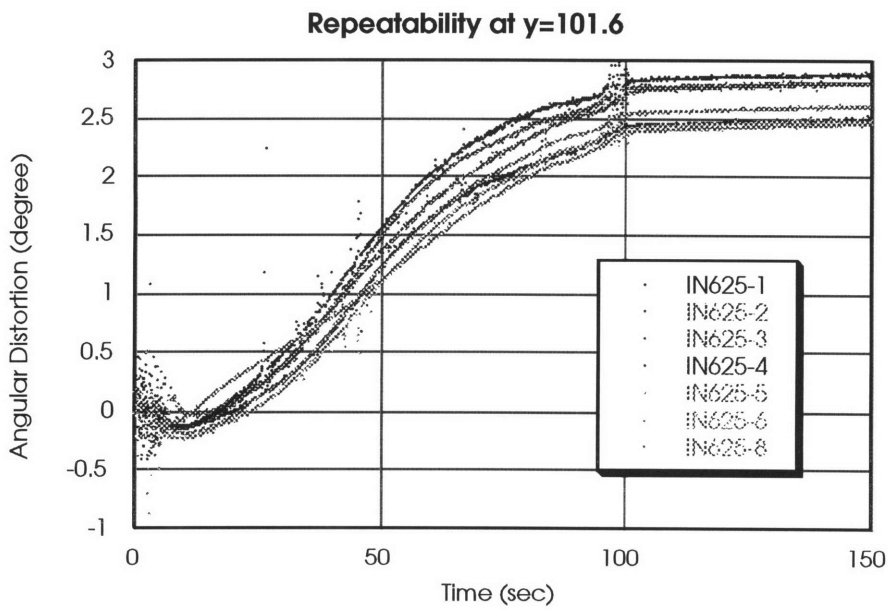


**Figure 3.4.4.3 Comparison of transient angular distortions of seven specimens**

### Chapter 3: Experiment

**Table 3.4.4.4 Comparison of final bending angles from the measurements of laser sensors and the three-dimensional coordinate machine**

Specimen ID	Position	Last Value of Transient Measurement (degree)	Value at the Final Shape (degree)
IN625-1	Y=101.6mm	2.56	3.8
	Y=203.2mm	N.A.	4.1
IN625-2	Y=101.6mm	2.88	3.6
	Y=203.2mm	N.A.	3.9
IN625-3	Y=101.6mm	2.87	3.5
	Y=203.2mm	N.A.	4.0
IN625-5	Y=101.6mm	2.70	2.75
	Y=203.2mm	N.A.	2.85
IN625-8	Y=101.6mm	2.76	3.4
	Y=203.2mm	2.96	3.7

#### **3.4.4.4 Comparison of the Final Bending Angles**

In Table 3.4.4.4, the final angular distortions measured by the laser sensors were compared with those measured by a three-dimensional coordinate-measuring machine at MIT. The former ones are less than the latter ones. The final angular distortions had also been reported by PSU on July 12, 1996. However, these angular distortions were measured by a simple and less-accurate method.

#### **3.4.4.5 Effects of a Multi-Pass Process**

A laser beam irradiated the specimen IN625-6 at the same position twice. The angular distortions of the plates for the first and the second pass of the laser heating at

### Chapter 3: Experiment

$y=101.6$  mm are shown in Figure 3.4.4.5. It shows that angular distortions in the first and the second passes were respectively 2.5 degrees. In other words, The final angular distortion after two passes was 5.0 degrees. Therefore, the bending angles can be superimposed for a two-pass laser forming process.

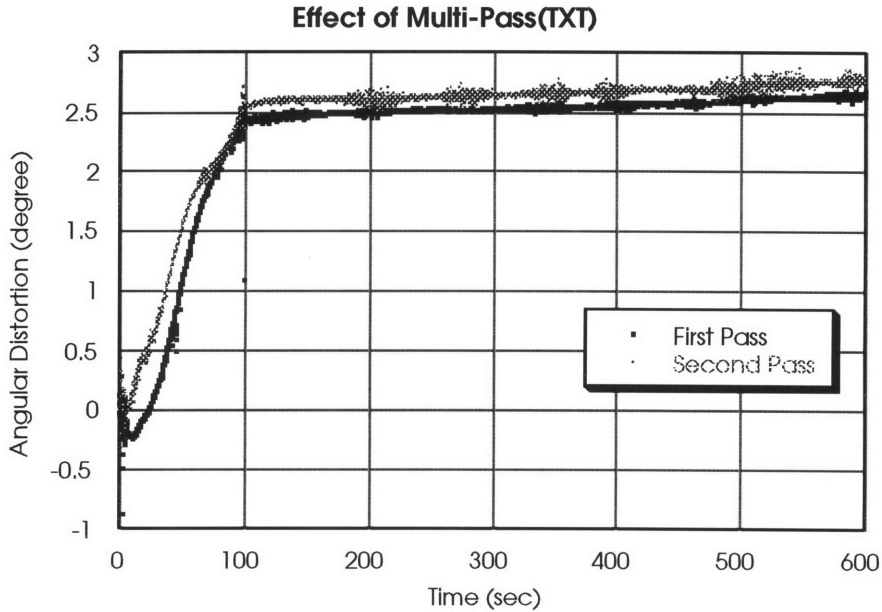
#### **3.4.4.6 Effects of the Initial Shape and Residual Stresses**

Figure 3.4.4.6.1 shows the comparison of the angular distortions at  $y=101.6$  mm in an Inconel 625 plate. The first pass was traveling in the middle of a plate while the second pass was perpendicular to the first pass. The transient angular distortion produced by the second pass was almost the same as that produced by the first pass. However, it decreased largely just before the end of the laser heating process and continued decreasing while the plate was cooled. Consequently, the final value of angular distortion by the second pass was smaller than that by the first pass by 14%.

Similarly, the comparisons of the angular distortions in an HSLA-80 plate are shown in Figure 3.4.4.6.2. In the figure, both angular distortions decrease just before the ends of the processes. All Inconel 625 plates were cut into squares by a mechanical shear. On the contrary, all HSLA-80 plates were cut by some thermal cutting methods (gas frame cutting or plasma cutting). Therefore, the HSLA-80 plates had significantly larger residual stresses. The decrease of the angular distortions in the HSLA-80 plates might be caused by the residual stresses induced by thermal cutting.

Chapter 3: Experiment

The second pass is the same as the first pass.  
Inconel 625, 12" x 12" x 0.25", Stove Black Coating



**Figure 3.4.4.5 Comparison between transient angular distortions during the first pass and the second pass at the same heating line**

The above mentioned cause of the decreases in the HSLA-80 plate is supported by the decrease of the angular distortion by the second pass shown in the Inconel 625 plate. When the first pass finished, the Inconel 625 plate has little residual stresses. After the first pass, the residual stresses were induced in the plate and these residual stresses caused the decrease of the angular distortion just before the end of the second process.

Chapter 3: Experiment

The second process line is perpendicular to the first process line.  
The results were measured at  $y=101.6$  mm on IN625-4 specimen.

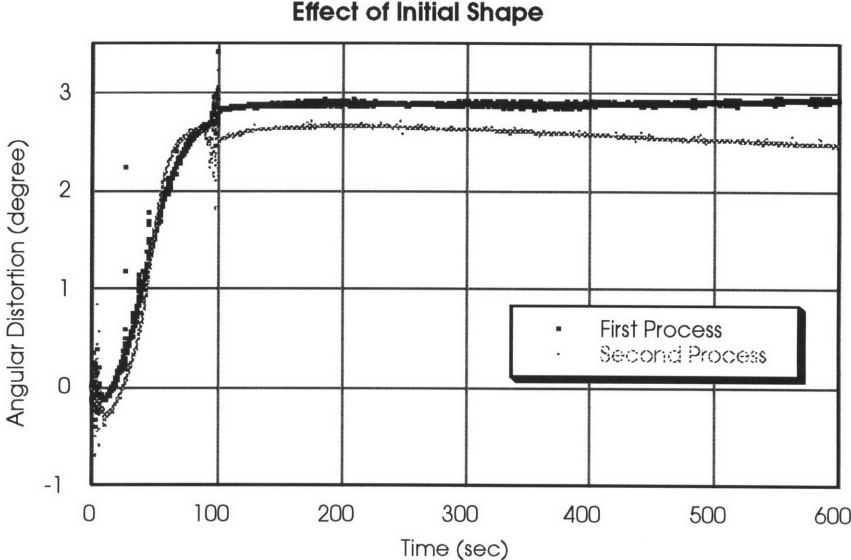


**Figure 3.4.4.6.1 Effect of initial shape before the process in an Inconel 625 plate  
(the second pass is perpendicular to the first pass)**

Chapter 3: Experiment

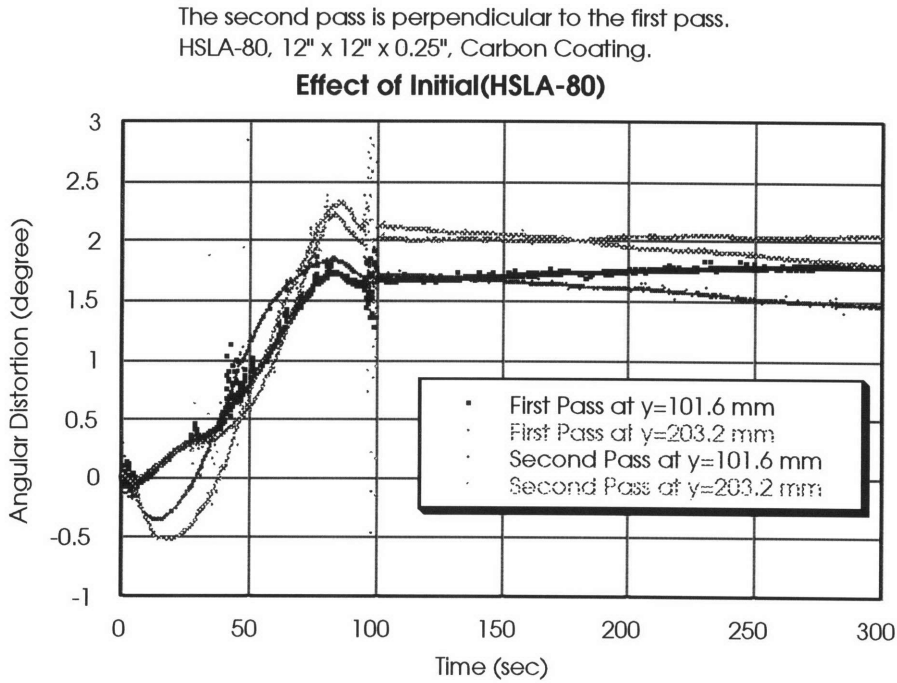


**Figure 3.4.4.6.2 Effect of initial shape and stresses in the HSLA-80 Plate  
(the second pass is perpendicular to the first pass)**

We can observe the slight declinations of the angular distortions by the second pass in the HSLA-80 plate after the heating process. The deformed shape by the first pass may cause the declination of angular distortion in the second pass. The same declination of the angular distortion by the second pass was observed in the Inconel 625 plate as shown in Figure 3.4.4.6.1.



## Chapter 3: Experiment

### **3.5 Experiment 4**

#### **3.5.1 Objective in Experiment 4**

Transient out-of-plane displacement and temperature were measured for various materials irradiated by a laser beam to validate the results of FEM analyses.

#### **3.5.2 Specimen and Processing Parameters in Experiment 4**

Table 3.5.2.1 lists the definition of specimens. Table 3.5.2.2 lists the processing conditions. The positions of the sensors are the same as those in the third experiment. Thermocouple 1 (TC1) is attached at the center of the non-irradiation side of the plate. Thermocouple 2 (TC2) is attached at 0.5 inches away from Thermocouple 1 in the transverse direction.

**Table 3.5.2.1 Specimen definitions in the fourth experiment**

Specimen	Length (in.)	Width (in.)	Thickness (in.)
Inconel 718 #1	12	12	0.25
Inconel 718 #2	12	12	0.25
Al 2219	12	12	0.25
Al 5053	12	12	0.25
Ti-15-3-3	12	12	0.0625
HY-80 #1	12	12	0.25
HY-80 #2	12	12	0.25

### Chapter 3: Experiment

**Table 3.5.2.2 Processing conditions in the fourth experiment**

Specimen	Delivery Power (kW)	Speed (cm/min.)	Spot size (cm)
Inconel 718 #1	2.60	20	2
Inconel 718 #2	2.60	20	2
Al 2219	2.60	20	2
Al 5053	2.60	20	2
Ti-15-3-3	0.75	60	2
HY-80 #1	2.60	20	2
HY-80 #2	2.60	20	2

### **3.5.3 Results of Experiment 4**

Figure 3.5.3.1 shows the temperature distribution of Inconel 718 #2. The peak temperature at TC1 was 480 °C. The temperature increased quickly just and decreased slowly. Figures 3.5.3.2 and 3.5.3.3 show the transient angular distortion of Inconel 718 #1 and Inconel 718 #2, which were 1.2 and 0.82 degrees. Figures 3.5.3.4 and 3.5.3.5 show the transient angular distortions of HY-80 #1 and HY-80 #2, which were 2.0 and 1.67 degrees for Inconel HY-80 #1 and HY-80 #2.

Chapter 3: Experiment

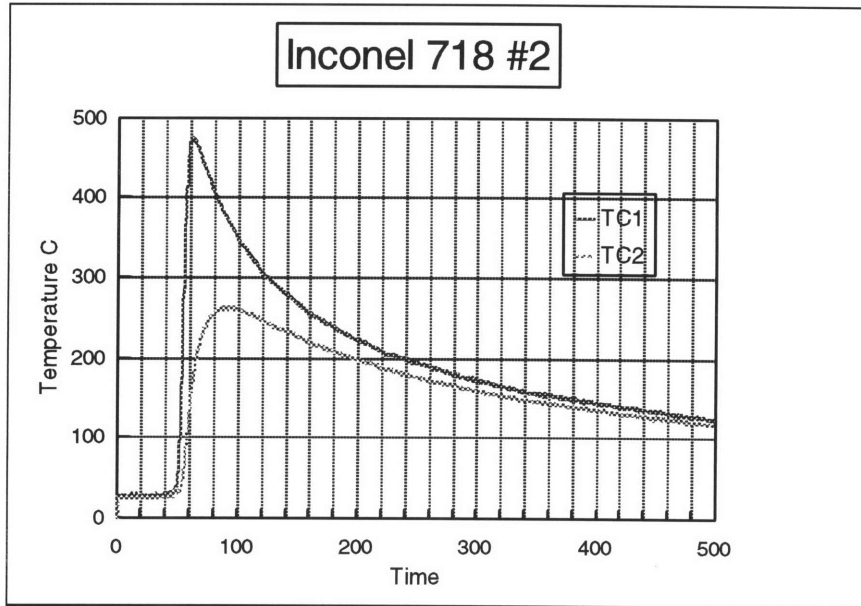


Figure 3.5.3.1 Temperature distribution of Inconel 718

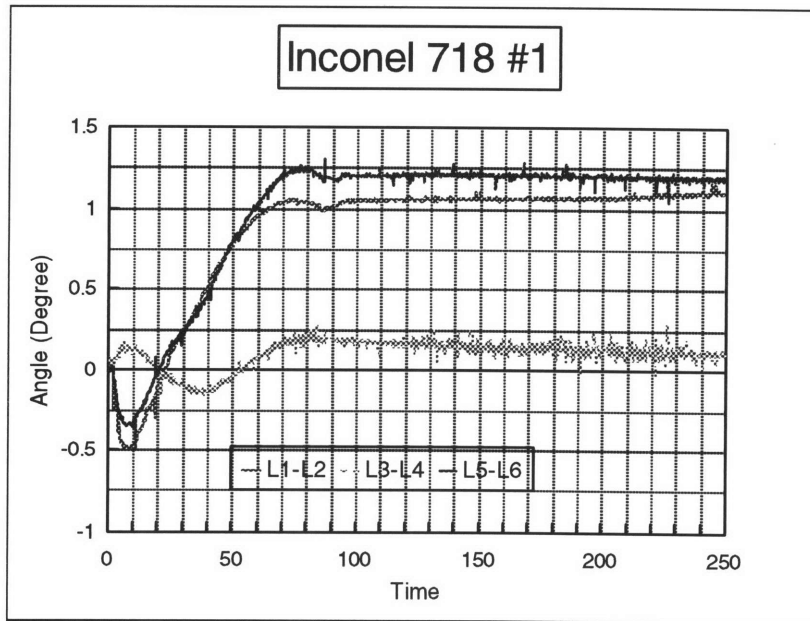


Figure 3.5.3.2 Transient angular distortion of Inconel 718 #1

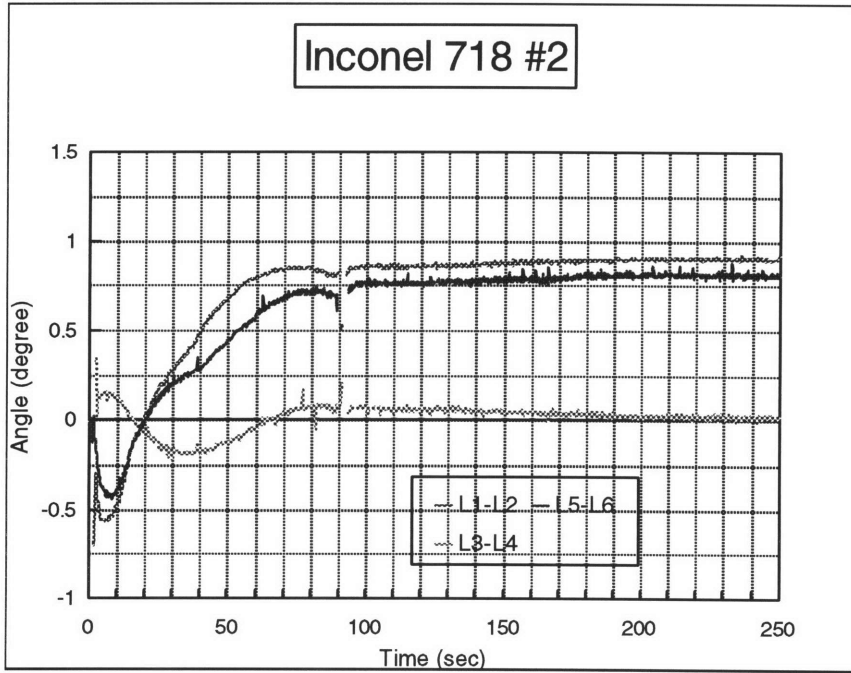


Figure 3.5.3.3 Transient angular distortion of Inconel 718 #2

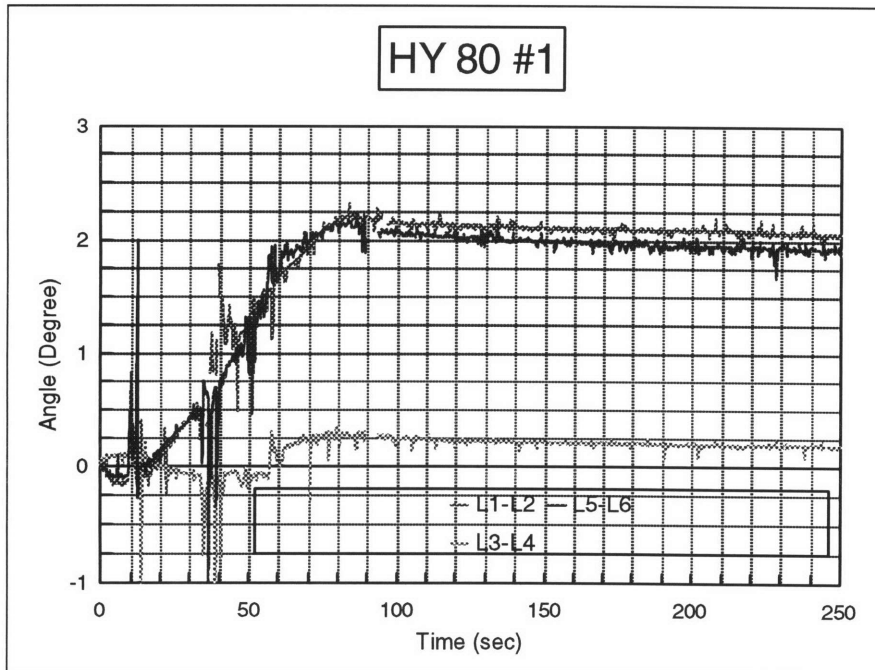
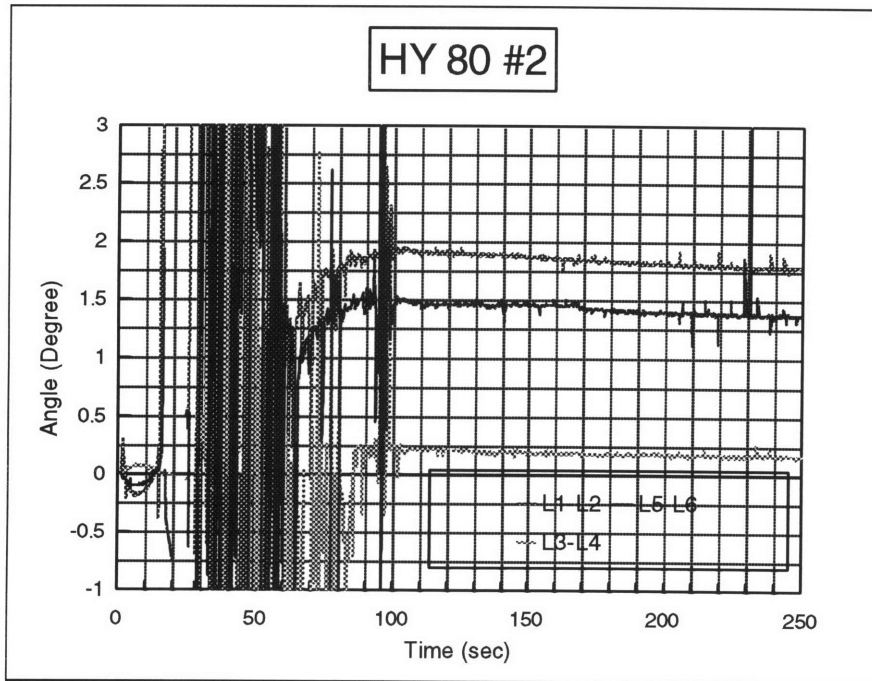


Figure 3.5.3.4 Transient angular distortion of Inconel HY 80 #1

Chapter 3: Experiment



**Figure 3.5.3.5 Transient angular distortion of Inconel HY 80 #2**

## **3.6 Experiment 5**

### **3.6.1 Objective in Experiment 5**

The objective is to investigate the effects of rolling direction on the angular distortion. The results showed that angular distortion increased when the heating direction was parallel to the rolling direction.

### **3.6.2. Specimen Definitions and Processing Parameters in Experiment 5**

Table 3.6.2.1 lists the definitions of specimens. Table 3.6.2.2 lists the processing conditions. The positions of sensors were the same as those in the fourth experiment.

**Table 3.6.2.1 Specimen definition in the fifth experiment**

Specimen	Length (in.)	Width (in.)	Thickness (in.)
HSLA80 #1	12	12	0.25
HSLA80 #2	12	12	0.25
Inconel #1	12	12	0.25
Inconel #2	12	12	0.25

**Table 3.6.2.2 Processing conditions in the fifth experiment**

Specimen	Power (kW)	Speed (cm/min.)	Spot size (cm)
HSLA80 #1	2.60	20	2
HSLA80 #2	2.60	20	2
Inconel #1	2.60	20	2
Inconel #2	2.60	20	2

### 3.6.3 Results in Experiment 5

Figures 3.6.3.1 and 3.6.3.2 show the transient angular distortions of the HSLA-80 plate which was irradiated by a laser beam moving parallel and perpendicular to the rolling direction respectively. The final average angular distortions of the HSLA-80 plates were 1.75 and 2.12 degrees respectively in the parallel and perpendicular directions. Therefore, the angular distortions of the HSLA-80 plates increased when the heating direction was transverse to the rolling direction. Figures 3.3 and 3.4 show the transient angular distortions of Inconel 625 specimen which was irradiated by a laser beam moving parallel and perpendicularly to rolling direction respectively. The final average angular distortions of Inconel 625 plates were 2.82 and 3.25 degrees respectively in the parallel and perpendicular directions. Therefore, the angular distortions of Inconel 625 plates increased when the heating direction was transverse to the rolling direction.

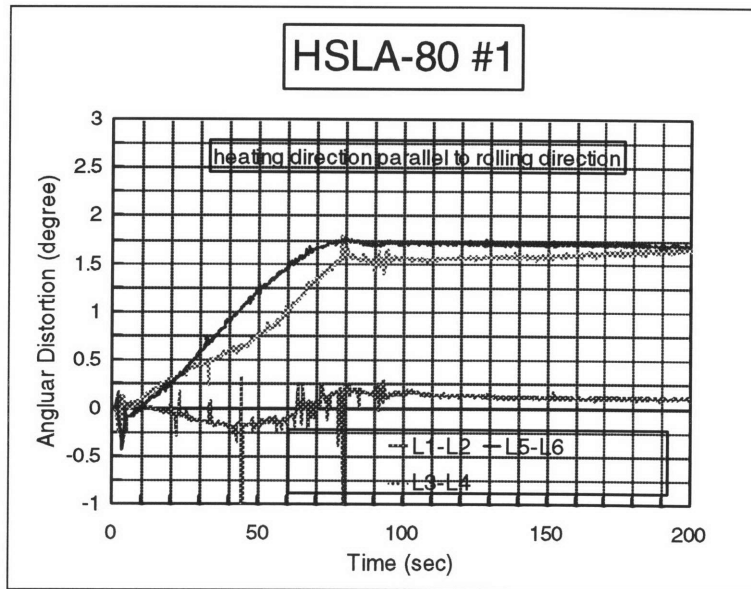


**Figure 3.6.3.1 Angular distortion of the HSLA-80 #1 plate  
(heating direction parallel to rolling direction)**

Chapter 3: Experiment

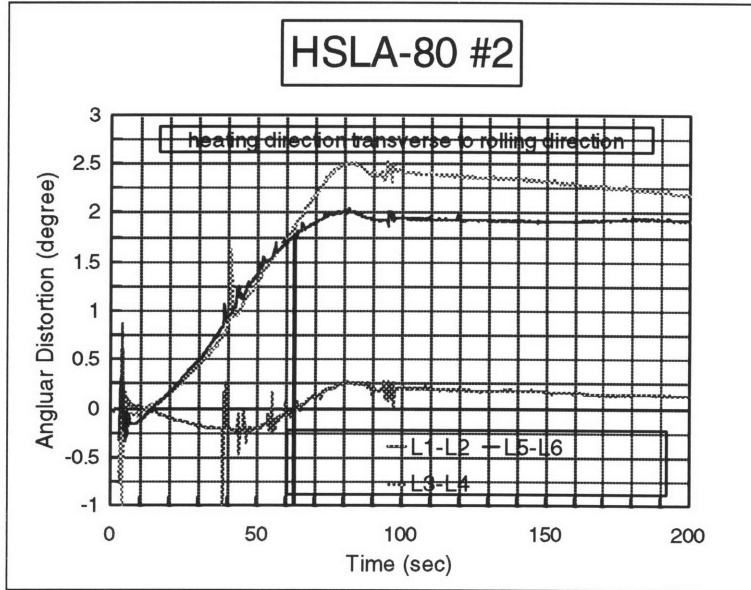


Figure 3.6.3.2 Angular distortion of the HSLA-80 #2 plate (heating direction transverse to rolling direction)

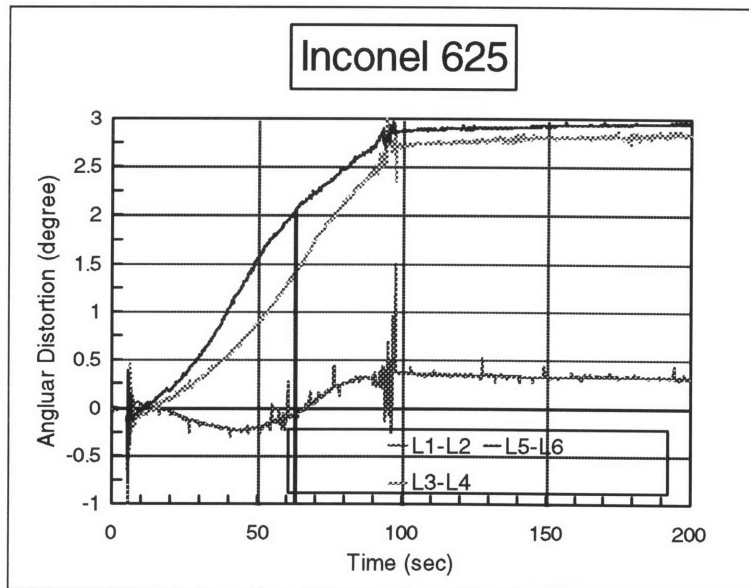
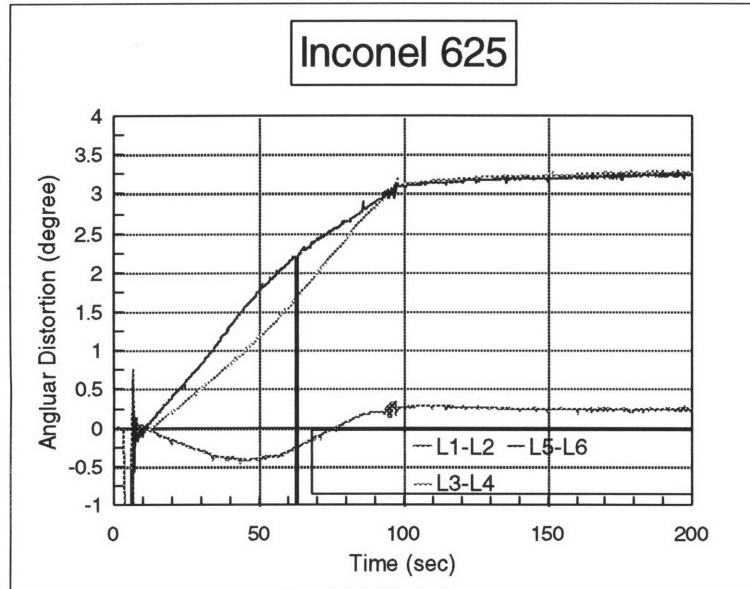


Figure 3.6.3.3 Angular distortion of the Inconel 625#1 plate (heating direction parallel to rolling direction)



Chapter 3: Experiment



**Figure 3.6.3.4 Angular distortion of the Inconel 625 #2 plate  
(heating direction transverse to rolling direction)**

## **Chapter 4 Mechanisms of Laser Forming**

### **4.1 Background**

The study of mechanisms of laser forming is beneficial to the development of laser forming technology. Mechanisms of laser forming provide the explanations of deformation produced by a specific laser heating pattern; evaluates the influence of material properties on deformation; decides significant processing parameters. The insight of mechanisms of laser forming is useful to perform a laser forming process, develop a predictive model, and make a good judgment of limitations on the laser forming process.

The mechanisms of laser forming can be depicted as an interaction between a laser beam and a workpiece in the point view of quantum mechanics. Laser can be considered as a group of high-energy light particles according to the matter characteristics of light. While light particles collide the surface of a workpiece, the internal energy of atoms is increasing. The increase of the internal energy leads to the increase of temperature in a macroscopic view. As a laser beam is moving on the surface of the workpiece, an uneven temperature distribution in the workpiece is generated. In thermal stress theory, an uneven temperature is a major source of thermal stresses. Thermal stresses produce the deformation of the workpiece. During a laser forming process, the gravitational force is much less than thermal stresses. The effect of gravity is not considered.

Mechanisms of laser forming are classified according to six types of deformation: angular change, transverse shrinkage, rotational distortion, longitudinal bending, longitudinal shrinkage, and bulking distortion as shown in Figure 4.1.1. [26].

Chapter 4 Mechanism of Laser Forming

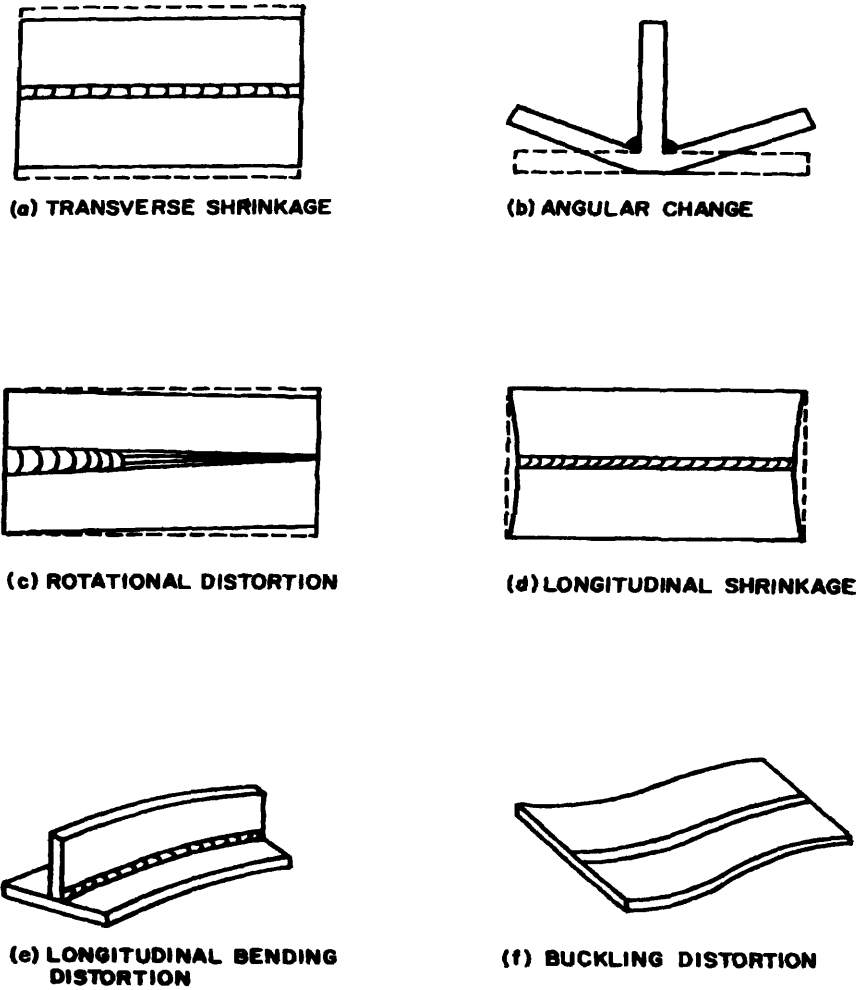


**Figure 4.1.1 Six types of the deformation during a laser forming process**

## Chapter 4 Mechanism of Laser Forming

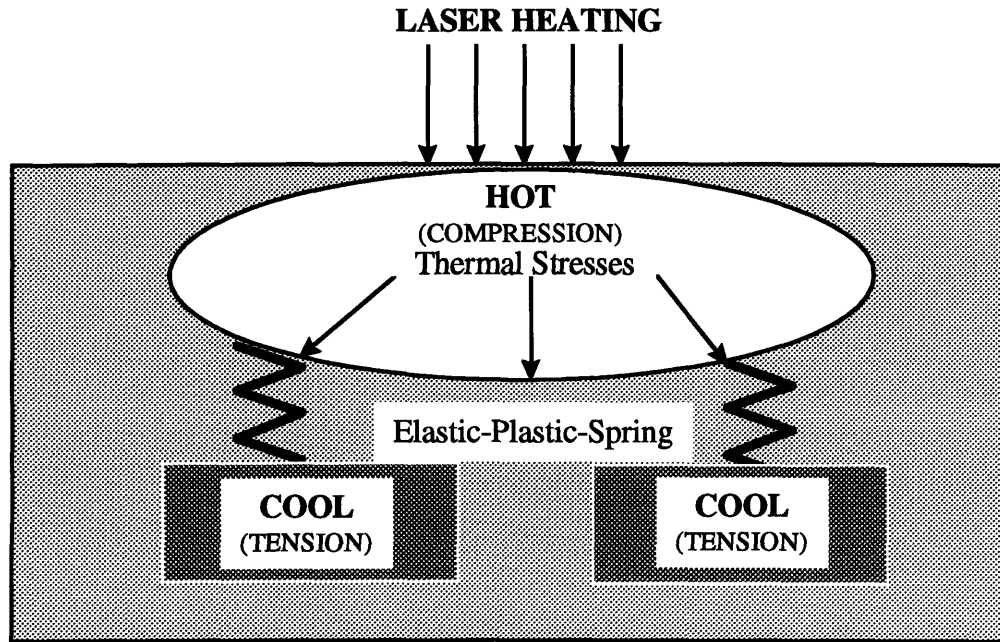
In one-dimensional laser forming process, angular change is more significant than other distortion. Buckling mechanism only occurs in the thin workpiece and specific processing condition. Therefore, angular bending mechanism is the major concern in this research. Angular bending mechanism includes bending toward or away a laser beam (upsetting mechanism). In this Chapter, thermal stress theory is introduced first. Thermal stress theory is used to explain angular bending mechanisms later.

### **4.2 Thermal Stresses Theory**

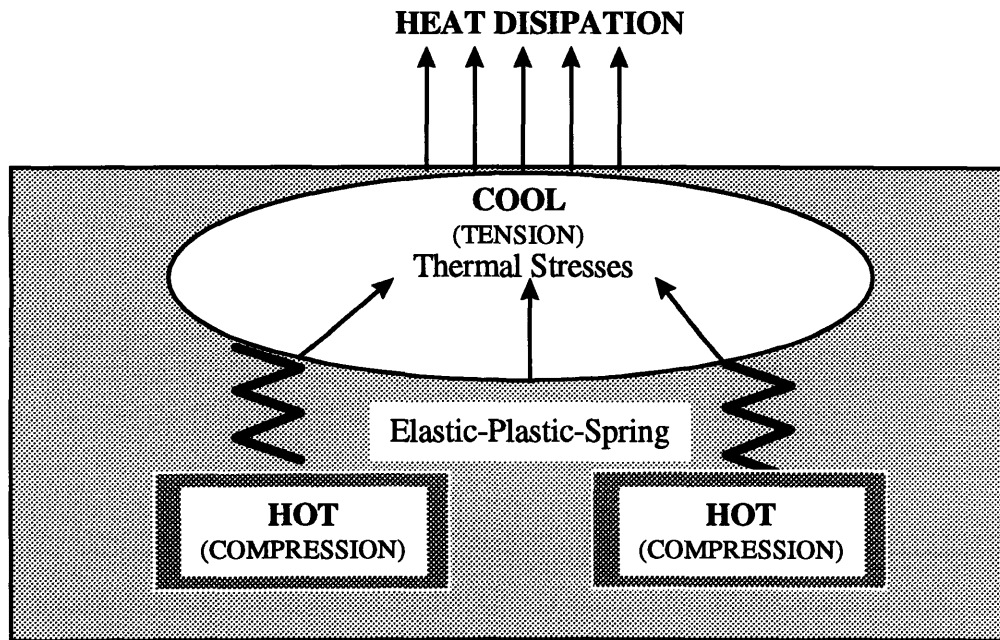
There are two ways to produce thermal stresses:

1. *Uniform temperature distribution with constraints*

A solid body expands or contracts without restraint under a uniform change of temperature. There are thermal deformation, but no thermal stresses in a solid body. Thermal strain is proportional to thermal expansion coefficient and the change of temperature. For example, a bar expands or contracts uniformly with a constant change of temperature through the body. As the solid body is confined at some regions under an uniform temperature change, thermal stresses are produced. For example, a bar is fixed at both ends. Given a constant positive temperature change through the body, it will expand, but outer constraints push the bar back. Therefore, compressive thermal stresses are produced in the solid body.

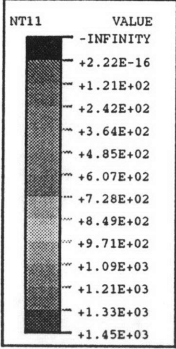


(a)

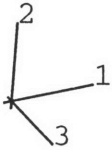
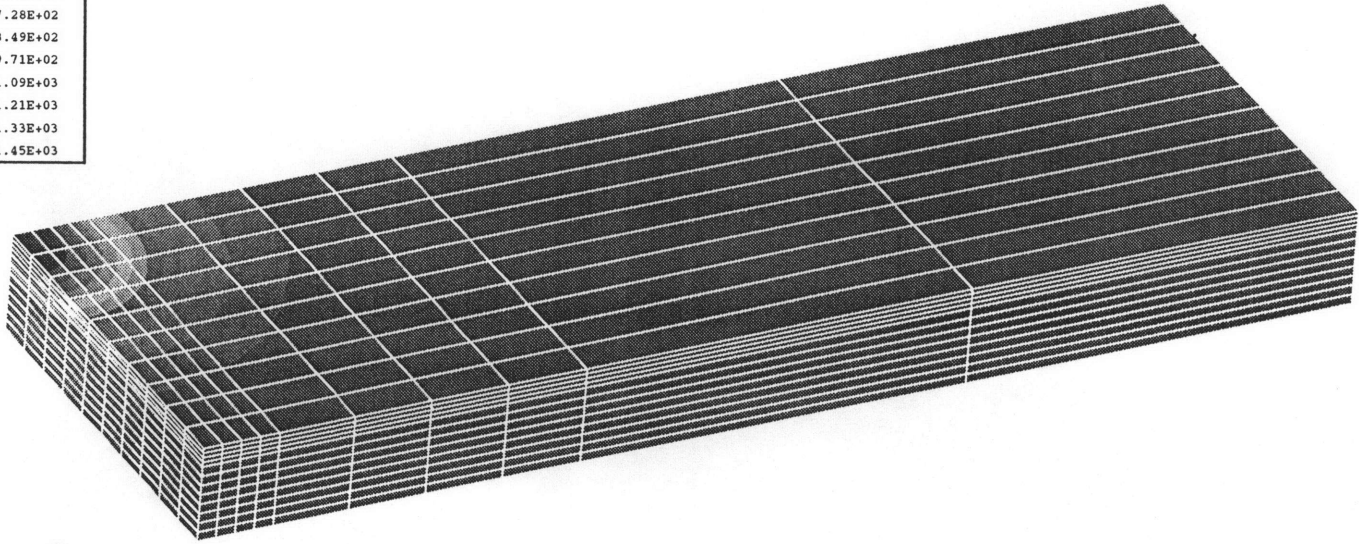


(b)

Figure 4.2.1 (a) and (b) Model of thermal stresses due to an uneven temperature distribution during heating and cooling



74



TIME COMPLETED IN THIS STEP .583 TOTAL ACCUMULATED TIME .583  
 ABAQUS VERSION: 5.5-1 DATE: 16-DEC-96 TIME: 20:53:10  
 STEP 1 INCREMENT 15

Figure 4.2.2 Three-dimensional temperature distribution during laser heating

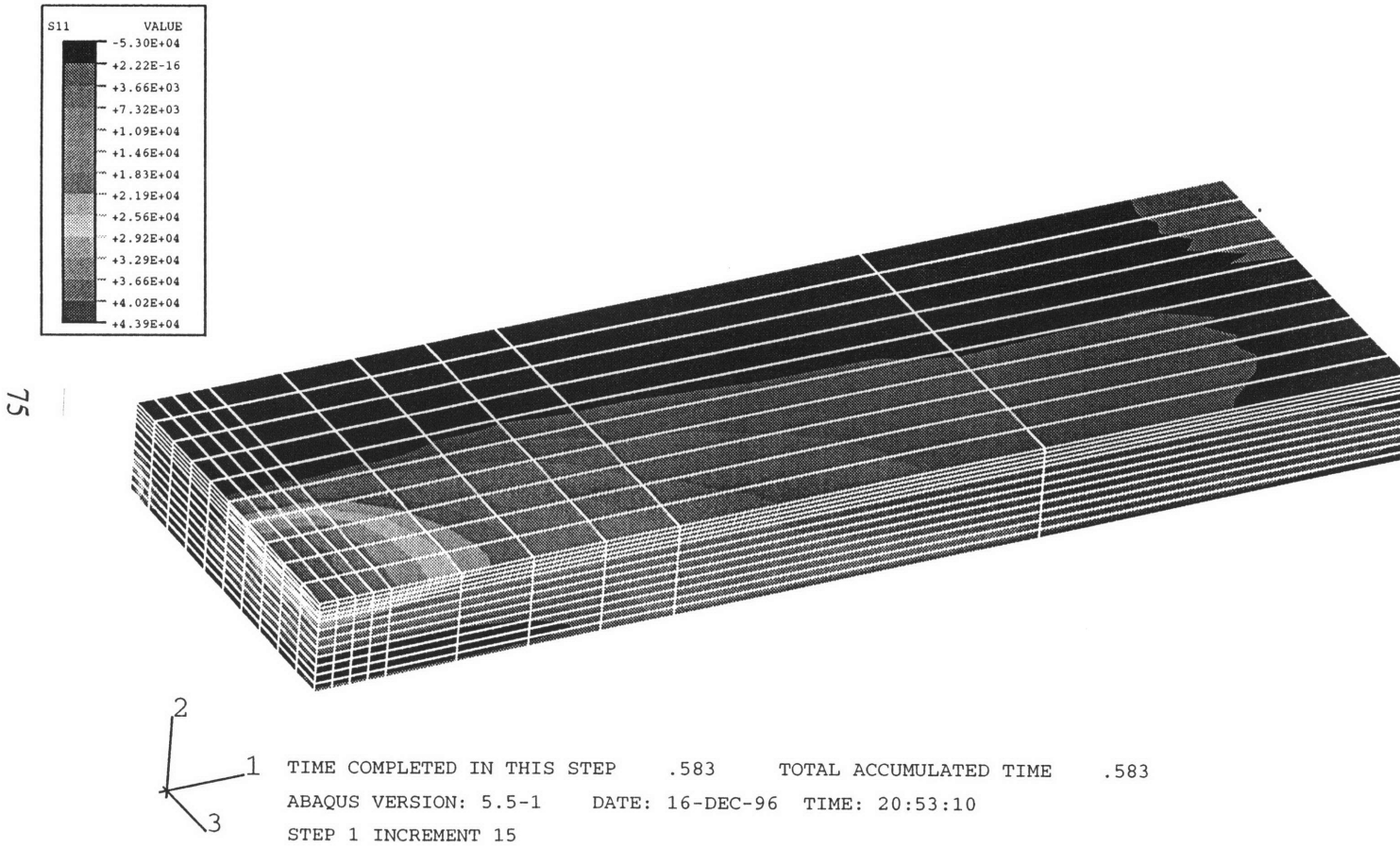
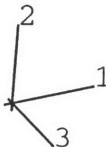
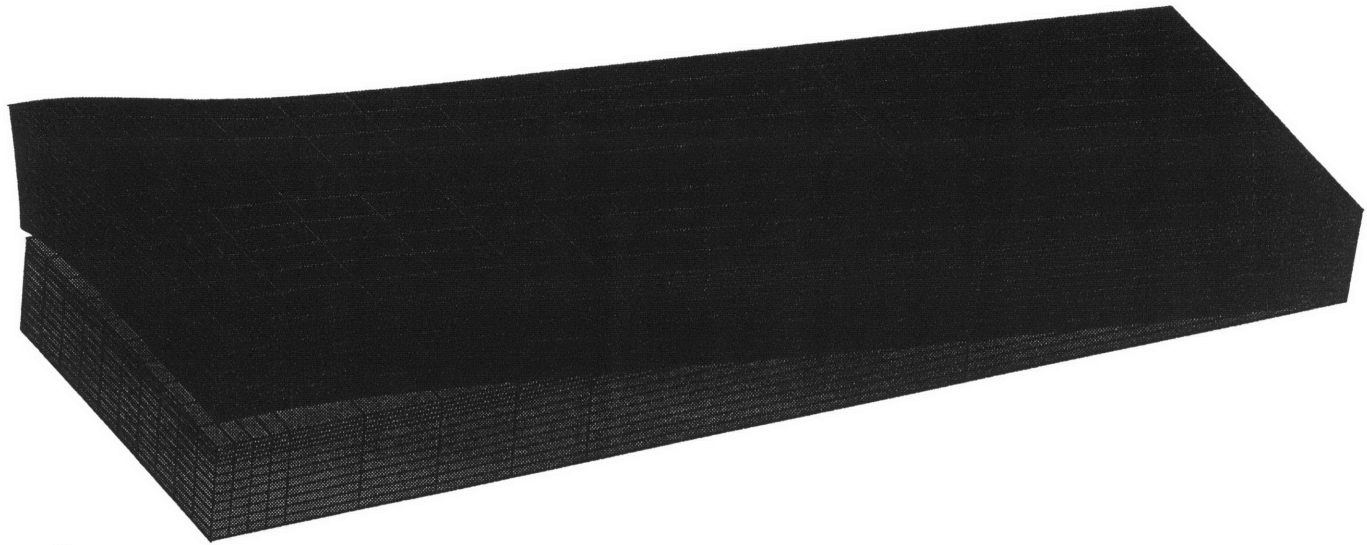


Figure 4.2.3 Thermal stress in x direction during laser heating



DISPLACEMENT MAGNIFICATION FACTOR = 31.9 ORIGINAL MESH DISPLACED MESH  
TIME COMPLETED IN THIS STEP .583 TOTAL ACCUMULATED TIME .583  
ABAQUS VERSION: 5.5-1 DATE: 16-DEC-96 TIME: 20:53:10  
STEP 1 INCREMENT 15

Figure 4.2.4 Three-dimensional deformation during laser heating



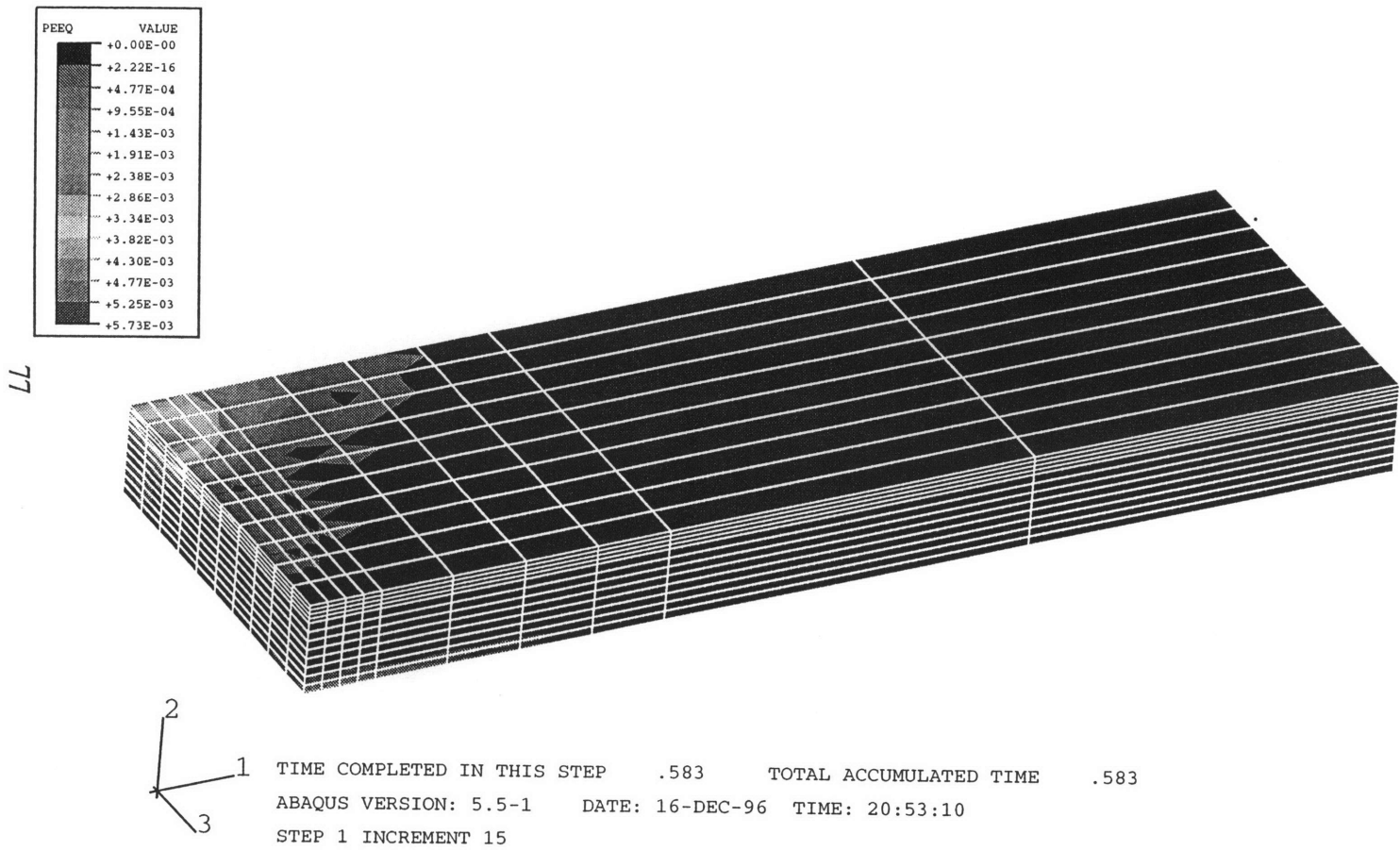
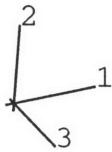
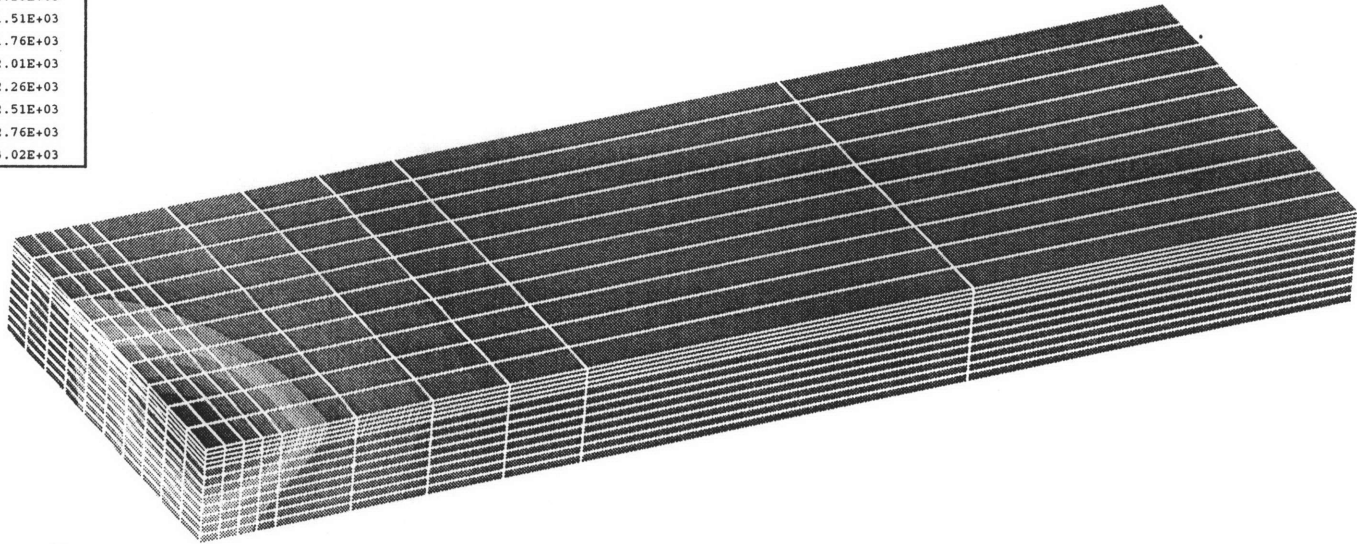
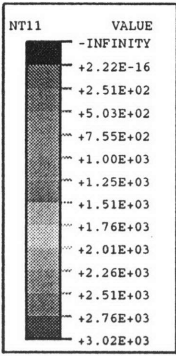


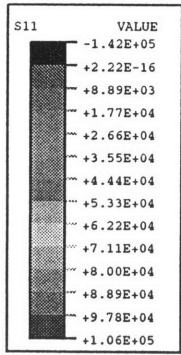
Figure 4.2.5 Effective plastic strain during laser heating

78

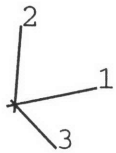
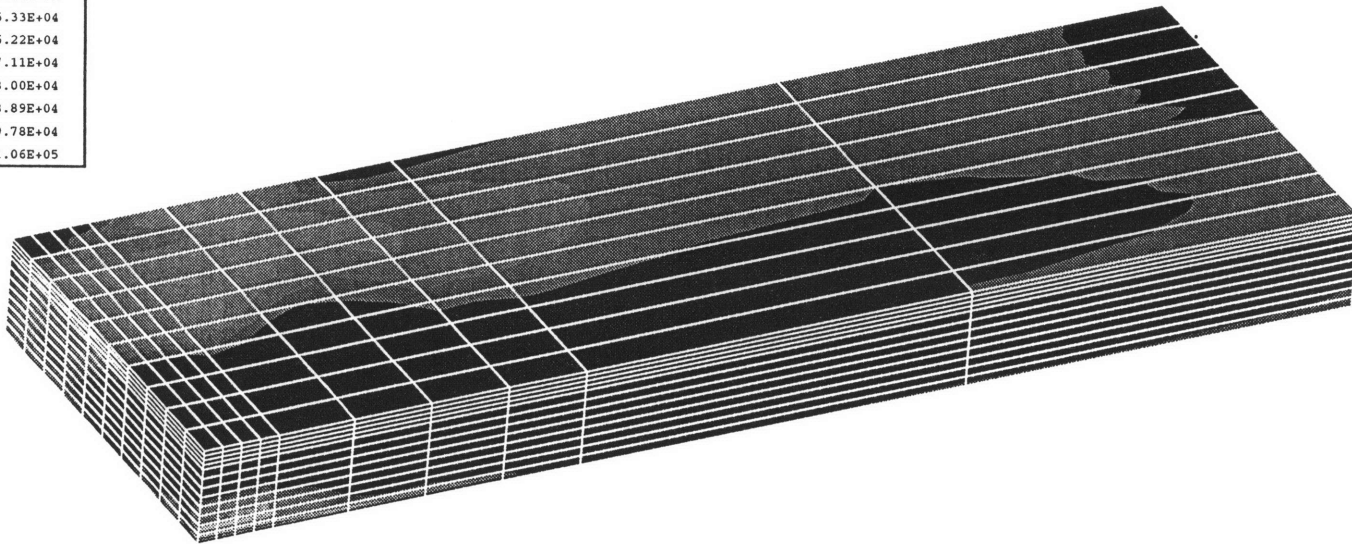


TIME COMPLETED IN THIS STEP 4.30 TOTAL ACCUMULATED TIME 4.30  
ABAQUS VERSION: 5.5-1 DATE: 16-DEC-96 TIME: 20:53:10  
STEP 1 INCREMENT 30

Figure 4.2.6 Three-dimensional transient temperature distribution at the end of laser heating



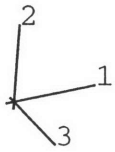
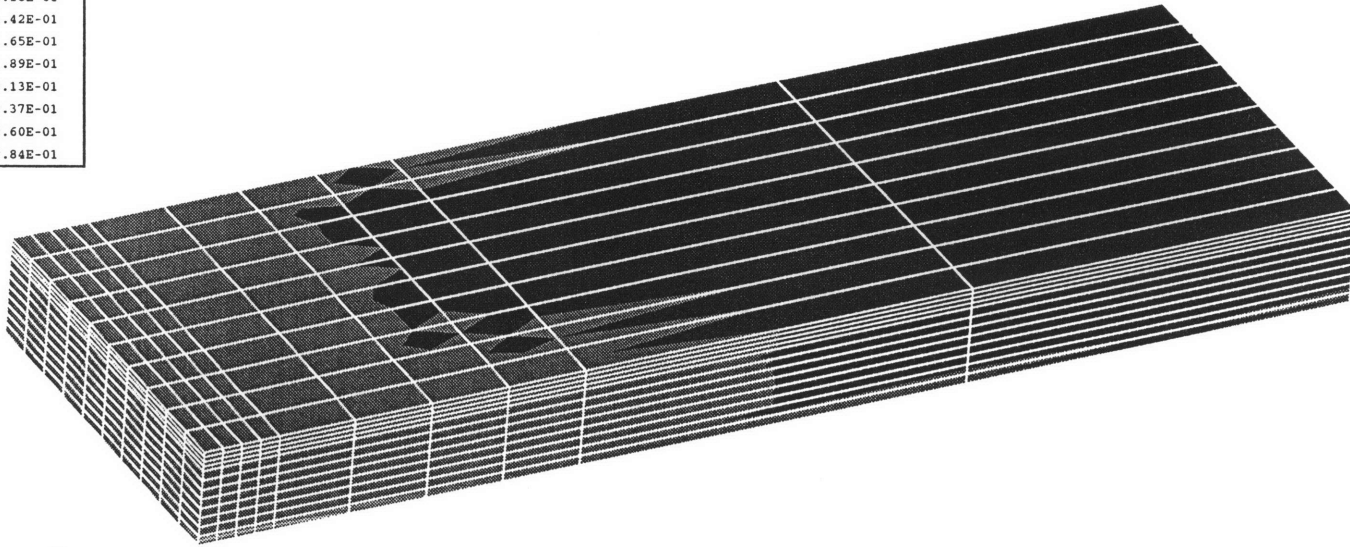
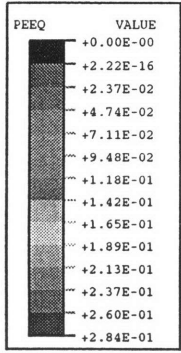
79



TIME COMPLETED IN THIS STEP 4.30 TOTAL ACCUMULATED TIME 4.30  
 ABAQUS VERSION: 5.5-1 DATE: 16-DEC-96 TIME: 20:53:10  
 STEP 1 INCREMENT 30

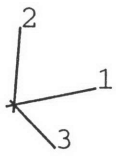
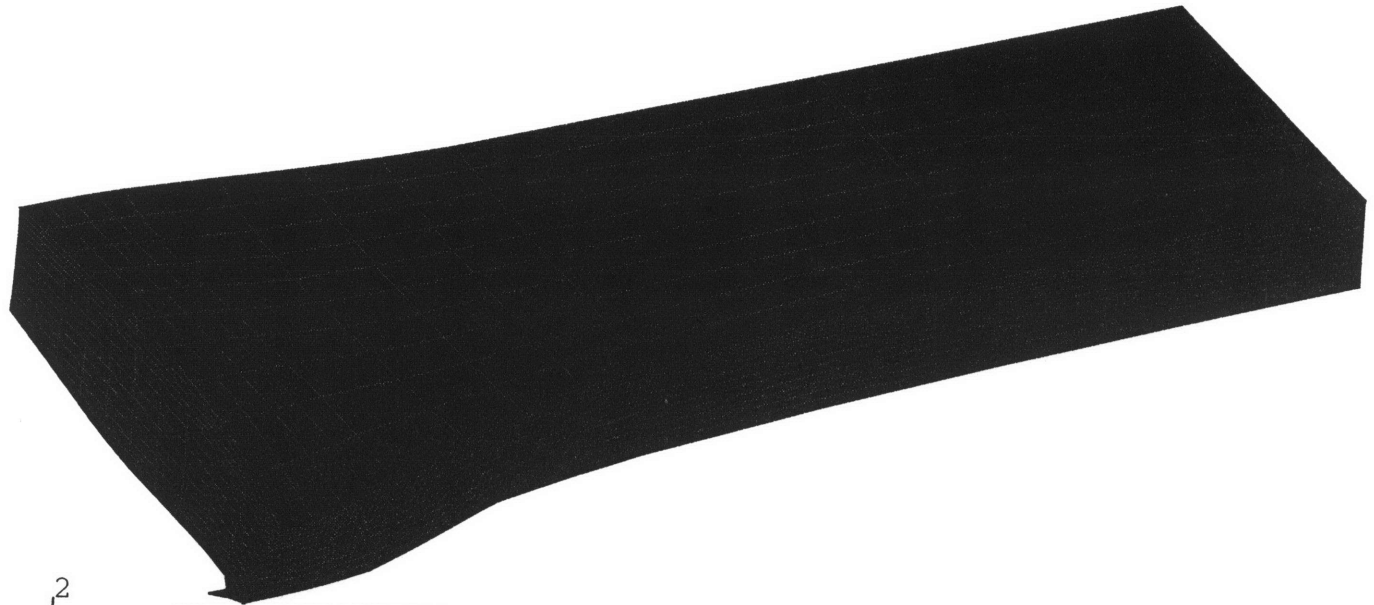
Figure 4.2.7 Thermal stress in x direction at the end of laser heating

80



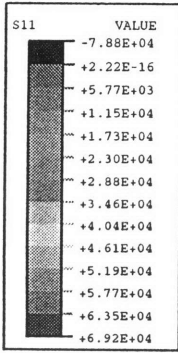
TIME COMPLETED IN THIS STEP 4.30 TOTAL ACCUMULATED TIME 4.30  
ABAQUS VERSION: 5.5-1 DATE: 16-DEC-96 TIME: 20:53:10  
STEP 1 INCREMENT 30

Figure 4.2.8 Effective plastic strain at the end of laser heating

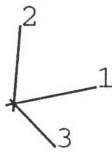
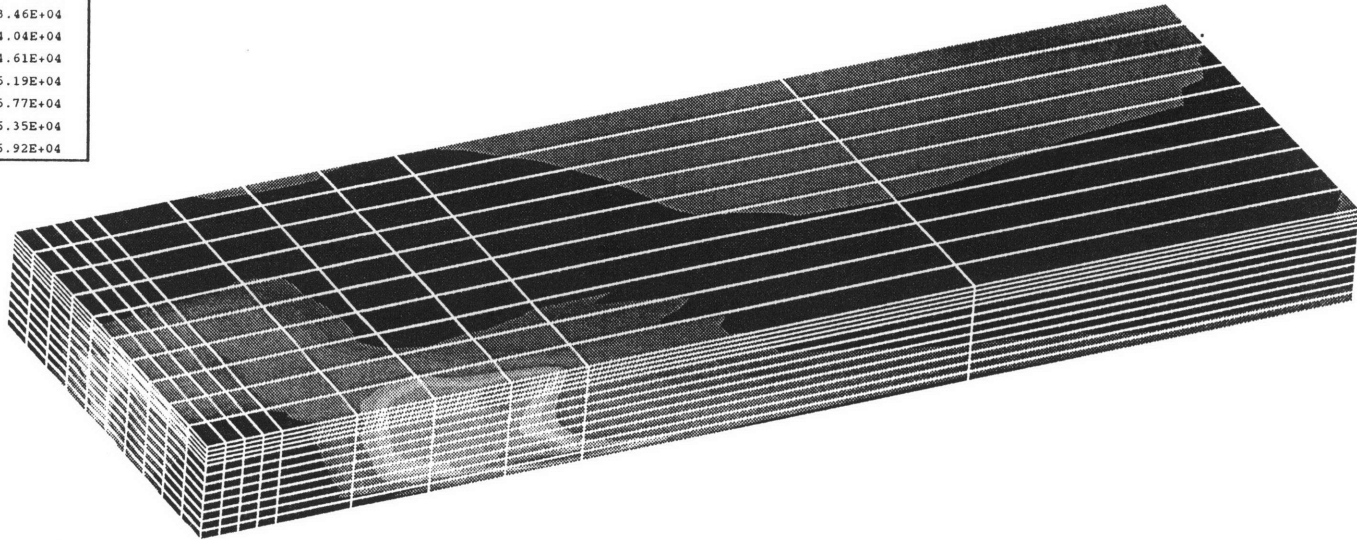


DISPLACEMENT MAGNIFICATION FACTOR = 27.9 ORIGINAL MESH DISPLACED MESH  
TIME COMPLETED IN THIS STEP 4.30 TOTAL ACCUMULATED TIME 4.30  
ABAQUS VERSION: 5.5-1 DATE: 16-DEC-96 TIME: 20:53:10  
STEP 1 INCREMENT 30

Figure 4.2.9 Transient deformation at the end of laser heating



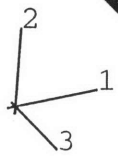
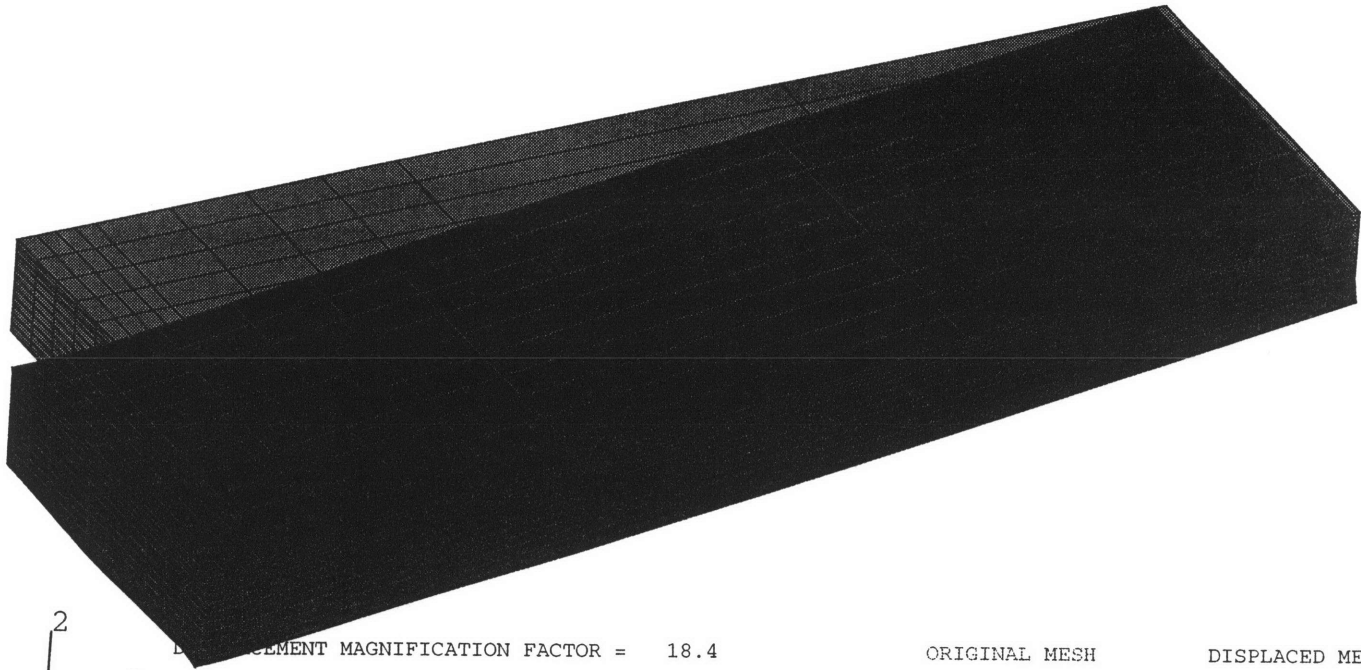
82



TIME COMPLETED IN THIS STEP 458. TOTAL ACCUMULATED TIME 458.  
 ABAQUS VERSION: 5.5-1 DATE: 16-DEC-96 TIME: 20:53:10  
 STEP 1 INCREMENT 55

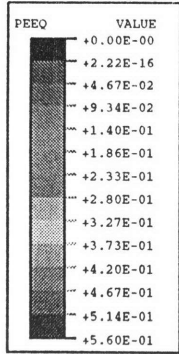
Figure 4.2.10 Thermal stress in x direction at the end of laser heating

83

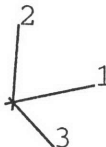
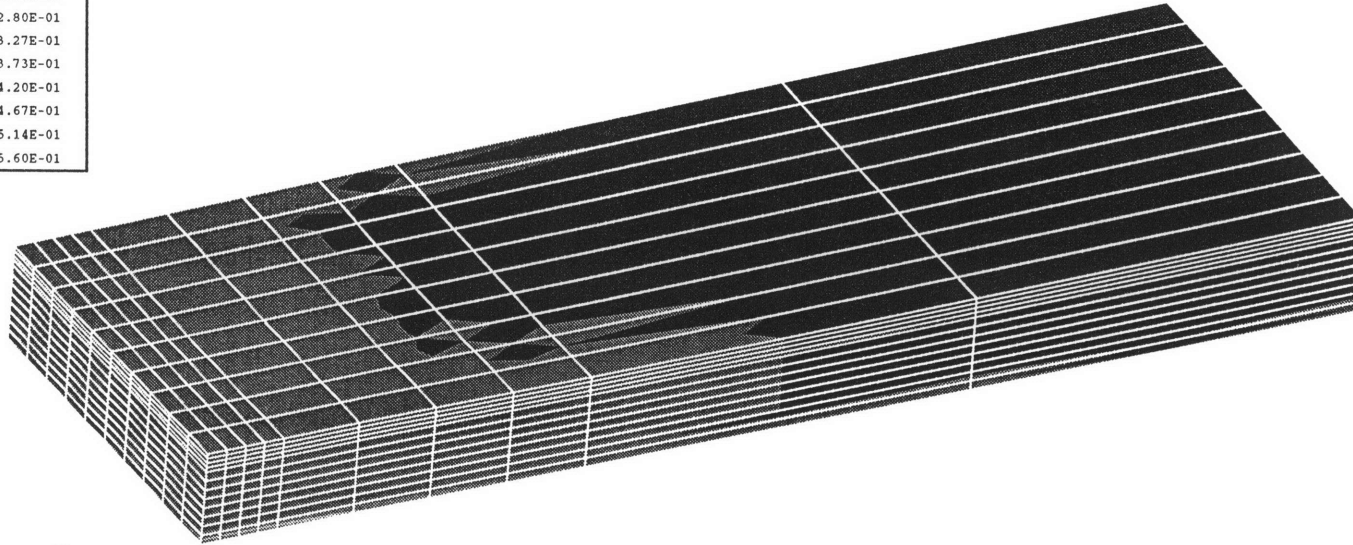


DISPLACEMENT MAGNIFICATION FACTOR = 18.4 ORIGINAL MESH DISPLACED MESH  
TIME COMPLETED IN THIS STEP 458. TOTAL ACCUMULATED TIME 458.  
ABAQUS VERSION: 5.5-1 DATE: 16-DEC-96 TIME: 20:53:10  
STEP 1 INCREMENT 55

Figure 4.2.11 Transient deformation at the end of laser heating



84



TIME COMPLETED IN THIS STEP 458. TOTAL ACCUMULATED TIME 458.  
 ABAQUS VERSION: 5.5-1 DATE: 16-DEC-96 TIME: 20:53:10  
 STEP 1 INCREMENT 55

Figure 4.2.12 Effective Plastic strain at the end of laser heating



## Chapter 4 Mechanism of Laser Forming

### 2. Uneven temperature distribution without constraints

A non-uniform temperature distribution produces the thermal stresses. The model can be depicted in Figure 4.2.1. Many springs are considered inside a body. Part (a) of Figure 4.2.1 occurs during the heating stage of a laser forming process. As the hotter parts of the body expand, the adjacent cooler parts tend to push back. Compressive thermal stresses are produced in hotter parts; tensile stresses in cooler parts. As thermal stresses meets yield condition, the spring undergoes plastic deformation. On the contrary, Part hotter.(b) of Figure 4.2.1 occurs during the cooling stage of a laser forming process. The origin hotter part of the body becomes cooler.

Therefore, the stresses are changed from compression to tension in the original hotter part. Residual stresses and strains remain at the end of cooling stage. It is noted that resultant forces and bending moments in a workpiece should be balanced if there are no external forces [5,12].

With basic concepts of thermal stress theory, we can give explanations of mechanisms of laser forming. During a laser forming process, a typical uneven temperature distribution during a heating stage is shown in Figure 4.2.2. The temperature in the upper surface of the plate is higher than in the lower one; the temperature of the leading edge of the laser beam is higher than the trail of that; the temperature near the heating line is higher than away from that. Therefore, the temperature is not uniformly distributed over the body. Figure 4.2.3 shows a stress distribution in the x direction corresponding to the uneven temperature distribution without constrains in Figure 4.2.2. The compressive thermal stresses will be produced in region near upper surface during

## Chapter 4 Mechanism of Laser Forming

heating. Tensile thermal stresses are produced in cold part while compressive thermal stresses are produced in hot part. At this time, the plate bends downwards as shown in Figure 4.2.4. The plastic strain occurs only near the heated region as shown in Figure 4.2.5. Figure 4.2.6 shows a typical temperature distribution at the end of a heating stage. Figure 4.2.7 shows the stress distribution in x direction. While the hot part of the plate cools down, compressive stresses change to tensile stresses. This change of stress can be observed in Figures 4.2.3 and 4.2.7. At this time, the plastic region expands to larger region as shown in Figure 4.2.8 and the plate bends upwards as shown in Figure 4.2.9. After stopping the laser beam, the plate cools down to room temperature 70 F. The residual stress in x direction is shown in Figure 4.2.10. The final deformed shape is bending toward the beam as shown in Figure 4.2.11. Figure 4.2.12 shows that plastic strain is concentrated on the region near the heating line.

### **4.3 Mechanisms of Laser Forming**

The explanation of mechanisms of laser forming is given in this section. The full understandings of mechanisms of laser forming rely on thermal-elastic-plastic analyses. The thermal-elastic-plastic analyses of a laser forming process will furnish the information of transient stresses and strains. The FEM thermal-elastic-plastic analyses will be performed in Chapter 6.

#### **4.3.1 Angular Bending Mechanism**

Angular bending mechanism can be explained by a simple beam with temperature difference through the thickness [13]. Figure 4.3.1 shows a beam of thickness  $h$  with a

## Chapter 4 Mechanism of Laser Forming

linear temperature difference through thickness.  $T_0$  is the initial temperature of the beam.  $T_1$  and  $T_2$  are the temperature at top and bottom of the beam respectively. The deflection equation of beam can be expressed as follows:

$$hd\theta = \alpha(T)(T_1(h) - T_0)dx - \alpha(T)(T_2(h) - T_0)dx$$

or

$$\frac{d\theta}{dx} = -\frac{\alpha(T)(T_2(h) - T_1(h))}{h}. \quad (4.3.1)$$

From equation (4.3.1), temperature gradient, thickness, and thermal expansion coefficient are important dependent parameters of angular deformation. In a laser forming process, an uneven temperature distribution through the thickness, as shown in Figures 4.2.1 and 4.2.3, is produced. Therefore, the workpiece bends away from the laser beam during a heating stage; bends toward the laser beam during a cooling stage. The mechanism is denoted as mechanism of bending toward the beam. However, the other mechanism (upsetting mechanism) occurs in the workpiece of thin thickness.

Chapter 4 Mechanism of Laser Forming

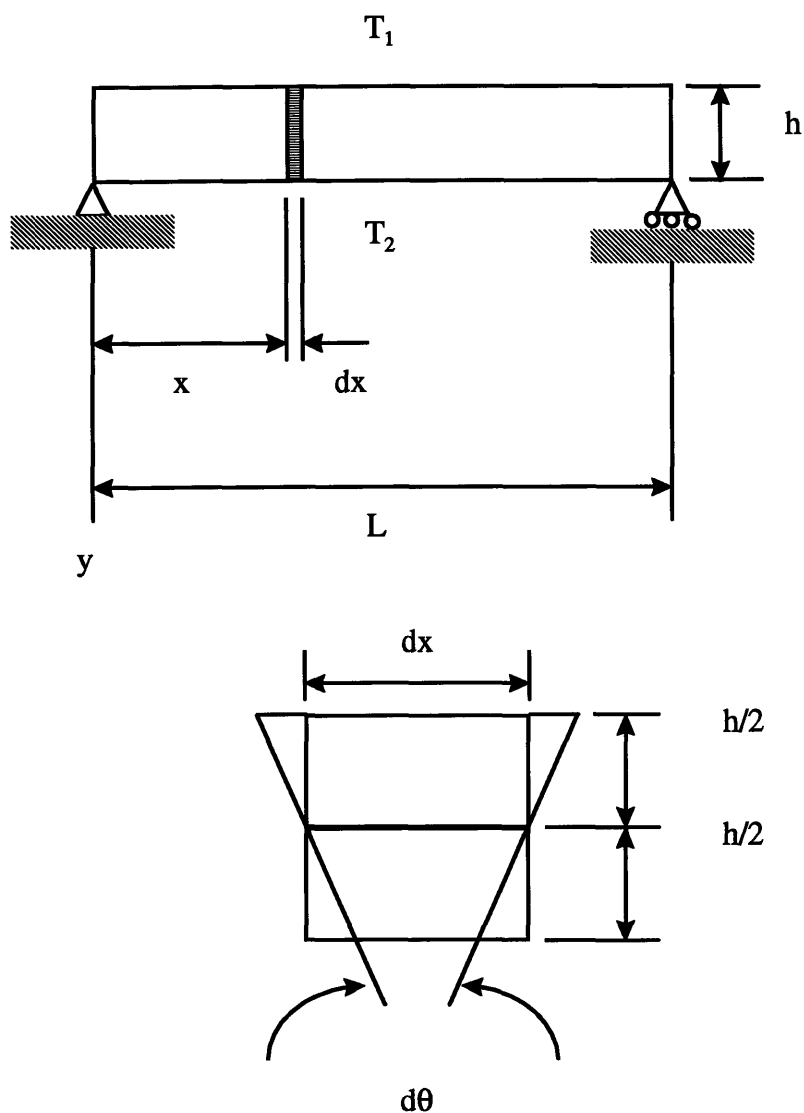


**Figure 4.3.1 A simple-supported beam with linear temperature difference through the thickness direction**

At the beginning of heating, the beam bends away from the laser beam due to a temperature gradient through the thickness direction. As heating time increases, heat diffuses from top to bottom of the workpiece. Temperature becomes uniform. In other

## Chapter 4 Mechanism of Laser Forming

words, temperature gradient (  $T_1(h) - T_2(h)$  ) is approaching through the thickness (h). The workpiece can not bend toward the beam.

### **4.3.2 Longitudinal Bending Mechanism**

Longitudinal bending mechanism is very similar to angular bending mechanism. The deflection equation can be expressed as

$$\frac{d\theta}{dx} = - \frac{\alpha(T)(T_2(v) - T_1(v))}{l} \quad (4.3.2)$$

where

$T_2(v)$  = temperature at bottom surface,

$T_1(v)$  = temperature at top surface,

$v$  = travel speed.

The travel speed of a laser beam is strongly related to the gradient of temperature in the heating direction. As the travel speed is increasing, the longitudinal bending angle is increasing.

### **4.3.3 Buckling Mechanism**

Thermal stresses may cause the structural instability of a workpiece during or after a laser forming process. The critical load of thermal stresses depends on power, spot size, travel speed, and the dimensions of the workpiece. The buckling mechanism is difficult to control.

## **Chapter 5 Analytical Solutions**

### **5.1 Background**

Mathematical theory of a laser forming process is presented in this Chapter. A simple theoretical solution of mathematical theory of the laser forming process is also discussed. In the preceding chapters, the laser forming process and mechanisms were introduced. The details of physical behaviors are further discussed to be associated with mathematical formulations in this Chapter. The mathematical theory of the laser forming process is involved with heat transfer and mechanical analyses. Two situations should be considered:

1. *Sequentially coupled heat transfer and mechanical analysis.*

A temperature distribution does not depend on stress and strain solutions. The temperature distribution is calculated from the heat transfer analyses. The temperature distribution from heat transfer analyses is used as a heat load in the mechanical analysis.

2. *Fully Coupled heat transfer and mechanical analysis.*

A temperature distribution from the heat transfer analyses depends on deformation and stresses in mechanical analyses; Deformation and stresses also depend on the temperature distribution.

In the laser forming process, dissipated plastic energy is much smaller than laser beam energy. Plastic deformation will not increase internal energy. In addition, deformation will not change the directions of heat conduction. Therefore, it is assumed

## Chapter 5 Analytical Solutions

that the temperature distribution is independent of stresses and strains. Sequentially coupled heat transfer and mechanical analyses are adopted for the mathematical theory of the laser forming process. Heat transfer and mechanical analyses are performing separately.

Analytical solutions of mathematical formulations of a laser forming process are not available due to the highly transient nonlinear governing equations and boundary conditions. The nonlinearity of the problem arises from the following factors:

- (1) *Material nonlinearity*: material properties are temperature-dependent including conductivity, expansion coefficient, Young's modulus, yield stress and so on. Thermal-elastic-plastic constitutive equations is highly nonlinear.
- (2) *Kinematic nonlinearity*: the relation between strains and displacement is nonlinear due to large deformation and strains produced during the laser forming process.
- (3) *Boundary nonlinearity*: radiation condition in heat transfer is nonlinear.

However, assumptions are made to simplify the nonlinear problems. Theoretical solutions of the temperature distributions in heat transfer analyses are obtained in simple cases. They were in good agreement with experimental results of welding processes at the regions far from the heating line. Therefore, the temperature distribution of theoretical solutions in simple cases can be used to verify the experiment in a laser forming process. In this Chapter, the simple theoretical solutions are introduced. However, a numerical method to solve the highly nonlinear equations is more feasible. The next chapter will use FEM to solve the problem.

## Chapter 5 Analytical Solutions

This chapter consists of two main parts:

1. Heat transfer theory applied to a laser forming process.
2. Mechanical theory applied to a laser forming process.

Each part starts with the investigations of physical phenomena of the laser forming process, which are followed by the mathematical formulations. The theoretical solutions of mathematical formulations are solved in simplified assumptions. Finally, FEM formulations of mathematical theories are presented.

## **5.2 Heat Transfer Analyses**

### **5.2.1 Physical Phenomena**

The physical aspects of heat transfer in a laser forming process are discussed as follow:

1. *Distribution of a heat source.* Heat is generated and distributes over a workpiece while a laser beam irradiates a workpiece. The power profile of the laser beam is assumed to be a Gaussian distribution as measured in the experiment in Chapter 3.
2. *Transient three-dimensional heat conduction.* The moving heat source with a constant speed produces the temperature distributions in a quasi-stationary state. Non-stationary states occur only at the start and the end of the laser



## Chapter 5 Analytical Solutions

forming process. The three-dimensional conduction occurs due to a moving heat source on the surface of the plates.

3. Convection and radiation boundary. High temperature difference between a workpiece and surrounding air results in natural convection and radiation heat transfer. If air is blown over the surface of the workpiece, forced convection occurs.
4. Gap heat transfer between a workpiece and a supporting post. The gap between a workpiece and a supporting post which holds the workpiece causes the interactions of heat transfer. Heat transfer between these two close surfaces is assumed to occur in the direction of surface normal. The heat flows from a workpiece to supporting stiffeners during a heating stage; the heat flows from a supporting post to the workpiece during a cooling stage. Gap conduction is geometrically nonlinear.
5. Nonlinear physical properties. Physical properties are strongly dependent on temperature including thermal conductivity and specific heat while the density is weakly dependent on temperature.
6. Phase Transformation and phase change. Materials may undergo phase transformation at elevated temperature during a laser forming process. The change of energy and material properties due to the phase transformation is neglected in the mathematical modeling. The surface of the workpiece is not melt during the laser forming process. The effect of phase-change and latent heat is not considered.

### 5.2.2 Theoretical Formulation

Mathematical analyses of heat transfer in welding, and laser forming processes have been widely studied [9,14,17,24,33,38,39,45]. Rosenthal and Cshmerbes [38], and Rykalin [39] have made mathematical analyses of heat flow due to a moving heat source in the quasi-stationary state. Masubuchi and Kusuda obtained solutions for three-dimensional non-stationary heat flow [24]. These models mentioned above made many assumptions.

The heat transfer of the laser forming process is nonlinear, transient, and three-dimensional. Finite difference methods can be used in heat transfer analyses, but FEM is used for the convenience of transferring data from heat transfer analyses to mechanical analyses. Zienkiewicz and Cheung introduced the application of FEM to the heat conduction problems.

The differential equation of three-dimensional heat conduction in a solid is

$$\rho c \frac{\partial \theta}{\partial t} = \dot{Q} + \frac{\partial}{\partial x} \left( \kappa_x \frac{\partial \theta}{\partial x} \right) + \frac{\partial}{\partial y} \left( \kappa_y \frac{\partial \theta}{\partial y} \right) + \frac{\partial}{\partial z} \left( \kappa_z \frac{\partial \theta}{\partial z} \right) \quad (5.2.2.1)$$

where

$\rho$  = density,

$c$  = specific heat,

$Q$  = heat generated per volume,

$\kappa_x, \kappa_y, \kappa_z$  = conductivity in the x, y, z directions,

$\theta$  = temperature.

## Chapter 5 Analytical Solutions

On the surface of the body, the following boundary conditions are satisfied:

$$\theta|_{S_\theta} = \theta^s \quad (5.2.2.2)$$

$$\theta|_{S_q} = q^s \quad (5.2.2.3)$$

$$S_\theta \cap S_q = \emptyset \text{ \& } S_\theta \cup S_q = S$$

(5.2.2.2) is called a force boundary condition; (5.2.2.3) is called a natural boundary condition. Force boundary conditions include convection and radiation boundary conditions. Convection boundary conditions are governed by

$$q^s = h(\theta, x, y, z)(\theta_e - \theta^s) \quad (5.2.2.4)$$

where

$q^s$  = heat flux,

$h$  = convection coefficient,

$\theta_e$  = environmental temperature,

$\theta^s$  = surface temperature.

Radiation boundary condition are governed by

$$q^s = \kappa(\theta_r - \theta^s) \quad (5.2.2.5)$$

$$\kappa = h_r(\theta_r^2 + \theta^{s2})(\theta_r + \theta^s) \quad (5.2.2.6)$$

$$h_r = \sigma f e \quad (5.2.2.7)$$

where

## Chapter 5 Analytical Solutions

$\sigma$  = Steffan Boltzmann coefficient,

$f$  = shape factor,

$e$  = emissivity,

$\theta_r$  = temperature of the external radiative source.

The values of  $\sigma$ ,  $f$  and  $e$  are  $5.67 \times 10^{-12} \text{ W/cm}^2 \text{ K}^4$ , 1.0, and 0.8 respectively.

### **5.2.3 Analytical Solutions**

#### **5.2.3.1 Rosenthal's Solution**

Rosenthal proposed the pioneer work of a temperature distribution due to a moving point heat source in 1941. Rosenthal obtained a mathematical solution for the temperature distribution under a moving point heat source. The solutions of three-dimensional plate with finite thickness are described as follow:

Assumptions are given:

- (a) Since the source is a point source, heat flux through the surface of the hemisphere drawn around the source must tend to the value of the total heat  $Q$ , delivered to the workpiece, as the radius of the semi-sphere tends to zero. Mathematically speaking, if  $R$  is the radius of the semi-sphere,

$$\lim_{R \rightarrow \infty} -2\pi R^2 \lambda \left( \frac{\partial \theta}{\partial R} \right) = Q_p$$

where

$$R = \sqrt{w^2 + y^2 + z^2}.$$

## Chapter 5 Analytical Solutions

- (b) Heat loss through the surface being negligible, there is no heat transmission from the workpiece to the surrounding atmosphere:

$$\frac{\partial \theta}{\partial z} = 0 \Big|_{z=0, t} \quad (t = \text{thickness})$$

- (c) The temperature of the workpiece remains unchanged at a very finite distance from the source, i.e.,

$$\theta = \theta_0 \Big|_{R \rightarrow \infty}$$

The solution is obtained as follows:

$$\theta - \theta_0 = \frac{Q\eta}{2\pi\lambda} e^{-\left(\frac{v}{2k}\right)w} \left[ \frac{e^{-\left(\frac{v}{2k}\right)R}}{R} + \sum_{n=1}^{\infty} \left( \frac{e^{-\left(\frac{v}{2k}\right)R_n}}{Rn} + \frac{e^{-\left(\frac{v}{2k}\right)R'_n}}{R'_n} \right) \right] \quad (5.2.3.1)$$

where

$$R_n = \sqrt{w^2 + y^2 + (2nT - z)^2},$$

$$R'_n = \sqrt{w^2 + y^2 + (2nT + z)^2},$$

$v$  = travel speed,

$\lambda$  = thermal conductivity,

$\kappa = \lambda/(c\rho)$  = thermal diffusivity,

$\rho$  = density,

$c$  = specific heat,

$\eta$  = efficiency,

$\theta_0$  = initial temperature,

## Chapter 5 Analytical Solutions

$Q$  = heat input.

It is assumed that material properties and process parameters are identical with those in the experiments in Chapter 3. Therefore,  $Q = 2600$  W;  $\eta = 0.8$ ;  $T = 0.25$  inch;  $v = 20$  cm/min;  $\lambda = 0.00047$  Btu/in-sec-F;  $\kappa = 0.014756$ ;  $\rho = 0.325$  lbm/in<sup>3</sup>;  $c = 0.098$  Btu/lbm-F. Figure 5.2.3.1 shows the temperatures of points at  $x = 0, 0.5, 1.0, 2.0,$  and  $3.0$  inches from the backside of heating line. Rosenthal's results are obtained from equation (5.2.3.1). The temperature approach infinity at  $x = 0$  (a singular point). However, the analytical results make good agreements with experimental data far from the laser heating line.

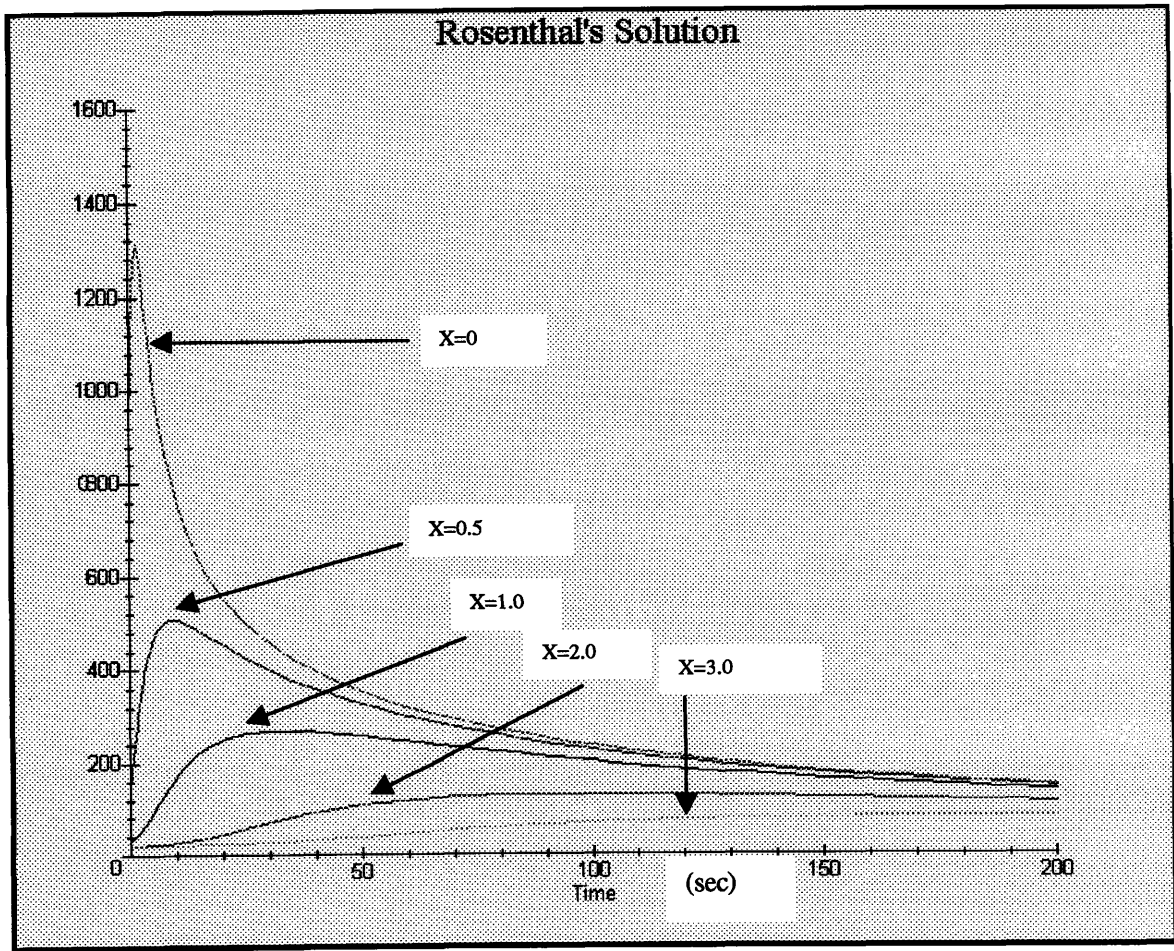


Figure 5.2.3.1 Rosenthal's solution

## Chapter 5 Analytical Solutions

### **5.2.3.2 Iwasake's Solution**

The disadvantages of Rosenthal's solution are inaccurate prediction of temperature near a heating line. It is justified that Rosenthal's solution is modified to fit the temperature distributions in the experiment. Iwasaki used experimental data to modify the point heat source equation and obtain a finite temperature value at the point source location [17]. Iwasaki's equation is defined as

$$T - T_0 = \frac{q}{2\pi ak} \sum_{n=-\infty}^{n=\infty} \frac{e^{-L(f(x) + ((2nz - f(z))^2 + f(y)^2 + f(x))^{1/2})}}{((2nz - f(z))^2 + f(y)^2 + f(x))^{1/2}} \quad (5.2.3.2)$$

where

$$f(x) = x / a ,$$

$$f(y) = (\delta a / \Delta w)(y / a) ,$$

$$f(z) = (1 - \delta) + \delta(z - vt) / a ,$$

$$\delta = a / (a + \Delta a) ,$$

$$L = av / (2\alpha) ,$$

$\alpha$  = thermal diffusivity,

$\kappa$  = thermal conductivity,

$a$  = thickness,

$q$  = heat input.

$\Delta a$  and  $\Delta w$  are assumed as 0.025 and 0.38 respectively. Thickness  $a$  is 0.25. Figure 5.2.3.2 shows Iwasaki's temperature distribution in the same processes parameters of experiment.



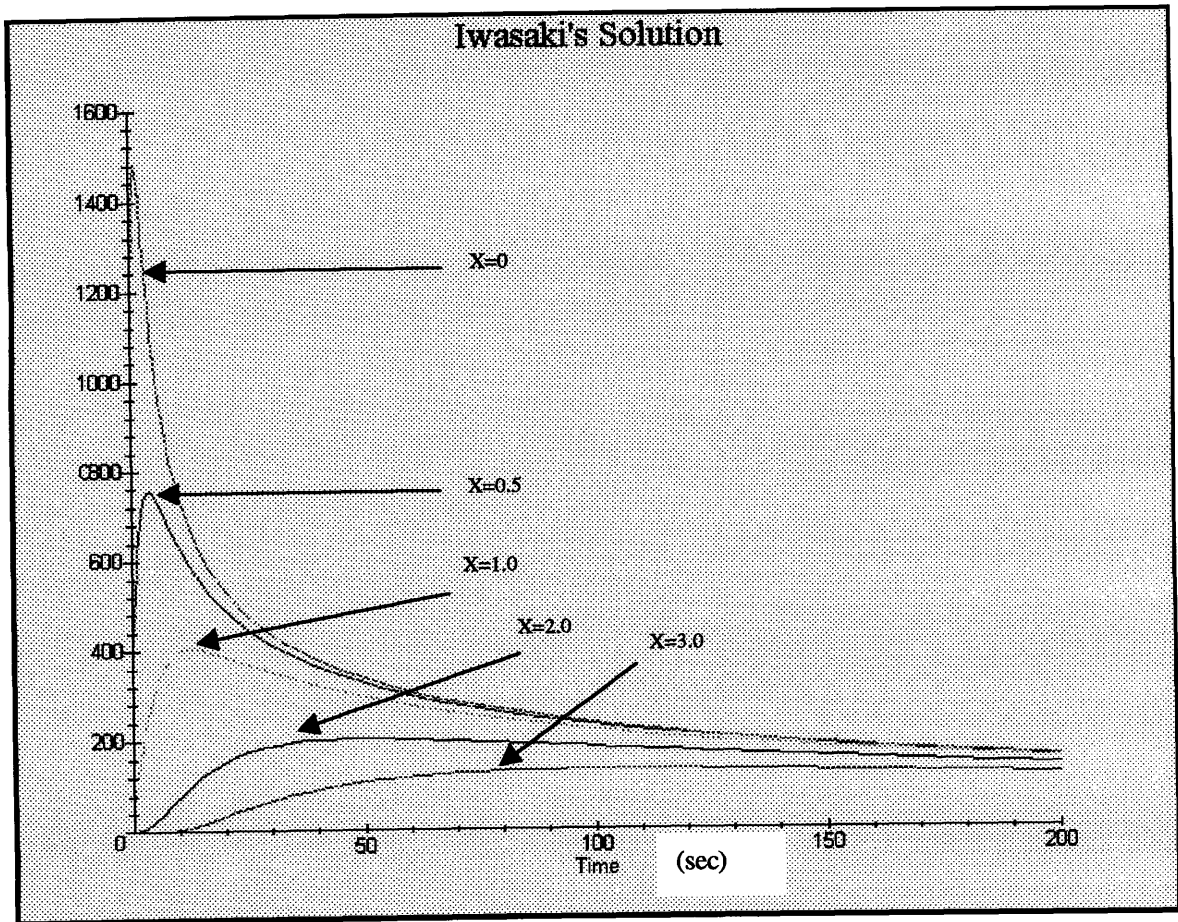


Figure 5.2.3.2 Iwasaki's solution

## **5.3 Mechanical Analyses**

### **5.3.1 Physical Phenomena**

The physical aspects of mechanical system are discussed as follows:

1. *Nonlinear Mechanical Material Properties*: The mechanical material properties are strongly dependent on temperature. Thermal expansion coefficient is slightly increasing as temperature is increasing. Young's modulus,  $E$ , yield stress,  $\sigma_y$ , Poisson's ratio,  $\nu$ , and strain hardening modulus are also functions of temperature.
2. *Boundary Conditions* : In a laser forming process, it is assumed that there are no external loads on a workpiece. One corner of the workpiece is clamped on the supporting post.
3. *Thermal elasticity and Thermal Plasticity*: The thermal-elastic-plastic state is produced during a laser forming process. Time-dependent plastic effects may be important in some rate-dependent materials. A plastic zone is created near the heating line.

### **5.3.2 Theoretical Formulation**

Transient thermal stresses have been studied since 1930s. However, it was not until 1968 that one-dimension thermal stress analysis was significantly improved by Masubuchi et al. In 1970s, Muraki developed a two-dimensional finite element code to calculate the thermal stress and distortion during butt-welding and bead on plate [34,35].

## Chapter 5 Analytical Solutions

There are two types of two-dimensional thermal stresses analyses for the laser forming process: plane stress and plane strain analysis. Up to date, few papers are devoted to the three-dimension thermal stress analysis. Since the advance of computer technology, the computation power has been increasing and more inexpensive than ever. An attempt to develop the analysis of the three-dimensional finite element model will be made.

The one-dimensional model is presented in this section. The one-dimensional equilibrium equation is expressed in differential form as follow:

$$\frac{\partial \sigma_x}{\partial x} = 0 \quad (6.3.2.1)$$

From equation (6.3.2.1), we can assume that  $\sigma_x = \sigma_x(y)$ . Without external forces, thermal stresses and thermal stress moment must be balanced. The equation (6.3.2.1) can be expressed in integral form:

$$\int_{-c}^c {}^{t+\Delta t} \sigma_x dy = 0 \quad (6.3.2.2)$$

$$\int_{-c}^c {}^{t+\Delta t} \sigma_x y dy = 0 \quad (6.3.2.3)$$

The superscript  $t+\Delta t$  of  $\sigma$  means the time of interest.

The constitutive equation is expressed:

$$d^t \sigma_x = E(d^t \varepsilon_x - \alpha \Delta^t \theta - d^t \varepsilon_x^p) \quad (6.3.2.4)$$

where

## Chapter 5 Analytical Solutions

$E$  = Young's Modulus,

$\alpha$  = thermal expansion coefficient,

$\Delta\theta$  = temperature difference,

$\epsilon_x^p$  = plastic strain.

Plastic strain can be obtained from (6.3.2.5).

$$d^t \epsilon_x^p = \frac{d^t \sigma_x}{E_t} \quad (6.3.2.5)$$

where

$E_t$  = tangent modulus.

The total stress  $\sigma^{t+\Delta t}$  at time  $t+\Delta t$  can be decomposed into  $\sigma^t$  and  $d\sigma^t$ .

Substituting (6.3.2.4) and (6.3.2.5) into (6.3.2.3) and (6.3.2.2) enables to solve the problem.

## **Chapter 6 Finite Element Method**

### **6.1 Background**

A thermal-elastic-plastic analysis of laser forming is similar to the analyses of flame forming, or welding [3,16,18,32,46]. The similar technique can be used in the analysis of laser forming. A major goal of the thermal-elastic-plastic analysis is to relate power, travel speed, spot size and plate thickness to deformation.

### **6.2 Procedures of Finite Element Method**

FEM is widely used in engineering analyses. Successful FEM analyses depends on

- (1) the proper formulation of physical problems into FEM models,
- (2) the convergent solutions of FEM models,
- (3) the appropriate interpretation of FEM results.

In other words, the proper procedures of FEM analyses are the key of success. Figure 6.2.1 shows the procedures of FEM for simulating a laser forming process including important parameters. Sequential coupled heat transfer and mechanical analyses are used as stated in Chapter 5. Therefore, the procedures can be separated into two parts: heat transfer and mechanical analysis. First, process parameters and material properties are formulated in mathematical expression. A temperature distribution is obtained by heat transfer analysis. If the results are not satisfied, the procedure goes back to modify the FEM. model. For example, the contour of the temperature distribution is not smooth cross the boundaries of the elements.

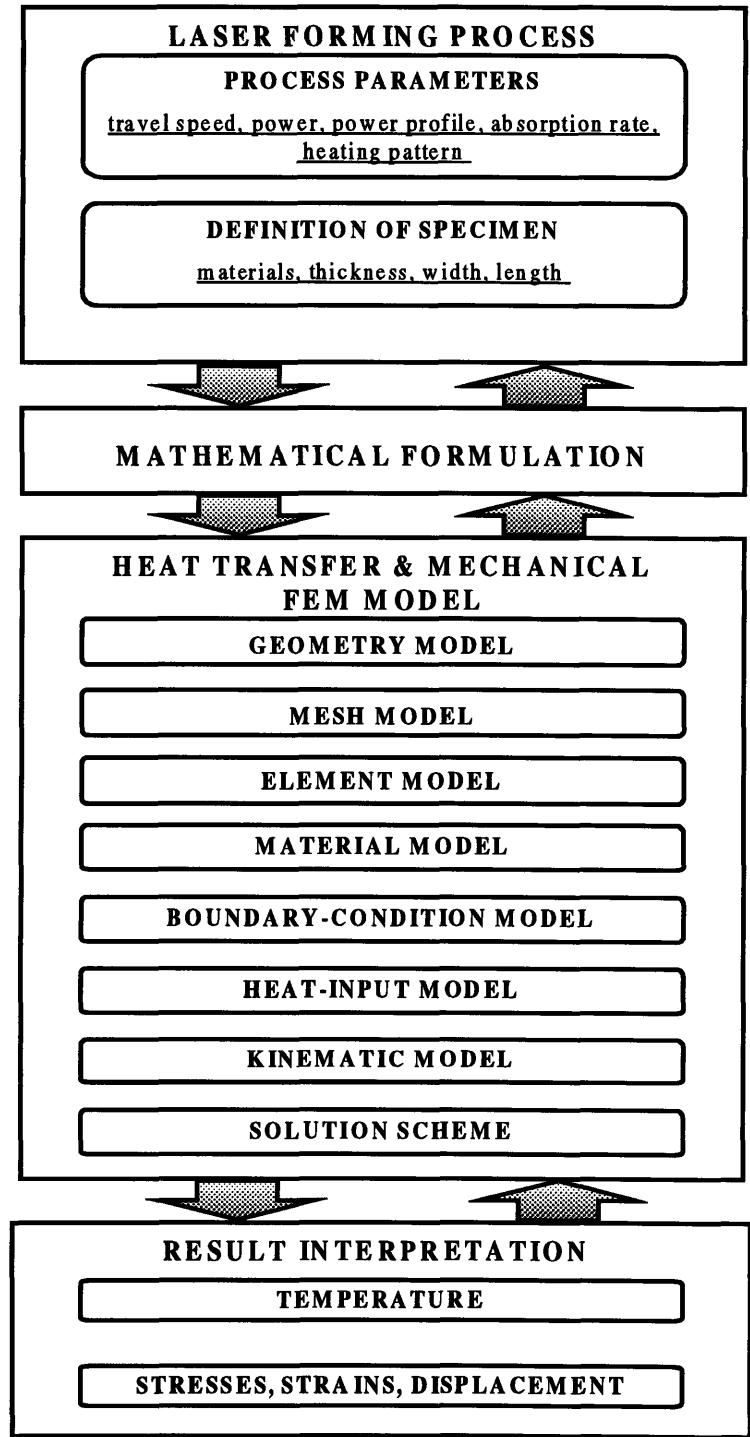


Figure 6.2.1 Procedures of finite element analyses

## Chapter 6 Finite Element Method

If the mathematical model can not accurately predict the temperature, modify the model. Second, the temperature distribution is used as heat loads in thermal-elastic-plastic analysis.

### **6.3 Formulation of Finite Element Method**

#### **6.3.1 Incremental Equations of Heat Transfer**

The interested domain is discretized into small fine elements. The temperature field variable within the element can be interpolated by

$$\theta = N^n \theta^n \quad (6.3.1.1)$$

where

$N^n$  = interpolation function,

$\theta^n$  = element nodal temperature.

Introducing this interpolation relation into the weak form of heat equilibrium equation, we obtain a set of equation [6]

$$\int_V N^n \rho \dot{U} dV + \int_V \frac{\partial N^n}{\partial x} \cdot k \cdot \frac{\partial N^m}{\partial x} dV \bar{\theta}^m = \int_V N^n r dV + \int_S N^n q dS \quad (6.3.1.2)$$

where

$U$  = internal energy per unit mass,

$r$  = heat flux per unit volume,

$k$  = thermal conductivity,

## Chapter 6 Finite Element Method

$\rho$  = density

$q$  = heat flux per unit of current area crossing surface  $S$ .

We can rewrite the set of equations in matrix form:

$$[C]\{\dot{\theta}\} + [K]\{\theta\} = \{Q\} \quad (6.3.1.3)$$

where

$$[C] = \int \rho c N^n N^m dV,$$

$$[K] = \int \left( \frac{\partial}{\partial x} N^n \right) k \left( \frac{\partial}{\partial x} N^m \right) dV,$$

$$\{Q\} = \int N^n r dV + \int N^n q dS.$$

### 6.3.2 Incremental Equation of Mechanical Analyses

The constitutive equations are given as follow [7,8]:

$${}^{t+\Delta t} \sigma = {}^{t+\Delta t} C^E ({}^{t+\Delta t} e - {}^{t+\Delta t} e^p - {}^{t+\Delta t} e^{th}) \quad (6.3.2.1)$$

The equilibrium equation is

$${}^{t+\Delta t} K^E {}^{t+\Delta t} U = {}^{t+\Delta t} R - \int_v B_L^T {}^{t+\Delta t} C^E ({}^{t+\Delta t} e^p + {}^{t+\Delta t} e^{th}) \quad (6.3.2.2)$$

$${}^{t+\Delta t} K^E = \int_v B_L^T {}^{t+\Delta t} C^E B_L dv \quad (6.3.2.3)$$



## Chapter 6 Finite Element Method

where

$K^E$  = elastic stiffness matrix,

$U$  = nodal point displacement vector,

$C^E$  = stress-strain matrix,

$B_L$  = strain-displacement matrix,

$R$  = nodal external force vector.

The FEM formulation in ABAQUS can not be found in ABAQUS theory manuals and ABAQUS lecture notes.

## **6.4 Finite Element Model for Heat Transfer Analysis**

### **6.4.1 Geometry Model**

The workpiece is 12 inch by 12 inch. The behaviors of the plate can be predicted by the analyzing a portion of the workpiece, so that the huge computation time can be reduced. The simplified geometry model is based on the assumption:

Laser beam is heating on the centerline of the specimen plate. In this situation, half of the workpiece is simulated due to the symmetric thermal and displacement field about the centerline.

## Chapter 6 Finite Element Method

### **6.4.2 Mesh Model**

The mesh has been graded such that it is finest in the region of highest and most rapid temperature gradient near the heat input. For this, ABAQUS offers a non-uniform mesh seed spacing.

### **6.4.3 Element Model**

DC3D20 elements were used in heat transfer analysis in ABAQUS. Each DC3D20 element was a three-dimensional diffusion element with twenty nodes. The element type in thermal stress analysis must be compatible with that in heat transfer analysis. For example, a three-dimensional solid element with twenty nodes is compatible with a three-dimensional solid element with twenty nodes. Eight-node elements are more efficient in heat transfer analysis but could not be used in thermal stress analysis due to the high nonlinearity of equations. ABAQUS version 5.5 does not support interpolating the nodal temperature of an eight-node element into that of a twenty-node element. In order to maintain the consistency of the element types, twenty-node element was used in heat transfer analysis. For this reason, more computation was needed in heat transfer analysis. ABAQUS version 5.6 may support the automatic interpolation of nodal temperature.

### **6.4.4 Heat Input Model**

A laser beam produces heat in the workpiece. The heat input is modeled as a moving heat source over the surface of the workpiece. The distribution of heat input is a Gaussian distribution. Rykalin have treated the distribution of a moving heat source as a Gaussian distribution [9]. According to Rykalin's model,

## Chapter 6 Finite Element Method

$$q = q_{\max} e^{(-kr^2)} \quad (6.4.4.1)$$

where

$q_{\max}$  = maximum heat flux at the center of the heat spot,

$k$  = heat flux concentration coefficient,

$r$  = radial distance from the center of the heat spot.

The total heat  $Q$  is equal to the total heat flux under the surface. In other words,

$$Q = 2\pi q_{\max} \int_0^{\infty} r e^{(-kr^2)} dr \quad (6.4.4.2)$$

Evaluating the integral.

$$q_{\max} = \frac{Qk}{\pi} \quad (6.4.4.3)$$

From equation (6.4.4.1), we assume that 5% of the heat flux intensity is at the radius of the spot size. In other words,

$$q(r_h) = q_{\max} e^{-kr_h^2} = 0.05q_{\max} \quad (6.4.4.4)$$

where

$r_h = d_h/2$  = radius of spot size,

$$r_h = \sqrt{(x - vt)^2 + y^2} \quad (6.4.4.5)$$

$v$  = travel speed = 0.1323 in/sec.

Therefore, the relationship between concentration coefficient and spot size is obtained.

## Chapter 6 Finite Element Method

$$d_h = \frac{3.46}{\sqrt{k}} \quad (6.4.4.6)$$

**Table 6.4.4.1 The relation between spot size and concentration coefficient**

$d_h(\text{mm})$	$d_h(\text{inch})$	$k(\text{inch}^{-2})$
10	0.3937	77.2360
15	0.5906	34.3271
20	0.7874	19.3090
25	0.9843	12.3578
30	1.1811	8.5818
35	1.3780	6.3050
40	1.5748	4.8272
45	1.7717	3.8141

As  $Q$  is 2080 W or 1.97 Btu/sec,  $q_{\max}$  is 12.1081 Btu/inch<sup>2</sup>. The heat flux distribution of a laser beam is shown in Figure 6.4.4.1. The heat flux distribution is approximated by the nodal heat fluxes of  $6 \times 6$  and  $12 \times 12$  meshes as shown in Figures 6.4.4.2. and 6.4.4.3. Mesh size should be sufficiently fine to approximate the heat flux distribution; otherwise, the error of temperature distributed is huge due to inaccurate heat input.

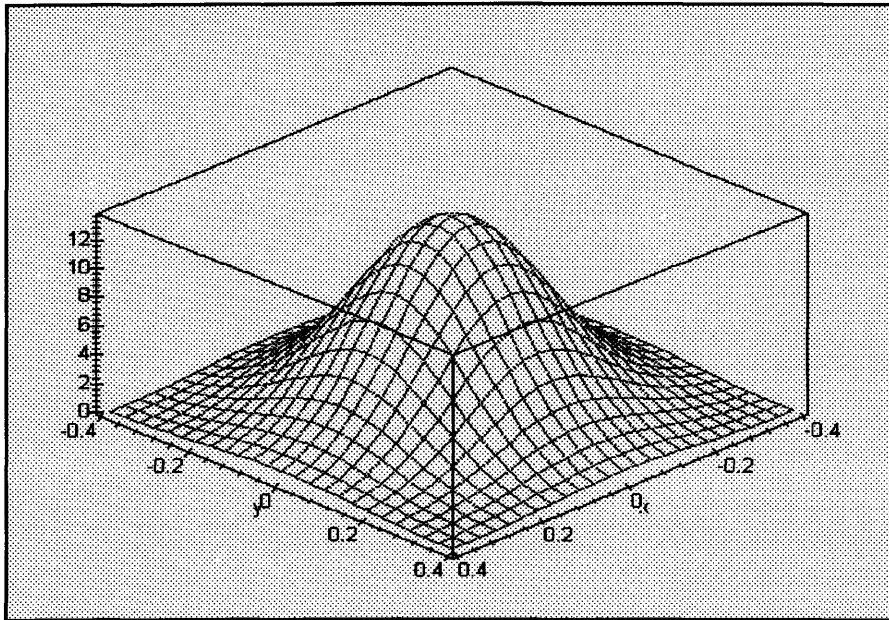


Figure 6.4.4.1 The Gaussian distribution of the heat flux of a laser beam

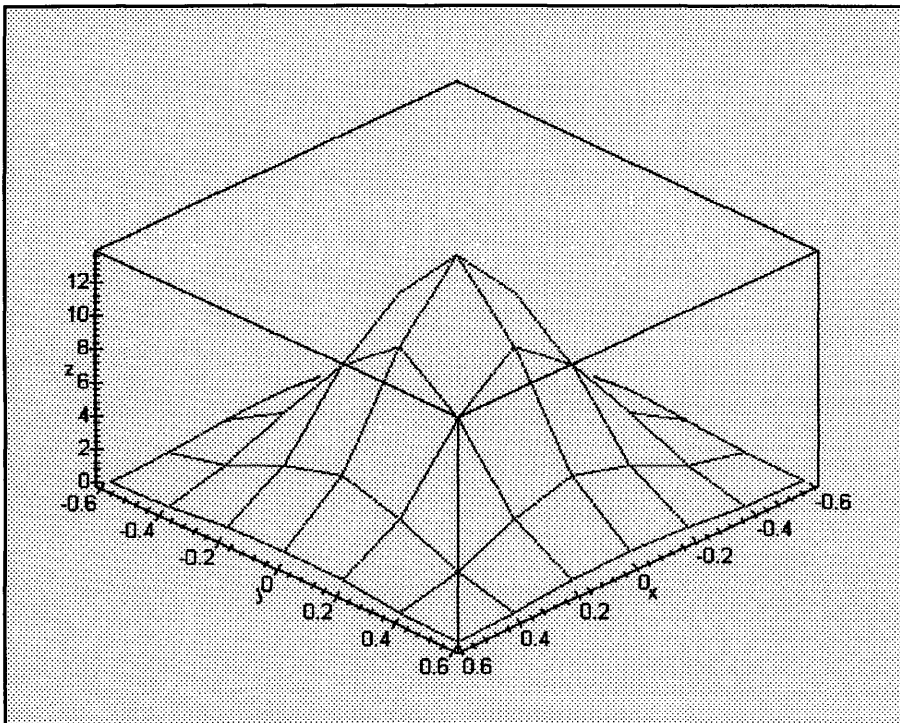
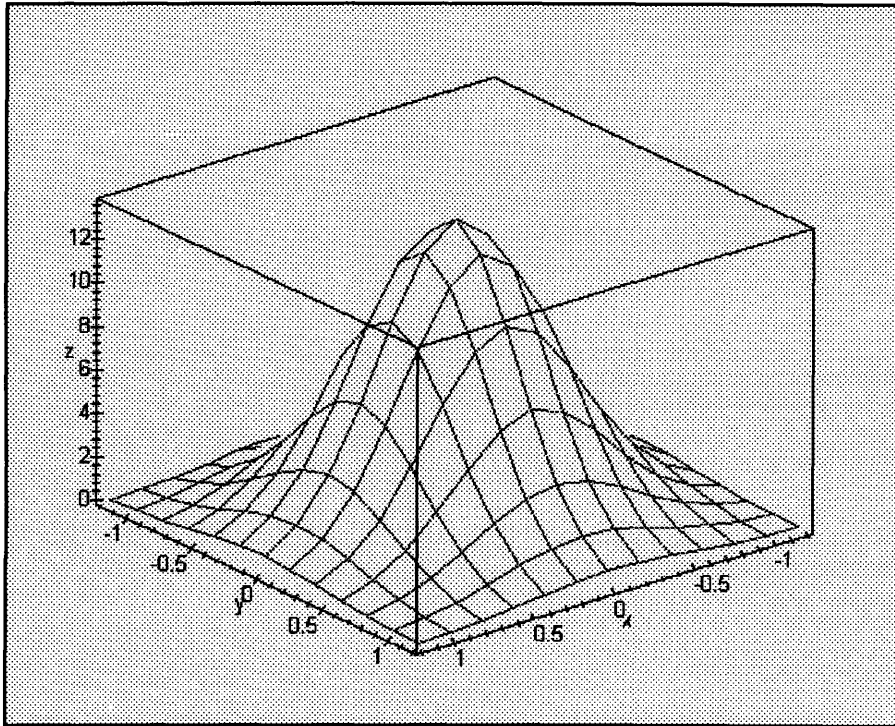


Figure 6.4.4.2 Heat flux distribution in 6x6 mesh size

## Chapter 6 Finite Element Method



**Figure 6.4.4.3 Heat flux distribution in 12×12 mesh size**

In ABAQUS, a user subroutine DFLUX is used to define the heat input function (6.4.4.1). It is easily to change the power, travel speed, and spot size in the user subroutine.

### **6.4.5. Material Model**

The temperature dependent material properties are important for the accurate calculation of a temperature distribution. Unfortunately, most material properties at elevated temperature are unknown due to the difficulty in measuring the properties at these temperatures. Table 6.4.5.1 list the density and specific heat of various materials at

## Chapter 6 Finite Element Method

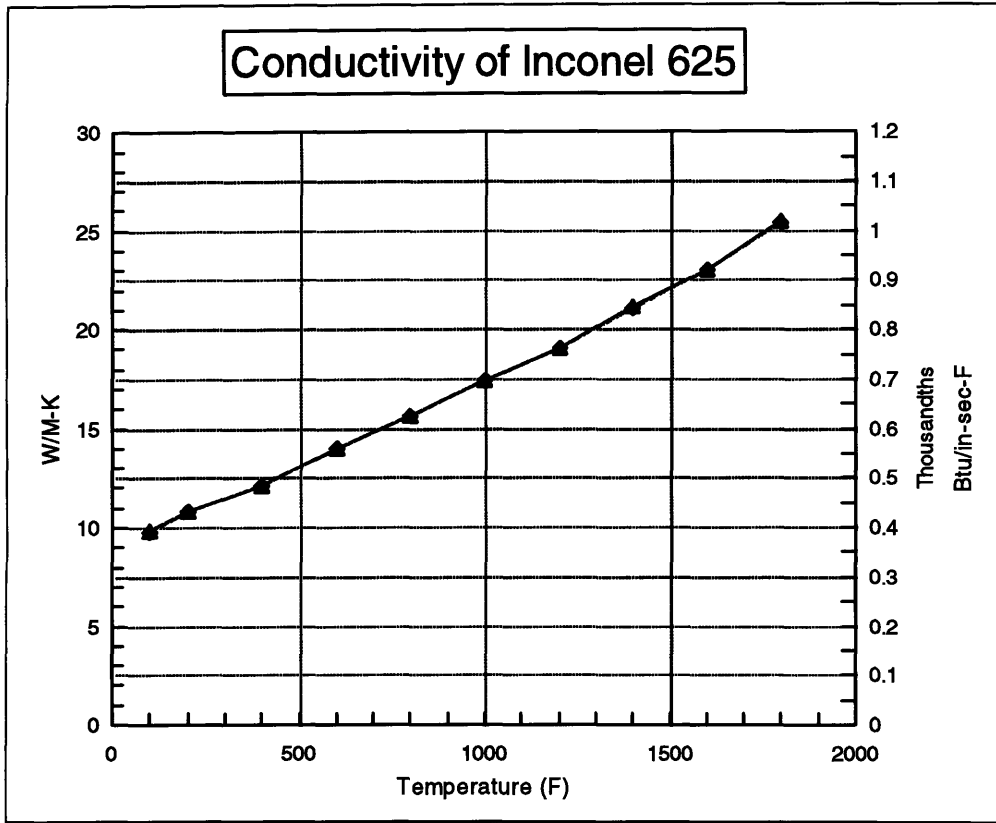
room temperature (70 °F). Table 6.4.5.2 lists the conductivity of Inconel 625. Its specific heat is 0.098 Btu/lbm-F.

**Table 6.4.5.1 Density and specific heat of Inconel 625 and Inconel 718**

Material	Density(lbm/in <sup>3</sup> )	Specific heat (Btu/lbm-F)
Inconel 625	0.305	0.098
Inconel 718	0.297	0.104

**Table 6.4.5.2 Conductivity of Inconel 625**

Temperature (F)	Conductivity(W/M-K)	(Btu/in-sec-F)
100	9.8	0.000392522
200	10.8	0.000432575
400	12.1	0.000484644
600	14.0	0.000560745
800	15.6	0.000624831
1000	17.4	0.000696926
1200	19.0	0.000761012
1400	21.1	0.000845123
1600	23.0	0.000921225
1800	25.4	0.001017352



### 6.4.6 Boundary Conditions Model

A workpiece is surrounded by air at room temperature. The top surfaces of the top elements of the model and the bottom surfaces of the bottom elements of the model are subject to convection heat transfer. The initial temperature of the workpiece and the surrounding air is 70 °F. The convection coefficient is temperature-dependent. Table 6.4.6 lists the relations between temperature and convection coefficient for mild steels in atmosphere.

There is no heat flux across the symmetric line. Gap conduction between plate and supporting posts is disregarded.



**Table 6.4.6 Convection coefficient with respect to temperature**

Temperature	Btu/(hr-ft-ft-F)	Btu/(sec-in-in-F)
70	450	8.6806E-04
100	700	1.3503E-03
1100	1300	2.5077E-03
2100	1500	2.8935E-03
3100	1600	3.0864E-03

### 6.4.7 Solution Scheme

For transient analysis, the initial minimum time increment in ABAQUS should be considered to obtain the satisfactory results. The initial minimum time increment is

$$\frac{1}{6} \frac{\rho c \Delta l^2}{k} < \Delta t_{min} \quad (6.4.7)$$

where

$\Delta t_{min}$  = minimum useful time increment,

$\rho$  = density,

$c$  = specific heat,

$k$  = conductivity,

$\Delta l$  = the smallest element dimension near surface with high temperature gradients.

## **6.5 FEM Model for Mechanical Analyses**

Mathematical formulation of laser forming process is a boundary-value problem. It involves high nonlinearity in material and geometry. The modeling method is discussed in the following subsections.

### **6.5.1 Mesh Model**

The same mesh model is used in heat transfer and mechanical analyses. The natural errors in F.E.M. arise from discretization. To investigate the discretization error, a sequence of meshes is used. In the sequence of meshes, the same kind of elements were used and the element size were uniformly decreased. This approach is referred to as the h-method of analysis. If the high order of displacement interpolate function is used, this approach is referred to as the p-method.

### **6.5.2 Element Model**

#### **Element Type**

Solid structures are approximated by many small elements. Those small elements must be reasonable to present the behaviors of the solid structures. Therefore, beams, plate, shell, plane-stress, plane-strain, and three-dimensional elements with various numbers of nodes are developed to simulate the behaviors of the various structures. Each type of element has its assumptions and applications. In the application of laser forming, bending deformation is important. Therefore, general plane-stress element should be used in two-dimensional analysis. Plate elements may not approximate well for the regions of the plate near the heating line due to

## Chapter 6 Finite Element Method

too many assumptions in this type of element. However, plate elements may be appropriately used in the elastic regions. This can reduce computation time by using plate elements instead of three-dimensional solid elements.

In the laser forming process, Poisson ratios at elevated temperature for particular materials may approach 0.5. Displacement-based elements need an unusually fine mesh to obtain accurate results. Stresses based on the displacement-based elements are inaccurate. In this case, hybrid elements should be used to improve the convergence rate.

### **Integration Order**

Material and geometric nonlinearity demands high integration order to obtain accurate results. Therefore, twenty-node three-dimensional solid elements are used. The displacement interpolation function is quadratic in that element. Reduced-integration order element may be considered in this case to reduce computation time. If reduced-integration order elements are used, the results should be checked by different mesh schemes to avoid the ghost mode of strain energy. In three-dimension hybrid solid elements, pressure is independent of the interpolation function. In ABAQUS, three-dimensional 20-node solid elements were used to simulate the laser forming process in this thesis.

### 6.5.3 Material Model

#### 6.5.3.1 Decomposition of Total Strain

The constitute equations of thermal-elastic-plastic analysis is based on the incremental form. The increment of total strain during a laser forming process can be decomposed into

$$d\epsilon_{ij} = d\epsilon_{ij}^e + d\epsilon_{ij}^p + d\epsilon_{ij}^c + d\epsilon_{ij}^{th} \quad (6.5.3.1)$$

where

- $d\epsilon_{ij}$  = increment of component of the total strain tensor,
- $d\epsilon_{ij}^e$  = increment of component of elastic strain tensor,
- $d\epsilon_{ij}^p$  = increment of component of plastic strain tensor,
- $d\epsilon_{ij}^c$  = increment of component of creep strain tensor
- $d\epsilon_{ij}^{th}$  = increment of component of thermal strain tensor.

Each strain increment contributes to the total strain increment as discussed in the following sections.

#### 6.5.3.2 Creep Model

Metal at elevated temperature is sensitive to creep. In a laser forming process, the plate is heated from room temperature and cooled to room temperature in what is called a thermal cycles. The thermal cycle of a plate is between 15 and 20 minutes. The plate is only loaded in a short time. Therefore, the effect of creep is neglected in this study and  $d\epsilon_{ij}^c$  is zero. Equation (6.5.3.1) can be simplified to

## Chapter 6 Finite Element Method

$$d\epsilon_{ij} = d\epsilon_{ij}^e + d\epsilon_{ij}^p + d\epsilon_{ij}^{th} \quad (6.5.3.2)$$

Creep may be important for some materials due to high thermal stresses and temperature. The creep effect should be further studied.

### **6.5.3.3 Metal Elasticity Model**

In isotropic linear elasticity,  $d\sigma$  can be expressed in the following form:

$$d\sigma = Kd\epsilon_{kk}\delta_{ij} + 2Gde_{ij} \quad (6.5.3.3)$$

where

$$K = \frac{E}{3(1-2\nu)},$$

$$G = \frac{E}{2(1+\nu)}.$$

K and G depend on temperature but do not depend on deformation. The elastic strains are assumed to be small in the elastic-plastic finite element model in ABAQUS. The elastic properties of annealed Inconel 625 are shown in Table 6.5.3.3. The data is obtained from a chart provided by Boeing.

**Table 6.5.3 Elastic properties of anneal Inconel 625**

Temperature ( F )	Poisson Ratio	Young's Modulus (MSI)
0	0.304	29.9
200	0.305	29.2
400	0.308	28.4
600	0.308	27.5
800	0.310	26.5
1000	0.320	25.5
1200	0.325	24.4
1400	0.335	23.3

#### **6.5.3.4 Metal Plasticity Model**

The feasibility of laser forming in several materials is studied. They include HSLA80, HY80, Titanium, Aluminum, Inconel 625, and Inconel 718. The mechanical behaviors of these materials are distinct. The mathematical model of the plastic deformation must be based on the experimental results from a simple tension test. From the simple tension test, a metal plasticity model can be determined. In a metal plasticity model, three aspects should be considered [10].

- (1) *Yield criterion*: The existence of an initial yield surface, which defines the elastic limit of the material in a multi-axial state of stress.
- (2) *Hardening rule*: The hardening rule that describes the evolution of subsequent yield surfaces.
- (3) *Flow Rule*: The flow rule that is related to a plastic potential function defines the direction of incremental plastic strain vector in a strain space.

## Chapter 6 Finite Element Method

For example, mild steel exhibits plastic flow under constant stress. The behavior can be modeled as a perfect plasticity model. For aluminum, work-hardening behavior can be modelled with the work-hardening theory of plasticity.

In addition to these three basic aspects, the features of the loading and the large deformation in a laser forming process should be taken into consideration for a metal plasticity model. The details of the material plastic model used in FEM by ABAQUS are described below.

### ***Yield Criteria***

The plate is loaded in a combined stress state into plastic deformation during a laser heating process. The yield surface, or the yield condition, can be expressed as

$$\begin{aligned} f(\sigma_1, \sigma_2, \sigma_3, T, \kappa_1, \kappa_2, \dots) &= 0 \text{ or} \\ f(I_1, J_2, J_3, T, \kappa_1, \kappa_2, \dots) &= 0 \text{ or} \\ f(\sigma_{ij}, \epsilon_{ij}^p, \kappa(\epsilon_{ij}^p), T) &= 0 \end{aligned} \quad (6.5.3.4.1)$$

where

$\sigma_1, \sigma_2, \sigma_3$  = principal stresses,

T = temperature,

$\kappa_i$  = internal variables,

$I_1$  = first stress invariant,

$J_2, J_3$  = deviatoric stress invariant.

## Chapter 6 Finite Element Method

The yield surface is a function of stresses, temperature, and internal variables. The important fact for metals is that the effect of hydrostatic pressure on the yielding is neglected. Therefore, the yield function can be rewritten as

$$f(J_2, J_3, T, \kappa_1, \kappa_2, \dots) = 0 \quad (6.5.3.4.2)$$

This pressure-independent yield criterion is used to model the metal behavior in a laser forming process. In the elastic range, the entire internal variable evolution rate will vanish if strain aging is neglected [11].

The yield criterion of the plate during a laser forming process is assumed to follow the von Mises criterion which is a pressure independent yield criterion. In isothermal state, the von Mises yield criterion takes the form:

$$\frac{1}{6} [(\sigma_1 - \sigma_2)^2 + (\sigma_2 - \sigma_3)^2 + (\sigma_3 - \sigma_1)^2] = \kappa^2 \text{ or}$$
$$f(J_2) = J_2 - \kappa^2 \quad (6.5.3.4.3)$$

where  $\sigma_1$ ,  $\sigma_2$ , and  $\sigma_3$  are principal stresses.

$\kappa$  can be determined from the following expression in a uniaxial tension experiment.

$$\frac{1}{3} \sigma_y^2 = \kappa^2 \quad (6.5.3.4.4)$$

where  $\sigma_y$  is the yield stress in the uniaxial tension experiment.

In ABAQUS, von Mises yield criterion is used in plastic analysis.



## Chapter 6 Finite Element Method

### ***Hardening Rule***

There are several hardening rules to define the subsequent yielding surfaces: isotropic, kinematic, and mixed hardening rules. In isotropic hardening von Mises model,  $f$  can be expressed as

$$f(\sigma_{ij}, k) = \frac{3}{2} s_{ij} s_{ij} - \sigma_e^2(\epsilon_p) = 0 \quad (6.5.3.4.5)$$

For kinematic hardening, the general form of the yielding surface is expressed as

$$f(\sigma_{ij}, k) = F(\sigma_{ij} - \alpha_{ij}) - K^2 = 0 \quad (6.5.4.4.6)$$

Bauschinger effect is considered in the laser forming process. Therefore, the kinematic hardening is adopted to include Bauschinger effect in the finite element analysis by ABAQUS.

In ABAQUS, linear work hardening model is used as shown in Figure 6.5.3.4 [12]. Table 6.5.3.4 lists the plastic properties of DH36. The inadequate work hardening data of Inconel 625 may result in the inaccurate prediction.

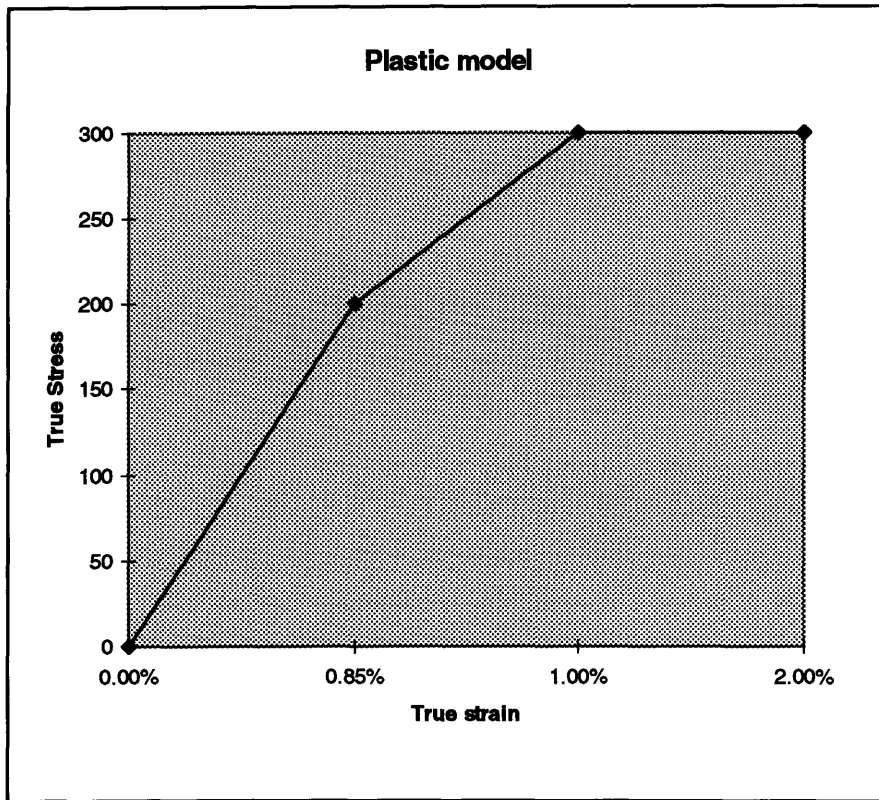


Figure 6.5.3.4 Linear strain hardening model in ABAQUS

Chapter 6 Finite Element Method

**Table 6.5.3.4 Plastic properties of DH36 steel**

Temperature (C)	Stress (Ksi)	Plastic Strain
20	444.67	0.00
20	522.67	0.01
100	443.80	0.00
100	521.80	0.01
200	426.12	0.00
200	504.12	0.01
300	390.01	0.00
300	465.51	0.01
400	335.45	0.00
400	390.45	0.01
500	262.45	0.00
500	307.45	0.01
600	171.01	0.00
600	206.01	0.01
700	67.50	0.00
700	95.00	0.01
800	43.50	0.00
800	63.50	0.01
900	25.50	0.00
900	40.50	0.01

***Flow Rule***

The plastic flow equation can be expressed as

$$d\epsilon_{ij}^p = d\lambda \frac{\partial g}{\partial \sigma_{ij}} \quad (6.5.3.4.6)$$

where

$d\lambda$  = a positive scalar function,

Chapter 6 Finite Element Method

$g =$  plastic potential function.

The plastic potential function can be associated with von Mises yield criterion. In other words, we take von Mises yield function  $f(\sigma_{ij}) = J_2 - k^2=0$  as the plastic potential function (i.e.,  $f = g$  ). Therefore,

$$d\epsilon_{ij}^p = d\lambda \frac{\partial(f)}{\partial\sigma_{ij}} = d\lambda s_{ij} \quad (6.5.4.7)$$

In this associated flow plastic model, the direction of flow is the same as the outward normal direction of the yield surface. Table 6.3.5 lists the plastic properties of Inconel 625 and Inconel 718. The mark “\*” denotes that the data is unavailable.

**Table 6.5.3.5. Plastic properties of Inconel 625 and Inconel 718**

	Temperature	Inconel 625	Inconel 718
Ultimate tensile strength	70 F (21 C)	103 ksi (710 MPa)	158 ksi (1090 Mpa)
	1000F (538 C)	74 ksi (510 Mpa)	*
0.2% yield strength	70 F (21 C)	51 ksi (350 Mpa)	133 ksi (915 Mpa)
	1000F (538 C)	34 ksi (235 Mpa)	*
Tensile elongation	70 F (21 C)	45%	11%
	1000F (538 C)	50%	*

## Chapter 6 Finite Element Method

### **6.5.3.5 Metal Thermal Expansion Model**

A change of temperature in a solid tends to produce thermal strain. The thermal strain  $d\epsilon_{ij}^{th}$  is given by the expression

$$d\epsilon_{ij}^{th} = \alpha dT \quad (6.5.3.5)$$

where

$\alpha$  = thermal expansion coefficient,

$dT$  = the change of temperature.

Table 6.5.3.6 gives the thermal expansion coefficients of annealed Inconel 625 at various temperatures. There is no expansion at temperature 21 °C (70 °F).

**Table 6.5.3.6 Thermal expansion of Inconel 625 with respect to temperature**

Temperature (°F)	Thermal Expansion (mm/m)
0	-0.8
200	0.9
400	2.4
600	3.9
800	5.8
1000	7.6
1200	9.4
1400	11.2
1600	13.4

### **6.5.4 Kinematic Model**

From displacement and strains in a laser forming process, three kinematic models should be considered:

## Chapter 6 Finite Element Method

- (1) small displacement and strains
- (2) large displacement and small strains
- (3) large displacement and large strains.

The stress and strain measures are different in three cases. For (1), infinitesimal strain is assumed. Engineering strain and stress are used. For (2), second Piola-Kirchhoff stress and Green-Lagrange strain are used. For (3), second Piola-Kirchhoff stress and Green-Lagrange strain are used. Three kinematic models are formulated in various ways to obtain reasonable solutions in FEM. The use of three models depends on practical situations. For example, the out-of-plane displacement of the Inconel 625 plate is from 3 to 6 mm in the experiment. It is very small compared with the dimension of the plate 300mm. Therefore, small displacement is assumed in this case. On the other hand, the out-of-plane displacement of Titanium plate may rise from 50mm to 100 mm while the dimension of the plate is 300 mm. In this case, large displacement should be assumed. As strain is above 10%, large strain should be assumed.

In ABAQUS, kinematic nonlinearity can be optionally included in the model to simulate large displacement and strains. The second and third kinematic models are not used by ABAQUS version 5.5. It is noted that calculation time increases significantly in large strains and displacement formulation.

### **6.5.5 Boundary Conditions**

In laser forming, one corner of a specimen is clamped on a supporting post. The displacement in the z direction is constrained on the supporting post. It is assumed that the angular distortion is symmetric about the heating; this disregards to the clamp at one

## Chapter 6 Finite Element Method

corner of the plate and the plate can move freely during the laser forming process. In these above-mentioned situations, extra constraints must be imposed on the specimen in F.E.M. to remove the rigid body motions. If no appropriate constraints were imposed to restrain the rigid body motions, the stiffness matrix in FEM would be singular. The equations of FEM formulation cannot be solved. Therefore, extra external constraints must be carefully considered:

- (1) They must remove the rigid body motions of the specimen
- (2) Metal movement of the specimen in FEM with extra constraints must match that in the experiment.

There are no displacements across the symmetric plane, because the specimen is symmetric along the heat line. Therefore, the rollers, which are parallel to the x-axis, are placed on the symmetric surface to constrain the displacement in the x direction. These rollers also constrain the moments in the y and z directions.

### **6.5.6 Solution Schemes**

There are three frequently used schemes to solve nonlinear equations: full Newton-Raphson, quasi-Newton, and modified Newton methods. They provide different convergence rates and computation cost in nonlinear analyses. In the full Newton-Raphson method, a tangent stiffness matrix is recalculated in each iteration, but this method provides a more accurate tangent stiffness matrix in each iteration. In contrary, the modified Newton method uses the initial tangent stiffness matrix in each iteration. The computation of the tangent stiffness matrix is reduced in each iteration. However, the total numbers of iterations needed to approach the convergence criterion increase due to

## Chapter 6 Finite Element Method

the inaccurate tangent stiffness matrix. The convergence rate is especially slow when the system suddenly softens in a solution step (e.g., a large amount of plastic straining). They also diverge when the system suddenly stiffens (e.g., elastic unloading from a plastic state or geometric nonlinearities). The quasi-Newton method is a compromise between full Newton-Raphson and modified Newton methods. A tangent stiffness matrix is recalculated once in several iterations in the quasi-Newton method.

In ABAQUS, we can use Newton or quasi-Newton methods. In this report, Newton method is used to avoid the possible divergence. If the convergent criteria are not properly set, the results obtained from the above schemes may be divergent or inaccurate.



## **Chapter 7 Parametric Study of a Laser Line Heating Process by F.E.M.**

### **7.1 Introduction**

Finite element method is used to investigate the effects of parameters including power ( $p$ ), travel speed ( $v$ ), and spot size ( $d$ ) on angular deformation caused by a laser heating process. The relations of the bending angle with respect to “ $p/v$ ”, “ $p/(tv^{1/2})$ ”, and “ $p/(tv^{1/2})$ ” is studied by experiments and FEM simulations. The relations from experimental and FEM studies are compared. The relation of bending angle with respect to spot size is only studied by FEM simulation. From these relations, the maximum bending angles of plates produced by laser line heating can be estimated. The effects of material properties on the bending angle can be also studied by changing the material properties in a FEM model. In experiments, it is difficult to study the effects of material properties on bending angle by finding two materials with the same heat conductivity, but different yield stresses. In FEM simulations, each material property can be easily isolated from others.

### **7.2 Mesh Definitions**

Mesh sizes of the FEM models play an important role in the convergence of FEM results. The convergence study of F.E.M. assures the reliability of the FEM results and also enables us to obtain the optimal FEM model. Therefore, various mesh-size models are used to investigate the convergence of FEM results. Table 7.2.1 gives the definitions of various mesh sizes for a rectangular plate. Each series presents different mesh schemes and various dimensions of the workpiece. Mesh density is denoted as the ratio of the

Chapter 7 Parametric Study of Laser Line Heating by F.E.M.

length to the number of divisions. For example, the dimension of “s” series is 1 inch in length, 1 inch in width, and 0.25 inch in thickness. The mesh densities of “s” series in x direction (transverse direction) are 0.2”-2 (0.2 inches divided by 2), and 0.8”-4 (0.8 inches divided by 4). The mesh of circular plate can be represented by mesh density in thickness, radius, and angular direction.

**Table 7.2.1 Mesh size definitions**

<i>Series</i>	<i>X Length-division Transverse Dir.</i>	<i>Y Length-division Thickness Dir.</i>	<i>Z Length-division Heating Dir.</i>	<i>Dimensions length-width-thickness</i>
<b>r</b>	1" - 5	0.24"-12	1"-10	1"-1"-0.24"
<b>s</b>	0.2"-2, 0.8"-4	0.25"-10	1"-10	1"-1"-0.25"
<b>t</b>	0.2"-4, 0.8"-4	0.05"-4, 0.20"-8	1"-10	1"-1"-0.25"
<b>u</b>	0.2"-8, 0.2"-2, 0.6"-3	0.05"-4, 0.20"-8	1"-20	1"-1"-0.25"
<b>v</b>	0.2"-4, 0.8"-8	0.05"-4, 0.20"-8	1"-10	1"-1"-0.25"
<b>w</b>	0.2"-4, 0.8"-4, 2"-2	0.05"-4, 0.20"-8	1"-10	1"-3"-0.25"
<b>x</b>	0.2"-4, 0.8"-4, 5"-5	0.05"-4, 0.20"-8	2"-10	2"-6"-0.25"
<b>y</b>	0.4"-4, 0.6"-3, 5"-5	0.05"-4, 0.20"-8	6"-60	6"-6"-0.25"

**7.3 Deformation and Parameters in A Rectangular Plate**

Through a series of FEM analyses, many important behaviors of the workpiece during the laser forming process are observed.

## Chapter 7 Parametric Study of Laser Line Heating by F.E.M.

### (1) **Effect of Plate Length**

The bending angle decreases as the length of the plate decreases, because the longer length of plate provides more cold metal to produce thermal stresses. The larger thermal stresses will produce larger angular deformation. The effect is shown in the FEM model in the “r” and “w” mesh schemes. The plate in the “w” mesh scheme is three times longer than in the “r” mesh scheme. The same material properties and heat input were used. The angular distortion of the mesh “w” was 0.72 degrees while that of the mesh “r” was 0.4240 degrees. Figures 7.3.1 and 7.3.2 show the effects of dimensions of plate on angular distortion respectively by FEM simulations, and experiments. Two figures show that angular distortion increases as heating length increases. It should be noted that there is an upper limit in the angular distortion with respect to the heating length. In other words, a bending angle approaches a specific value as heating length increases toward infinite. If the plate is short, in-plane bending is produced.

### (2) **Effect of Boundary Condition**

If the edge of the rectangular plate is clamped parallel to the heating direction, the angular distortion will change. The elastic pre-strain is imposed at both edges of the rectangular plate. The final deformed shape is shown in Figure 7.3.3. The angular change is zero near the clamped edge due to the clamping. The plate was released from the clamp after the laser forming process, and the final angular change is calculated near the heating line. The clamped edge in the elastic region springs back after laser forming process. The elastic region does not change the final angular distortion. The angular change in elastic pre-strain is smaller than that in free edge.

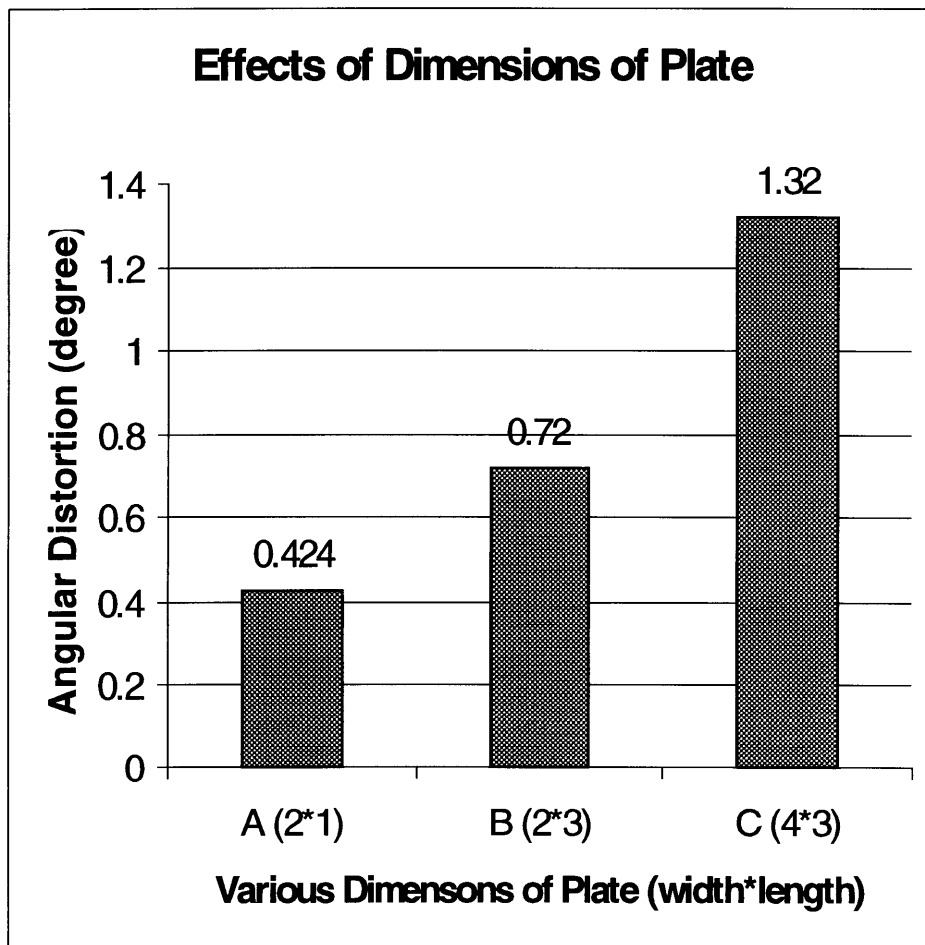


Figure 7.3.1 Effects of Dimension of Plate on Angular Distortion

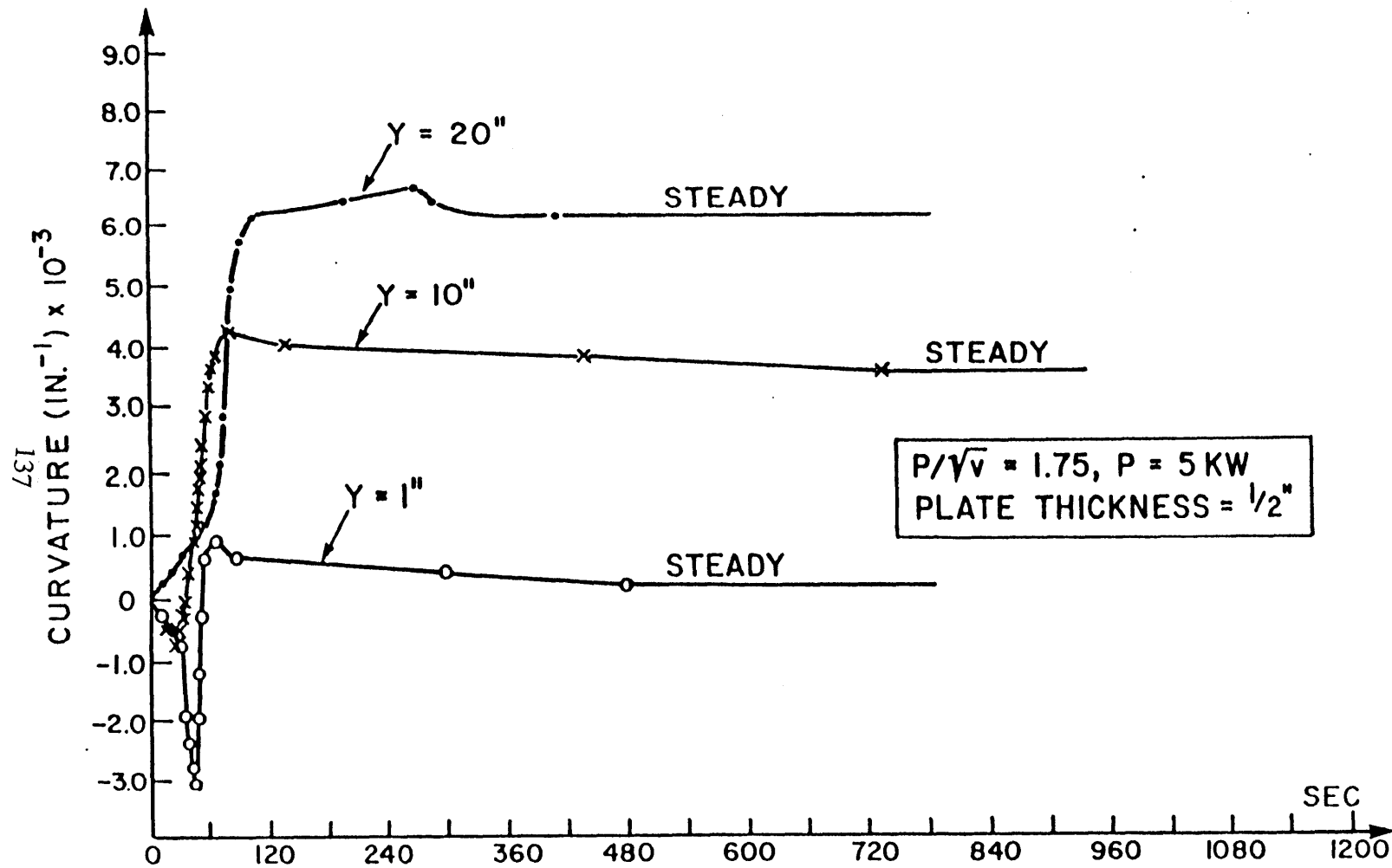
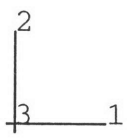


Figure 7.3.2 The effect of the heating length on the bending angle



DISPLACEMENT MAGNIFICATION FACTOR = 42.0 ORIGINAL MESH DISPLACED MESH  
TIME COMPLETED IN THIS STEP 600. TOTAL ACCUMULATED TIME 600.  
ABAQUS VERSION: 5.5-1 DATE: 28-DEC-96 TIME: 22:41:45  
STEP 1 INCREMENT 76

Figure 7.3.3 Deformation of a rectangular plate with elastic pre-strain

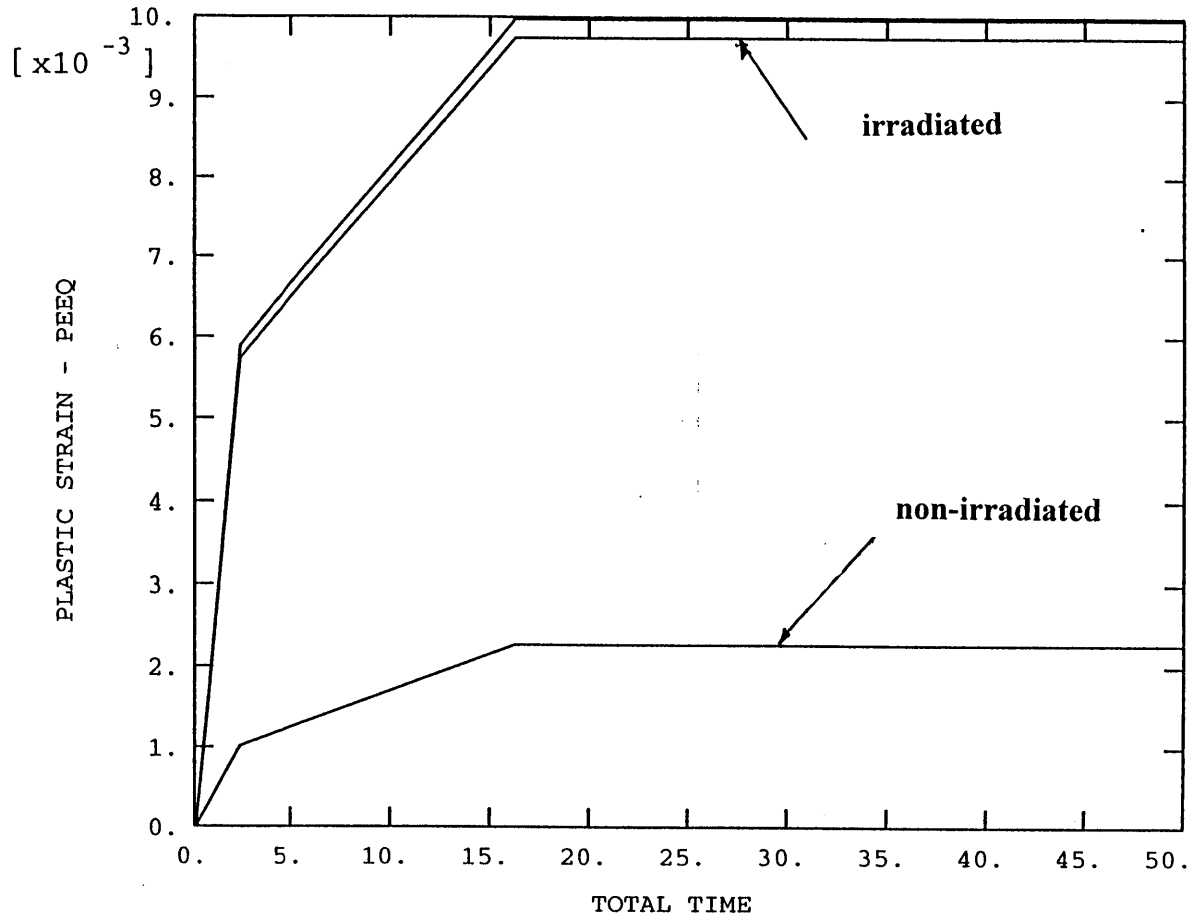


Figure 7.3.4 Effective plastic strains on irradiated and non-irradiated surfaces

(3) ***Effect of Heat Input***

Higher heat input usually produces larger angular distortion, but the angular distortion decreases after heat input rises beyond some critical values. The angular distortion depends on the peak temperature and the temperature gradient in a thickness direction. When heat input is too low, the peak temperature and thermal stresses are low. In this case, no plastic strains are produced in high yield-stress materials due to the low thermal stresses. As the peak temperature is too high, heat penetrates the thickness of the plate and the gradient of the temperature decreases. In this case, angular distortion decreases due to low temperature gradient. The relation between heat input and angular distortion is shown in Figure 7.5.7. If the plastic strain of the top surface is larger than that of the bottom surface, the plate bends upwards. Otherwise, the plate bends downwards. The effective plastic strains of the top and bottom surfaces, in the case of bending toward the laser beam, are shown in Figure 7.3.4.

(4) ***Effect of Travel Speed***

As the travel speed of the laser beam is very fast, the thermal cycle is very short. In other words, the heating and cooling rates are very fast. There is no time to produce any temperature gradient along the thickness direction while there is high temperature gradient produced along the heating direction. The longitudinal bending angle is hence very large. In the experiment of forming the titanium alloy plate, the travel speed was 60 cm per minute, and a huge longitudinal bending angle was observed. In addition, the angular distortion decreases as travel speed increases. The reason is that a lower temperature gradient in the thickness direction is produced with a higher travel speed. If the travel speed is too slow, heat will penetrate the thickness of the plate.



## Chapter 7 Parametric Study of Laser Line Heating by F.E.M.

Hence, angular distortion decreases due to low temperature gradient in thickness direction.

### (5) **Effect of Spot Size**

Angular distortion also depends on the spot size of the laser beam. The same heat input with different spot sizes is used to investigate the effects of the spot size on angular distortion. The angular distortion with a spot size of 12.5 mm is 0.5157 degrees, while that with a spot size of 10 mm is 0.3432 degrees. As the spot size increases, the angular distortion increases. The plastic zone is larger in a larger spot size. Therefore, angular distortion increases as spot size increases.

### (6) **Effects of Yield Stress at Room Temperature**

Effects of yield stresses of Inconel 625 on angular distortion are investigated by using three different yield stresses 0.444 ksi, 51 ksi, and 443.8 ksi at room temperature in the “r” series. Figure 7.3.5 shows that angular change increases as the yields stresses at room temperature increase.

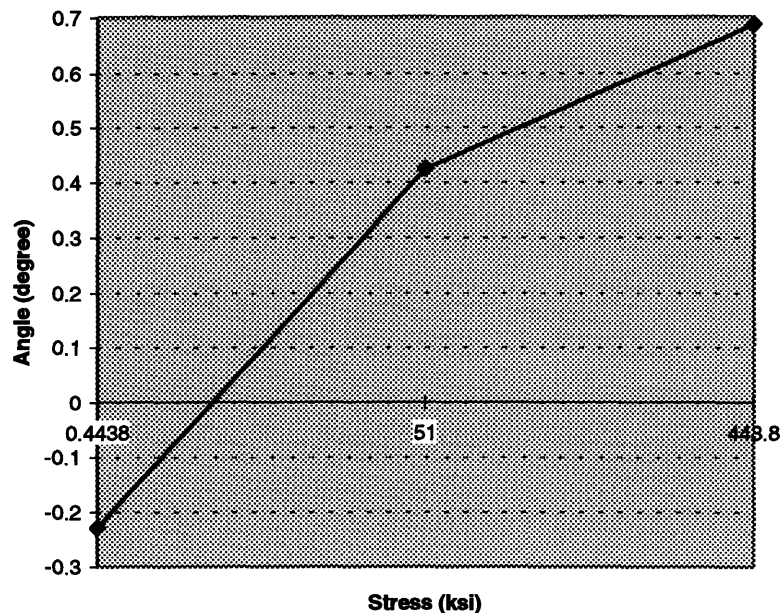


**Figure 7.3.5 Angular change with respect to yield stress at room temperature**

## **7.4 Parametric Study of A Circular Plate Irradiated by A Laser Beam**

A circular plate can be heated by a laser beam in various ways to produce different types of deformation. Three types of heating patterns are investigated:

- (1) The Gaussian distributed power profile of a laser beam irradiates the center of the circular plate.
- (2) The Gaussian distributed power profile of a laser beam moves along one circular path with 360 degrees on the top surface of the circular plate.

## Chapter 7 Parametric Study of Laser Line Heating by F.E.M.

- (3) The Gaussian distributed power profile of a laser beam moves along one circular path with 720 degrees on the top surface of the circular plate.

The temperature distribution and deformation is predicted by F.E.M.

### **7.4.1 Center Irradiation**

A laser beam irradiates the center of the circular plate. The circular Inconel 625 plate is 2.0 inch in diameter and 0.25 inch in thickness. The processing condition is listed in Table 7.4.1. The absorption rate is assumed to be 0.8.

**Table 7.4.1 Processing condition of center irradiation**

Specimen	Power (kW)	Heating Time (sec)	Spot size (cm)
Inconel 625	2.60	5	2

The circular plate goes down during the heat stage, and goes up during the cooling stage. The final distortion is shown in Figure 7.4.3. There is no out-of-plane distortion in the circular plate, while there is in-plane expansion. The deformation is produced by the higher temperature gradient in the radius direction, rather than the thickness direction.

### **7.4.2 Circular Irradiation in 360 Degrees**

The laser beam is moved along a circle of diameter one inch concentric with the circular plate. The processing condition is listed in Table 7.4.2. The transient temperature distribution is shown in Figure 7.4.4. There are five groups of curves shown in Figure 7.4.3. Each group presents a different angular position: 0, 90, 180, 270, and 360 degrees.

## Chapter 7 Parametric Study of Laser Line Heating by F.E.M.

In each group, there are four curves in different radius positions: 0, 0.25, 0.5 and 1 inches. As the laser moves from 0 to 270 degrees counterclockwise, the temperature of the entire plate rises quickly. When the laser beam is at 270 degrees, the temperature of angular position 0 degrees began to cool down. However, the temperature at angular position 0 is heated up again at time 36 seconds, since the laser beam returns to the angular position 0 again. After 36 seconds, the laser beam stops irradiating the surface of the circular plate, and the plate cools down. In each group, the highest temperature occurs at radius 0.5 inch on the path of the laser beam. The temperature of the outer and inner radius positions is lower, due to the distance away from the laser beam.

**Table 7.4.2 Processing condition of circular irradiation in 360 degrees**

Specimen	Power (kW)	Speed (degree/sec)	Spot size (cm)
Inconel 625	2.60	10	2

### **7.4.3 Continuous Circular Irradiation in 720 Degrees**

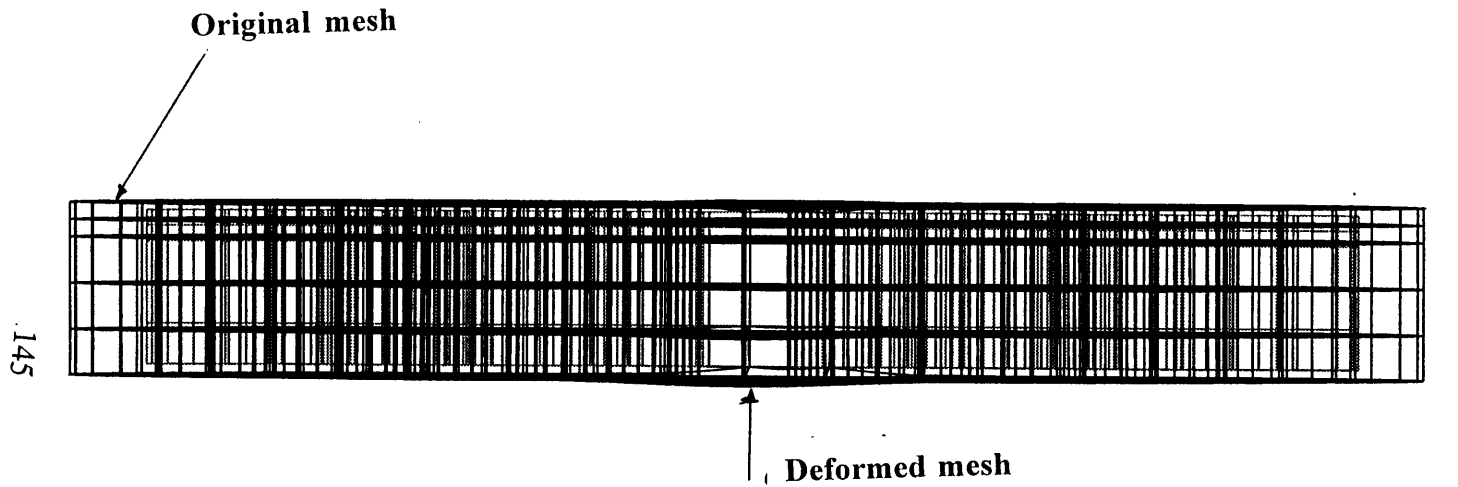
The effects of continuous circular irradiation are investigated.

**Table 7.4.3 Processing condition of continuous circular irradiation**

s

Specimen	Power (kW)	Speed (degree/sec)	Spot size (cm)
Inconel 625	2.60	18	2

If the diameter of the circular plate is small compared to the spot size, continuous circular irradiation will heat up the plate without temperature gradient after several cycles.



2  
3 1

DISPLACEMENT MAGNIFICATION FACTOR = 7.18 ORIGINAL MESH DISPLACED MESH  
 TIME COMPLETED IN THIS STEP 560. TOTAL ACCUMULATED TIME 560.  
 ABAQUS VERSION: 5.5-1 DATE: 01-JAN-97 TIME: 10:11:32  
 STEP 1 INCREMENT 50

**Figure 7.4.2 Final deformed shape of circular plate with central irradiation**

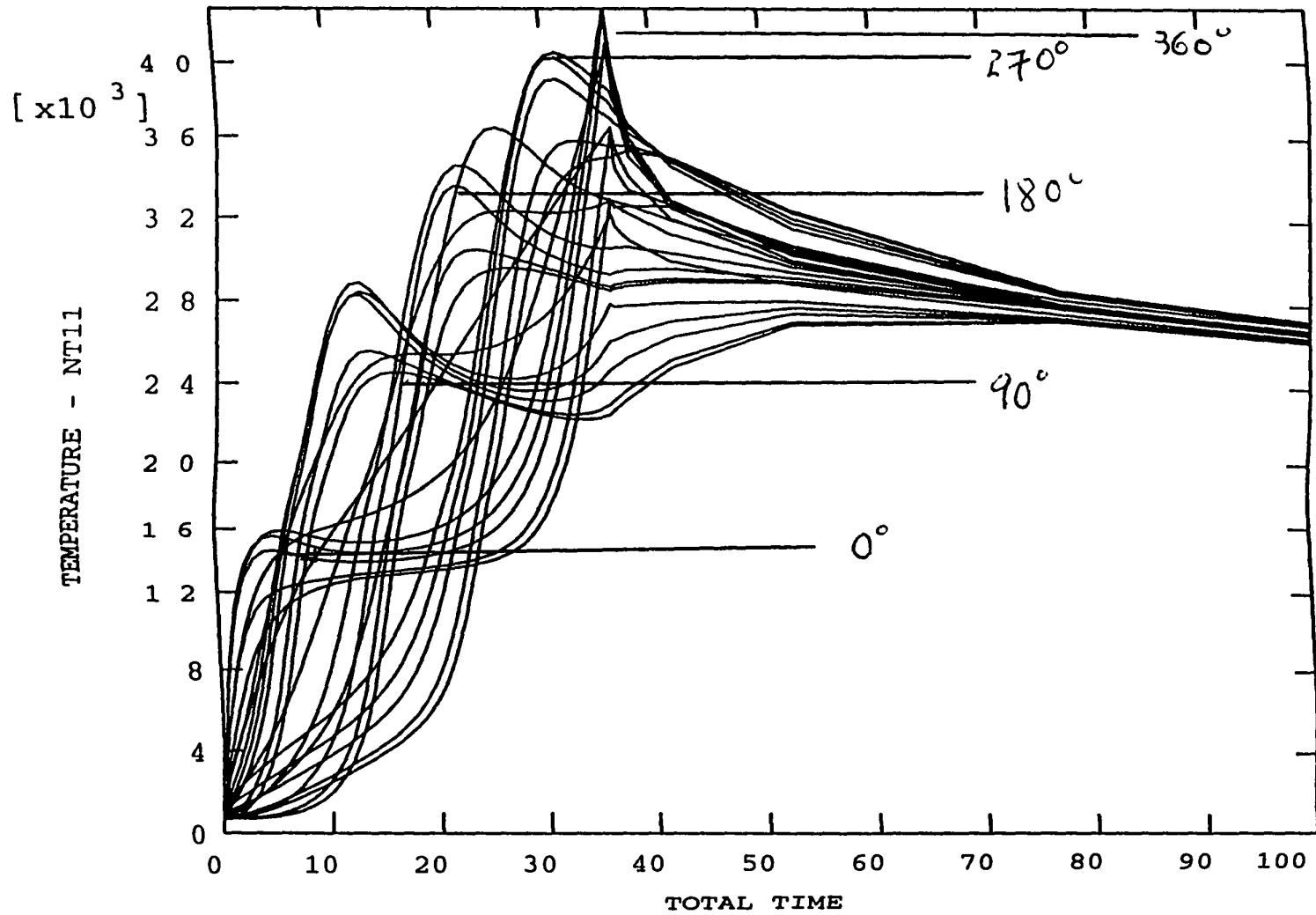


**Figure 7 4 3 Temperature distribution of a circular plate with circular irradiation in 360 degrees**

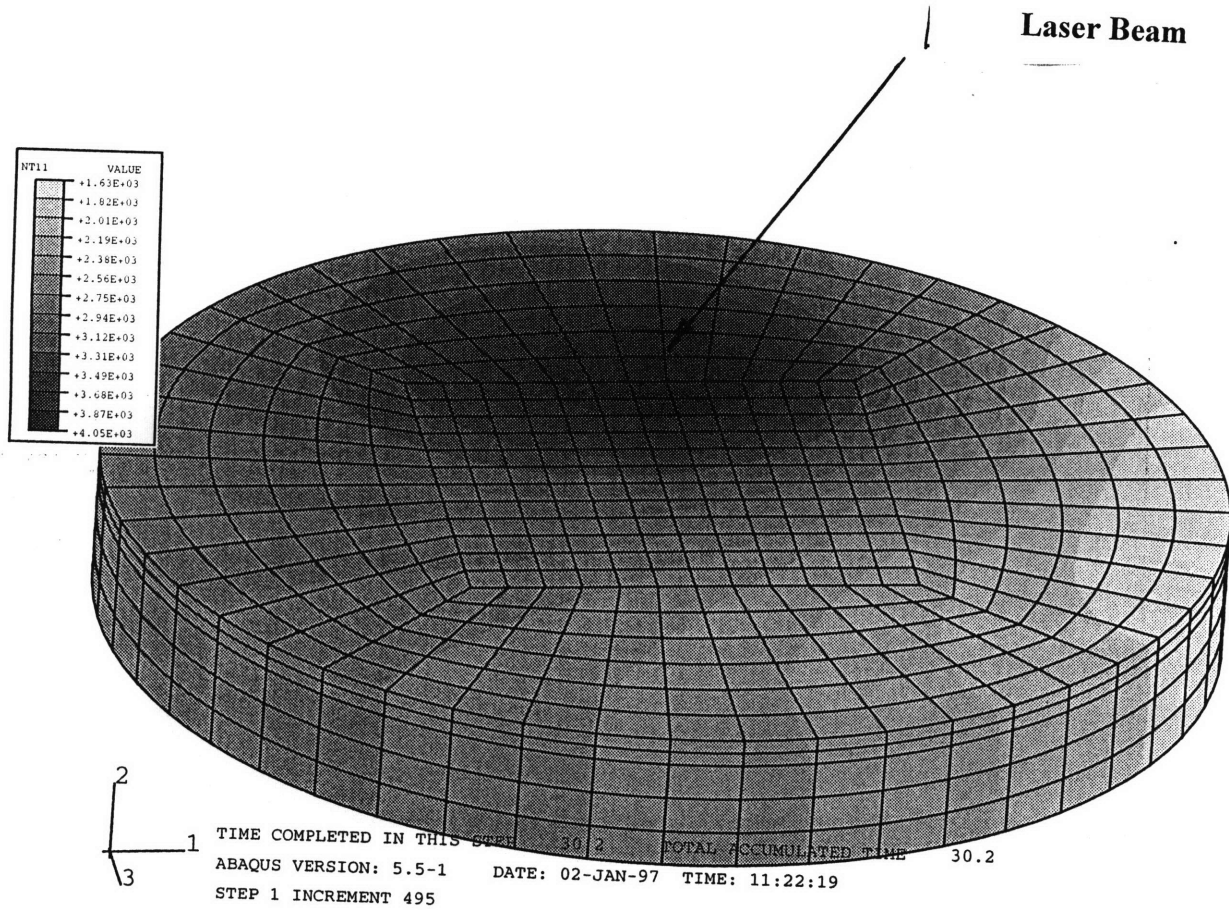


**Figure 7.4.4 Transient temperature distribution of a circular plate with circular irradiation in 360 degrees**

## **7.5 Parametric Study of A Rectangular Plate Irradiated by A Laser Beam**

The parametric study was performed by computer simulation to investigate the relation among angular distortion and parameters. Figures 7.5.1, 7.5.2 and 7.5.3 show the parametric study conducted by the experiment [28]. The figures indicate that angular distortion increases as “ $p/v$ ”, “ $p/(vt)$ ”, and “ $p/(v^{1/2}t)$ ” increase. For a ¼ inch plate, the angular distortion suddenly decreases as three parameters rises beyond some critical values.

The results of the parametric study by computer simulation are shown in Table 7.5.1. From this table, we can observe the relation among parameters and angular distortion.

- (1) Constant Power: The relations of angular distortion with respect to “ $p/v$ ”, “ $p/(vt)$ ”, and “ $p/(v^{1/2}t)$ ” from FEM simulations are shown in Figures 7.5.4, 7.5.5, and 7.5.6. In these figures, the same parameters may not result in the same angular distortion. In other words, these parameters do not exhibit the relations between processing conditions and angular distortion. For example, the angular distortion could be 0.344 or 0.4584 degrees for “ $p/v$ ” = 0.16; the effect of doubling power on angular change is different from halving velocity while both result in the same value of the parameter  $p/v$ . Therefore, the modification of the parameters is necessary. However, a new parameter combining all parameters and material properties should be proposed on the basis of physical laws. Case1, Case2, and Case3 have the same power but different speeds. Figures 7.5.4, 7.7.5 and 7.5.6 show that the angular



Chapter 7 Parametric Study of Laser Line Heating by F.E.M.

distortion increases as the velocity increases, but distortion decreases once the velocity increases beyond some critical value. This behavior was observed in the experiment with ¼-inch plate, as shown in Figures 7.5.1.

- (2) Constant Velocity: Compare Case1 with Case4; Case2 with Case 5; Case3 and Case6. Figure 7.5.7 shows that the angular distortion increases as the power increases. In higher travel speed, the angular distortion is more sensitive to power.

**Table 7.5.1 The results of parametric study**

Parameter	P (kW)	v (in/sec)	V (ipm)	T (in)	P/v (KJ/in)	P/(t·V <sup>0.5</sup> ) (kW/(in·ipm))	P/V <sup>0.5</sup> (kW/ipm)	Angle (degree)
case1	1.25	0.1312	7.8738	0.25	0.16	1.78	0.45	0.3440
case2	1.25	0.2625	15.7476	0.25	0.08	1.26	0.31	0.1398
case3	1.25	0.0656	3.9369	0.25	0.32	2.52	0.63	0.2865
case4	2.5	0.1312	7.8738	0.25	0.32	3.56	0.89	0.5214
case5	2.5	0.2625	15.7476	0.25	0.16	2.52	0.63	0.4584
case6	2.5	0.0656	3.9369	0.25	0.64	5.04	1.26	0.3438

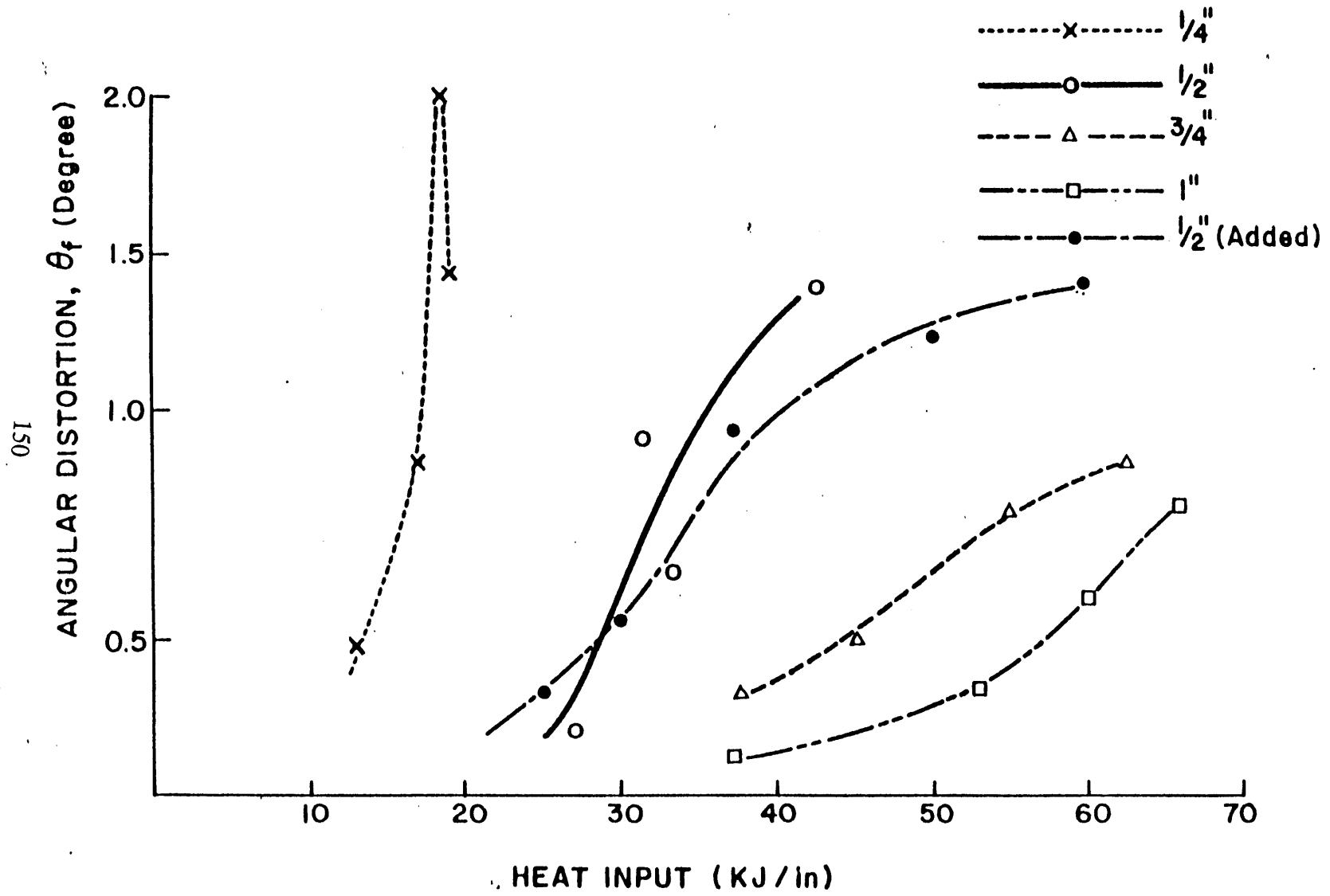


Figure 7.5.1 Angular distortion with respect to p/v from experimental study

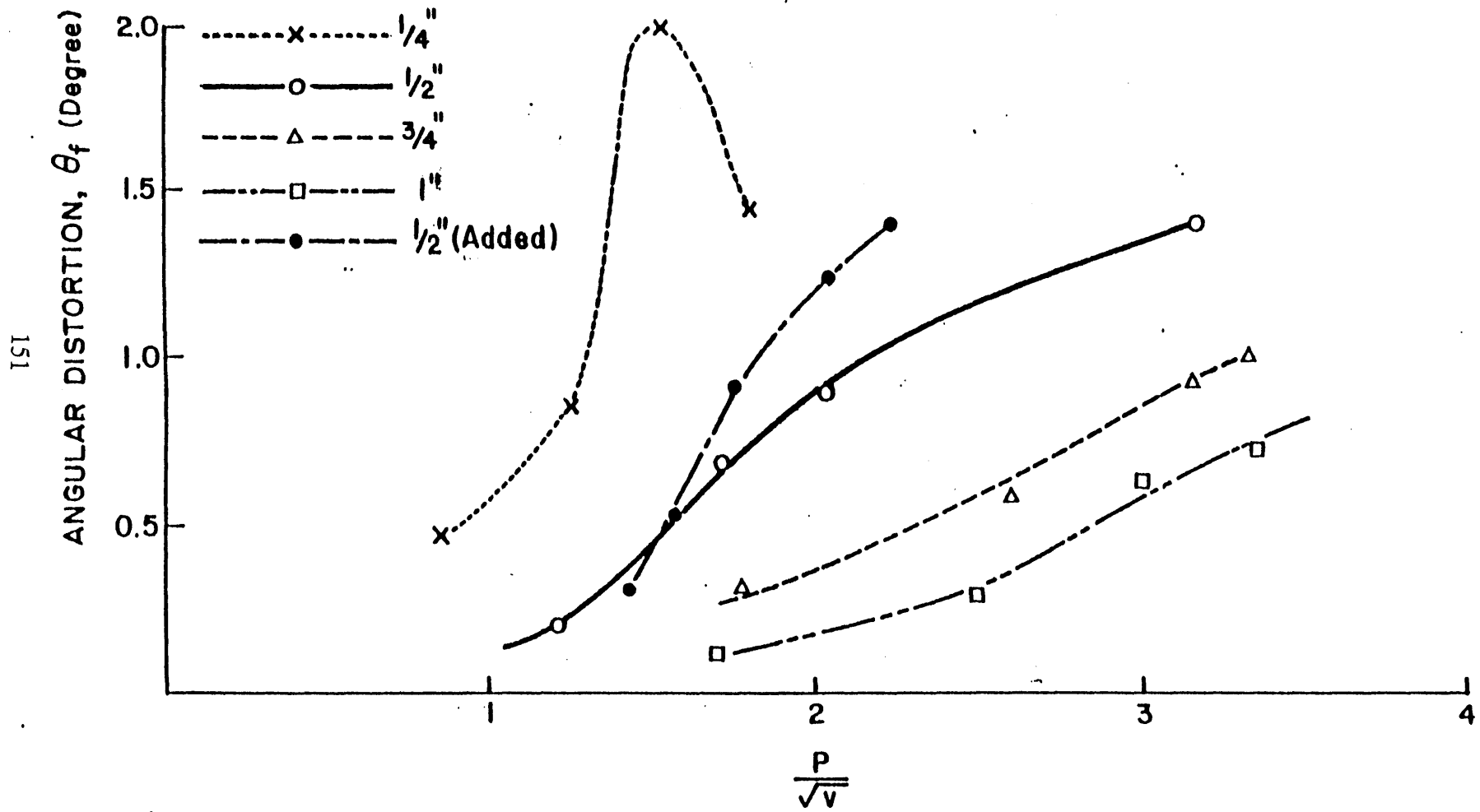


Figure 7.5.2 Angular distortion with respect to  $p/v^{0.5}$  from experimental study

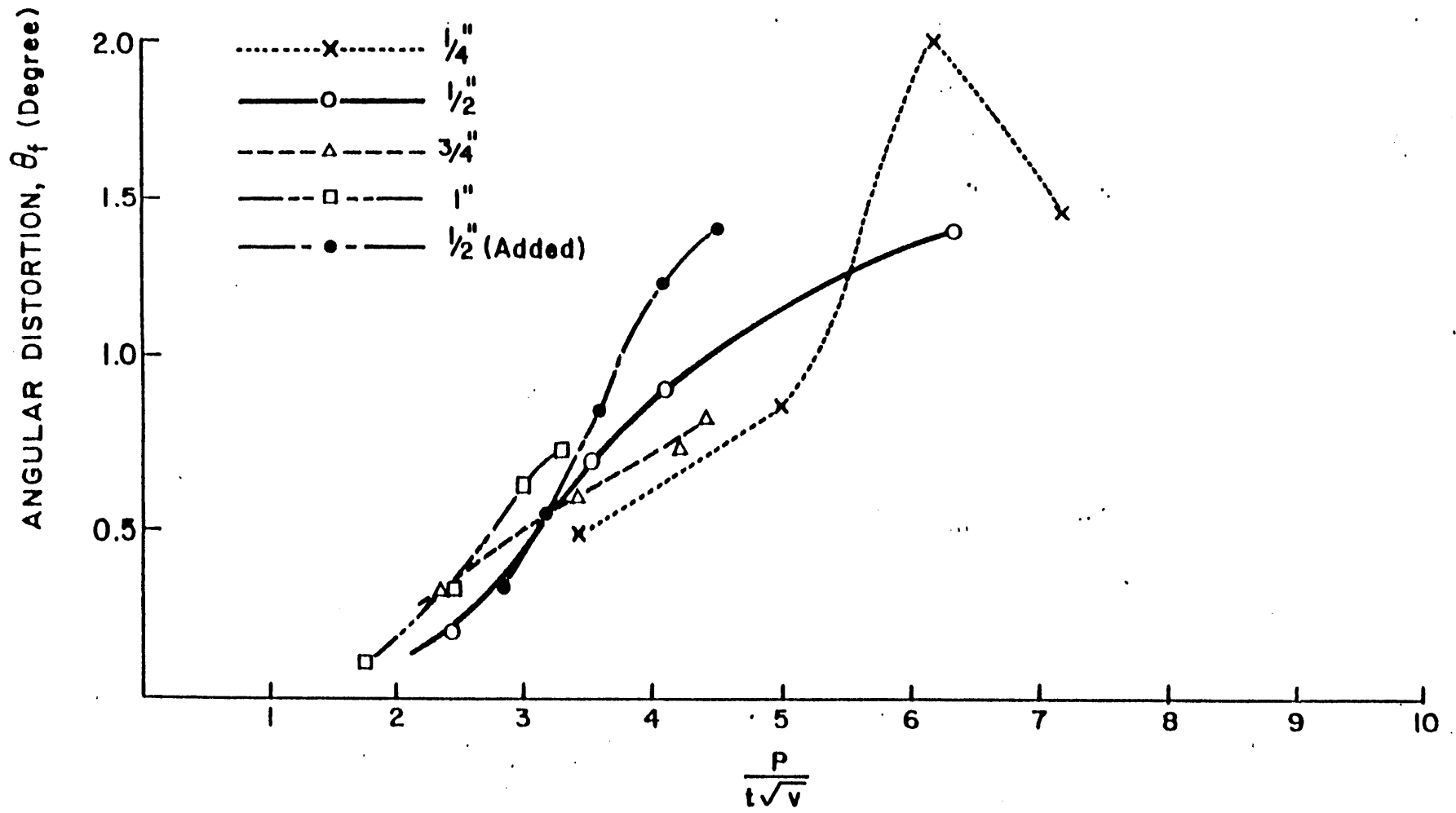


Figure 7.5.3 Angular distortion with respect to  $p/tv^{0.5}$  from experimental study

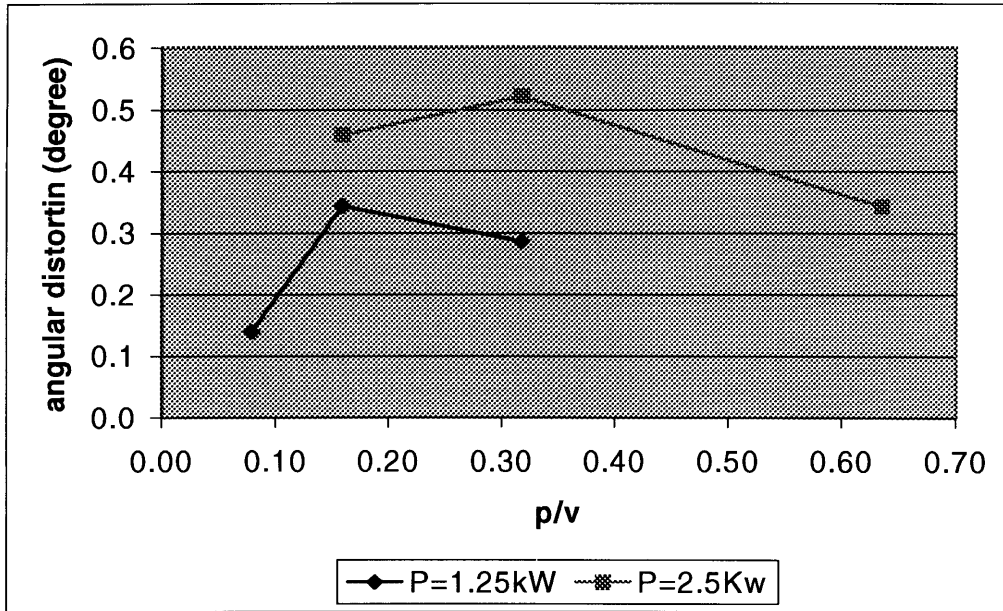


Figure 7.5.4 The relation between angular distortion and  $p/v$

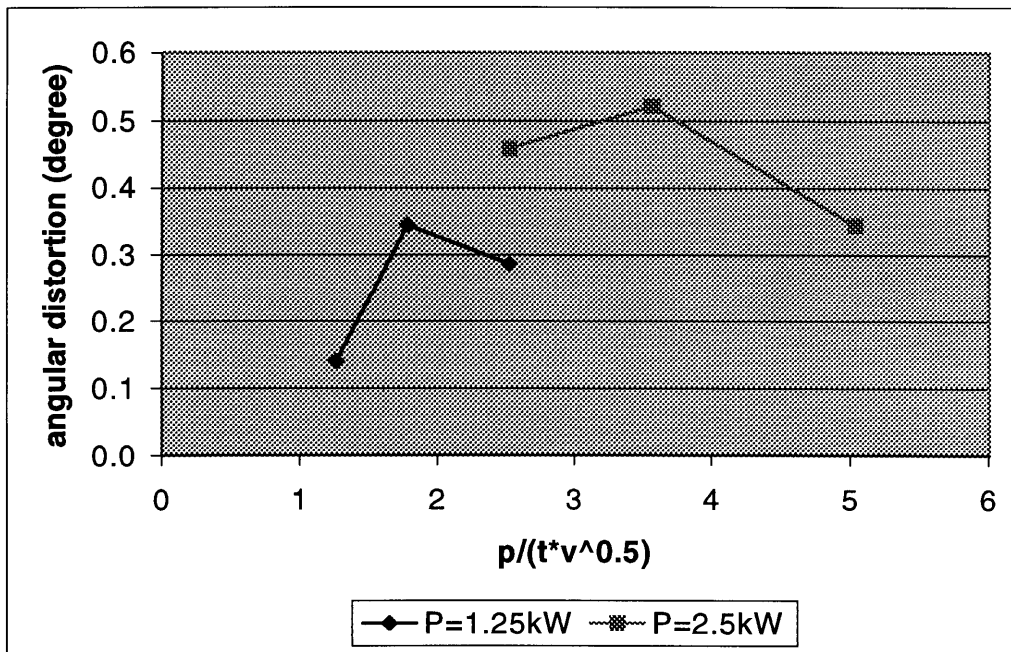


Figure 7.5.5 The relation between angular distortion and  $p/v^{1/2}$

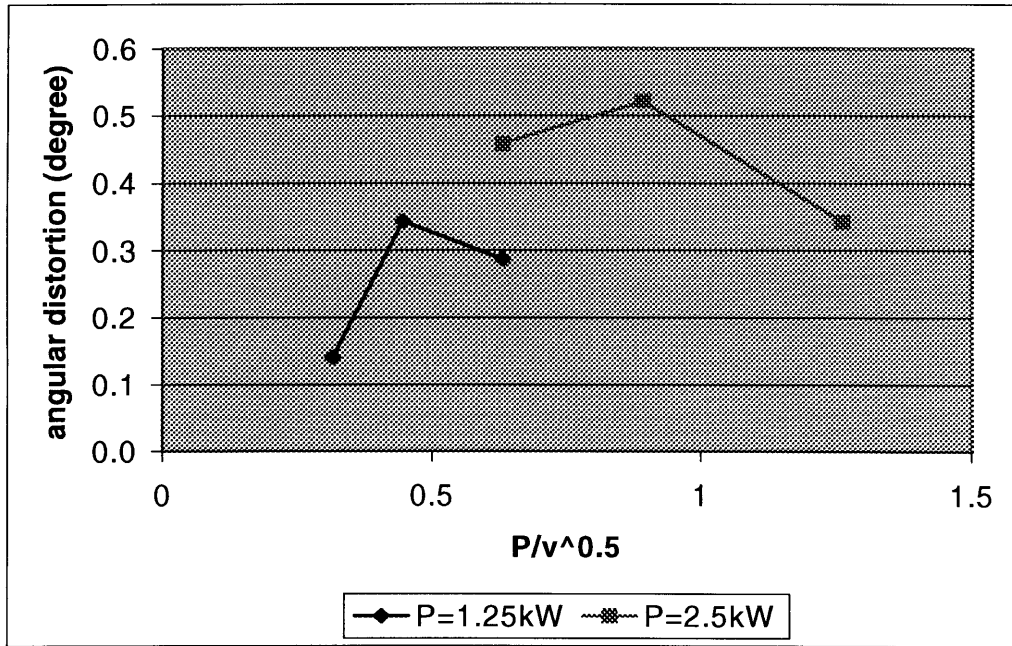


Figure 7.5.6 The relation between angular distortion and  $p/(v^{1/2})$

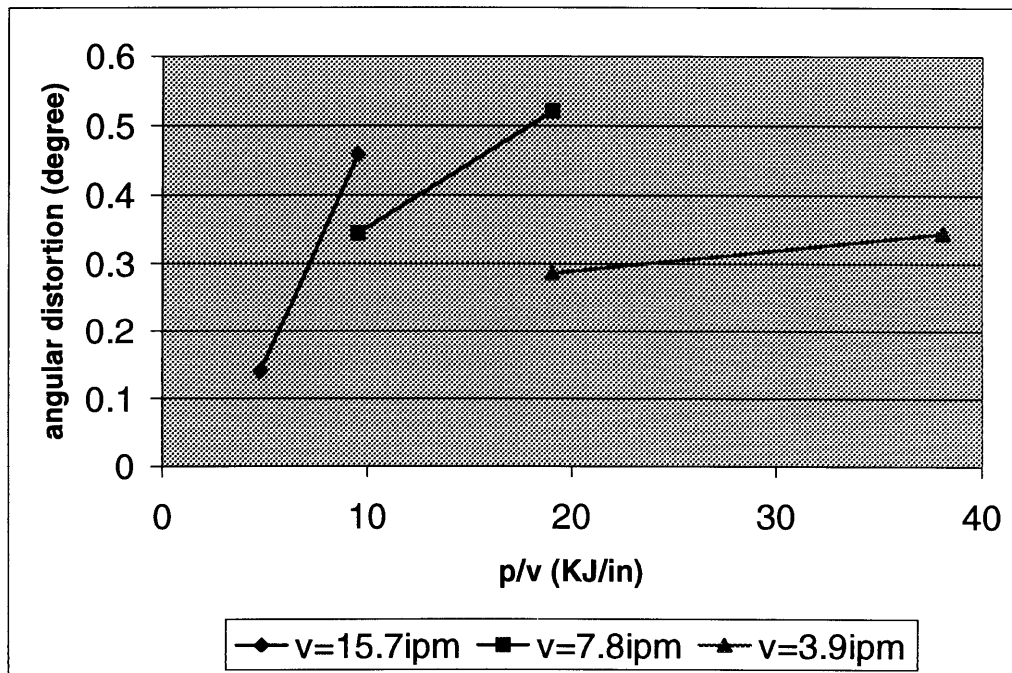


Figure 7.5.7 The relation between angular distortion and  $p/v$  at constant velocity

## **Chapter 8 Conclusion and Recommendations**

### **8.1 Conclusion and Recommendations**

This thesis presents new results in laser forming technology based on the experimental study and computer simulation. They can be summarized as follows:

- (1) Laser can be used to form sheets of various materials. Low-carbon steel, HY-80, HSLA steel, and Inconel alloys, are bent toward the laser beam in one single heating pass. However, there is no bending for aluminum alloys, due to their high conductivity.
- (2) Angular distortion increases as “ $p/v$ ”, “ $p/(vt)$ ”, and “ $p/(v^{1/2}t)$ ” increase. A angular distortion decreases one those parameters increase beyond critical values. This phenomenon is observed in both experiments and FEM analyses. In addition, FEM analyses indicated that parameters with the same value from different combinations of power and travel speed result in different bending angles. In other words, the effects of power and travel speed on the bending angle are different. The mechanism needs to be further investigated.
- (3) The bending angle increases as the heating length increases. Experiments and FEM analyses find the effects of a heating length on a bending angle. A 12”×12”×0.25” plate was used in the experiment. Due to the constraints of computation time and disk space, the simulation model is 3”×4”×0.24”. The inconsistency between the dimensions used in the simulation model and experimental specimen leads to the smaller bending angle in FEM analyses. The estimated computation time for the simulation of the full-scale model is 720 CPU hours on a HP 715/100 workstation.

## Chapter 8 Conclusions and Recommendations

The required hard drive space is 3.5 Gbytes. Much computer resources is needed to perform a three-dimensional thermal-elastic-plastic FEM analysis.

These new results suggest the following directions for future work:

- (1) Furthering the parametric study by computer simulation and experiment. The issue of the same value “ $p/v$ ” producing different bending angles can be studied by performing experiments. Due to limited variables studied in this thesis, it is necessary to perform simulation involving more variables. The next step is to integrate the results of the parametric study from experiment and computer simulation. The relation between parameters and bending angles has been established.
  
- (2) Using new techniques to reduce computation time. The angular distortion increases as the length of the plate increases. To reduce the computation time by only simulating the plastic parts of the structure can lead to huge errors by neglecting the coupling effect between the elastic and plastic parts of the structures. Therefore, simulating the entire structure needs fine mesh near the heating path and coarse mesh in elastic zone. The huge number of nodes and elements in three-dimensional FEM analysis leads to heavy computation in current computer technology. Rezoning and dynamic substructuring techniques can significantly reduce the computation time of FEM of a laser forming process. In the current finite element method, a fine mesh is used near the path of the moving heat source. The new method adopts a dynamic fine mesh only near the spot size of the moving heat source. In other words, the number of nodes and elements can be reduced to a minimum. These techniques have been successfully applied to FEM simulation of a welding process [6]. For the typical process of heating the top surface of the plate, the computation time with the new techniques



## Chapter 8 Conclusions and Recommendations

is less than 1/7 the CPU time of the current method. Professor Brown in the Department of Material Science at MIT and Dr. Song have developed a computer program with the new techniques, which is integrated into ABAQUS. They demonstrated good prediction on residual stress of a plate. The rezoning method was also successfully used to simulate the extrusion of a metal bar [7,8]. The elements undergo large distortion during the process so the original elements can not be used to predict the stress accurately. Remeshing of the deformed solid during the process can reduce the distortion of elements. In two-dimensional simulations, remeshing can be automatically generated by IDEAS. The new mesh is transferred to ABAQUS. In three-dimensional simulation, remeshing can be semi-automatically generated. Therefore, new techniques may feasibly reduce computation of the simulation of the laser forming process.

- (3) Using new constitutive equation to simulate phase transformation. Boeing examines the microstructure of materials. The microstructures of heat affected zone (HAZ) and base metal are different. The hardness of HAZ is softer than the base metal in Inconel 718. Using new constitutive equations in FEM model may improve the prediction of angular distortion.

## References

- [1] "ABAQUS Theory Manual," H.K.S. Inc., Pawtucket, RI, 1994.
- [2] "ABAQUS/STANDARD USER'S GUIDE," ver 5.5, H.K.S. Inc., Rhode Island, 1995.
- [3] Araki, M., Inoue, N., Horioka, M. and Ando, M., "On Angular Distortion of Hull Steel Plates by Line Heating Methods," Transaction of JWRI, Nov. 1994.
- [4] Bathe, K.J., "Finite Element Procedures", Prentice Hall, 1995.
- [5] Boley, B.A., Weiner, J.H., "Theory of Thermal Stresses," Robert E. Krieger Publishing Company, Inc., 1960.
- [6] Brown, S.B., Song, H, "Rezoning and Dynamic Substructuring Techniques in FEM Simulations of Welding Processes," Journal of Engineering for Industry, Vol. 115, Nov. 1993
- [7] Chen W.F. D.J. Han, "Plasticity for Structure Engineering," Gau Lih Book Co., Taipei, Taiwan, 1995.
- [8] Cheng, Liao, 1996 ABAQUS Taiwan Users' Conference.
- [9] Eagar, T.W., Tsai, N.-S., "Temperature Fields Produced by Traveling Distributed Heat Sources," Welding Journal, Dec. 1983.
- [10] Festa., R., "A Comparison between Models of Thermal Fields in Laser and Electron Beam Surface Processing," Int. J. Heat Mass Transfer. Vol. 31, No. 1, 1988.
- [11] Gao, Cheng, 1996 ABAQUS Taiwan Users' Conference.
- [12] Gatewood, B.E., "Thermal Stresses," Mcgraw-Hill, New York, 1957.
- [13] Gere, J., Timoshenko, S., "Mechanics of Materials," PWS-Kent Publishing Company, 3<sup>rd</sup> ed., 1990
- [14] Goldak, J., Chakravarti, A., Bibby, M., "A New Finite Element Model for Welding Heat Sources," Metallurgical Transactions B, Vol. 15B, Jun. 1984.

- [16] Iwamura, Y. and Rybicki, E.F., "A Transient Elastic-Plastic Thermal Stress Analysis of Flame Forming," *Journal of Engineering for Industry*, Feb, 1973.
- [17] Iwasaki, Y., "Study on the Forming of Hull Plate by Line Heating Method," *Mitsubuchi Juko Giho*, Vol. 19, No. 3, 1975.
- [18] Lindgren, Lars-Erik, "Temperature Fields in Simulation of Butt-Welding of Large Plates," *Communications in Applied Numerical Methods*, Vol. 2, 1986, pp. 155-164.
- [19] Lubliner J., "Plasticity Theory," Macmillan Publishing Co., New York, 1990.
- [20] Malaret, H.A. "Mechanisms in Thermal Mechanical Forming of Plate," M.S. thesis for Mechanical Engineering and Ocean Engineering, M.I.T., 1987.
- [21] von Allmen, M., Blatter, A., "Laser Beam Interactions with Materials," 2<sup>nd</sup> Ed., Springer-Verlag, 1995.
- [22] Martukanitz, P.R., G.K. Sumnicht, "Accuracy and Variability of Temperature Excursion and Displacement Measurements During Thermomechanical Forming of Inconel 625 with a Nd:YAG laser," subtask completion report, July, 1996.
- [23] Martukanitz, P.R., G.K. Sumnicht, "Interim Report Concerning Sponsored Research on Task I of Laser Forming for Flexible Fabrication," submitted from ARL, PSU to Rocketdyne, May, 1996.
- [24] Masubuchi, K. and Kusuda, T., "Temperature Distribution of Welded Plates", *Journal of the Japan Welding Society*, 22(5), pp. 14-17, 1953.
- [25] Masubuchi, K., Hsiao, Y.C., Shimizu, H., "Monthly Progress Report July 1996 on Laser Line Heating," submitted to Recketdyne, July, 1996.
- [26] Masubuchi, K., "Analysis of Welded Structures", Pergamon Press, 1980.
- [27] Masubuchi, K., "Studies at M.I.T. Related to Applications of Laser Technologies to Metal Fabrication," *Proceedings of LAMP*, 1992.
- [28] Masubuchi, K., and Luebke, W.H., "Phase II Report: Laser Forming of Steel Plates for Ship Construction," submitted from Massachusetts Institute of Technology to Todd Pacific Shipyards Corporation, March, 1987.

- [29] Masubuchi, K., and Shimizu, H., "A Review of Past and Current Studies Related to Metal Forming by Laser Line Heating," submitted from M.I.T. to Rocketdyne, Oct. 1995.
- [30] Masubuchi, K., W.J.C. Cook, D.L. Deacon, J.S. Fan, G. Haidemenopoulos, R.C. John, and R.W. McCarthy, "Phase I Report: Laser Forming of Steel Plates for Ship Construction," submitted from Massachusetts Institute of Technology to Todd Pacific Shipyards Corporation, Feb., 1985.
- [31] Michael Bass, "Material Processing Theory and Practices," Vol 3., North-Lolland Publishing Company, 1985.
- [32] Moshaiov, A. and Shin, J. G., "Modified Strip Model for Analyzing the Line Heating Method - Part 2: Thermo-Elastic-Plastic Plates," Journal of Ship Research, Vol. 35, No 3, Sep. 1991, pp. 266-275.
- [33] Moshaiov, A., Latorre, R., "Temperature Distribution During Plate Bending by Torch Flame Heating," Journal of Ship Research, Vol. 29, No,1, Mar. 1985.
- [34] Muraki, T., Bryan, J.J., and Masubuchi, K., "Analysis of Thermal Stresses and Metal Movement During Welding, Part I: Analytical Study, and Part II: Comparison of Experimental Data and Analytical Results, Journal of Engineering Materials and Technology, ASME, Jan. 1975.
- [35] Muraki, T., Masubuchi, K., "Manual on Finite Element Program for Two Dimensional Analysis of Thermal Stresses and Metal Movement During Welding," Department of Ocean Engineering, Massachusetts Institute of Technology, 1975.
- [36] Namba, Y., "Laser Forming of Metals and Alloys," Proceeding of LAMP, 1987.
- [37] Odumodu, K.U., "Finite Element Simulation of Laser Shaping," PhD. Thesis, University of Detroit-Mercy, 1995.
- [38] Rosenthal, D. and Schmember, R., "Thermal Study of Arc Welding", Welding Journal, Supplement 208, 1938.
- [39] Rykalin, N. N., "Calculation of Heat Process in Welding", printed in 1960 in Moscow, U.S.S.R.

- [40] Rykalin, N.N. and Nikolaev, A., "Welding Arc Heat Flow," *Welding in the World*, pp.112-132, September, 1971.
- [41] Scully, K., "Laser Line Heating," *Journal of Ship Production*, Vol. 3, No 4, Nov., 1987.
- [42] Shercliff, H.R., Ashby, M.F., "The Prediction of Case Depth in Laser Transformation Hardening," *Metallurgical Transactions A*, Vol. 22A, Oct. 1991.
- [43] Sluzalec, A., "Thermal Effects in Laser Microwelding," *Computer & Structures*, Vol.25, No. 1, 1987.
- [44] Snyder, M.D., Bathe, K.J., "A Solution Procedure for Thermo-Elastic-Plastic and Creep Problem," *Journal of Nuclear Engineering and Design*,1981.
- [45] Tekriwal, P., Mazumder, J., "Finite Element Analysis of Three-Dimensional Transient Heat Transfer in GMA Welding," *Welding Journal*, Jul. 1988.
- [46] V.J. Papazoglou, K. Masubuchi, "Numerical Analysis of Thermal Stresses During Welding Including Phase Transformation Effects", *Journal of Pressure Vessel Technology*, Transactions of ASME, pp. 149-154, 1982.
- [47] Vollersten, F. and Holzer, S., "3D-thermomechanical Simulation of Laser Forming," *Simulation of Material Processing*, 1995.
- [48] Wooten, J., "Technical Proposal Laser Forming for Flexible Fabrication," 1995.

# Appendix A: Using ABAQUS in Laser Forming Simulation

## A.1 Introduction

ABAQUS is a general-purpose finite element software developed by Hibbit, Karlsson & Sorensen Inc. ABAQUS consists of several program modules:

ABAQUS/Pre – Interactive preprocessor. ABAQUS/Pre generates an ABAQUS input file that defines nodes, elements, materials, loads, and analysis types.

ABAQUS/Standard – batch processor. ABAQUS/Standard compiles the ABAQUS input file into an executive file. This executive file solves the equations and outputs the results.

ABAQUS/Post – postprocessor. ABAQUS/Post reads the results from ABAQUS/Standard. The results are shown in various formats.

ABAQUS including element library, material library, procedure library, and built-in loading library can be widely applied to various engineering problems. In this Appendix, special emphasis is put on the modeling techniques of using ABAQUS for laser forming simulation. The detail descriptions of ABAQUS commands and terminology should be referred to ABAQUS manual. The basic knowledge on finite element analysis and the experience of using ABAQUS is assumed. Programming for ABAQUS is very flexible because ABAQUS input file is a text file. Any text editor can modify the commands of the input file. In addition, ABAQUS input file can be generated by other CAD system such as IDEAS. In Chapter 6, the procedure of finite element analysis (FEM) has been described. This Appendix will follow the procedure to create an ABAQUS input file by ABAQUS/Pre. In a sequential-coupled thermal-elastic-plastic

analysis, two ABAQUS input files are created. One is for heat transfer analysis; the other is for thermal stress analysis. The typical ABAQUS input files for laser-forming simulation are illustrated. ABAQUS runs the input files and generates the results. The results should be carefully examined. The explanation of the results is discussed.

### A.2 Definition of Geometry, Mesh and Element Set

The metal sheet before heated by a laser beam is assumed to be flat without any initial deflection. Because the flat plate is symmetric about the laser-heating path, half of the width of the plate is simulated. The half of the flat plate can be divided into several regions due to mesh schemes and heat loads. Mesh schemes require a fine mesh near heat-affected zone and a coarse mesh in other parts. Therefore, the plate is divided in two regions in the width direction. Each region in width direction can be subdivided into up and down regions due to heat loads. A laser beam irradiates the up regions. There are at least four regions in the flat plates as shown in Figure A.1. More regions can be subdivided from these four regions according to the need of mesh size.

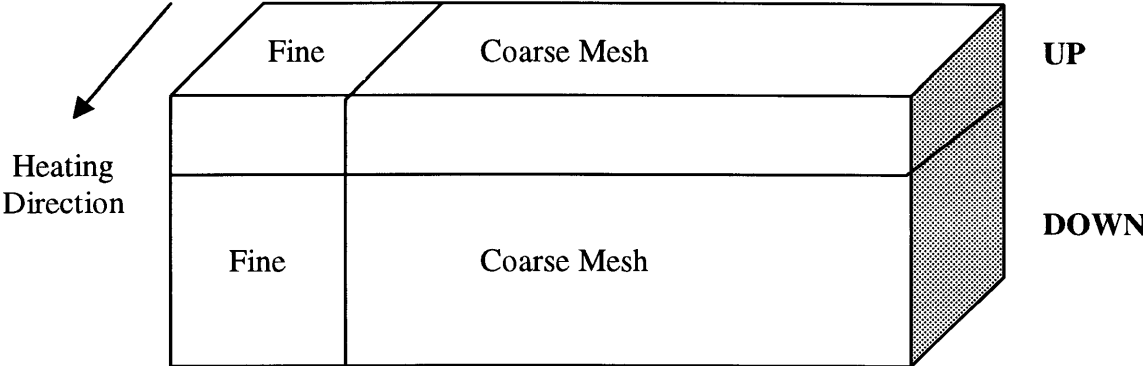


Figure A.1: Mesh Scheme

Two element sets are defined: up\_element, and down\_element. The element set is a set of elements. The up\_element element set is defined as the set of the elements with surfaces heated by a laser beam.

ABAQUS/Pre is used to define the nodes and elements of model. The brief steps are described as the following:

- (1) Create a new database.
- (2) Create four solids by XYZ definition in Geometry Menu.
- (3) Define mesh seeds and generate mesh in each solid in FEM Menu.
- (4) Eliminate two node numbers assigned to the same node.
- (5) Define up and down element sets.

The definition of nodes and elements in ABAQUS input file is listed as follows:

```
*NODE, NSET=NALL
  1,      0.,      0.
  2,      0.,     -0.00625
  3,      0.,     -0.0125
  4,      0.,     -0.01875
```

- *NALL, the set of all nodes, is defined by NSET.*
- *This line indicates nodal number and coordinates of the node.*



```
*ELEMENT, TYPE=DC3D20, ELSET=UP
1,      1,      3,      17,      15,      91,      93,      107,      105,
2,      11,     16,      10,      92,      101,     106,
100,    66,     67,      72,      71
```

- *The element type is a three-dimensional diffusion continuum element with twenty nodes in heat transfer analysis.*
- *UP, the set of elements, is defined by ELSET.*
- *This line indicates element number and nodal number in the element.*

```
*ELEMENT, TYPE=C3D20, ELSET=UP
```

- *The element type is a three-dimensional solid element with twenty nodes in structural analysis.*

Element type in thermal stress analysis must be compatible with that in heat transfer analysis. For example, a three-dimensional solid element with twenty nodes is compatible with a three-dimensional solid element with twenty nodes. Eight-node element is more efficient in heat transfer analysis but can not be used in thermal stress analysis due to high nonlinearity of equations. ABAQUS ver 5.5 does not support to interpolate the nodal temperature of an eight-node element into that of a twenty-node element. In order to keep the consistency of element type, twenty-node element is used in heat transfer analysis. For this reason, the unnecessary computation is increasing in heat transfer analysis. ABAQUS ver 5.6 may support the automatic interpolation of nodal temperature.

### A.3 Definition of Material

Material properties can be constant or a function of various variables. ABAQUS provides different keywords to define various material properties. These keywords in the ABAQUS input file can be generated by using ABAQUS/Pre or any text editor. There is no inherent units in ABAQUS. Users need to keep the consistency of units. Definition of material properties for heat transfer analysis is given as follows:

```
*MATERIAL, NAME=INCOL625
**
*DENSITY
    0.325,
**
*SPECIFIC HEAT
    0.098,
**
*CONDUCTIVITY, TYPE=ISOTROPIC
    51.9E-3, 00
    51.5E-3, 50
    51.1E-3, 100
    49.8E-3, 150
    48.6E-3, 200
```

If the plate is melting during the laser forming process, latent heat of material must be considered.

```
*LATENT HEAT
247e3, 1455, 1554
```

In thermal stress analysis, the following material properties are necessary in the input file.

```
*ELASTIC, TYPE=ISOTROPIC
.299E+08, .304, 0.
.292E+08, .305, 200.
.284E+08, .308, 400.
.275E+08, .308, 600.
.265E+08, .310, 800.
```

- *The values of the previous line in order are Young's modulus, Poisson ration, and temperature.*

```
*EXPANSION, TYPE=ISO, ZERO=70.
0.71E-5, 200.
0.78E-5, 1000.
0.88E-5, 1600.
```

- *The values of the previous line in order are thermal expansion coefficient, and temperature.*

```
*PLASTIC, HARDENING=KINEMATIC
51000., .0, 70.
80000., .01, 70.
34000., .0, 1000.
60000., .01, 1000.
```

- *The values of the previous line in order are yield stress, plastic strain, and temperature.*

## A.4 Property Reference

All elements in a model must have a property reference. The property reference associates elements with material properties, coordinate systems, or specific properties.

For example,

```
*SOLID SECTION, ELSET=UP, MATERIAL=INCONEL6
1.,
**
```

## A.5 Definition of Heat Load

The moving laser beam is defined as a moving surface heat flux. The moving surface heat flux can be expressed in a mathematical function of coordinates and time. ABAQUS provides a user subroutine to define the heat flux function. The DFLUX user

subroutine is a FORTRAN subroutine. The coordinates of each node at the up\_element set are transferred into the DFLUX subroutine. The DFLUX subroutine will return the heat flux value calculated from the mathematical function to each node.

The DFLUX subroutine is given as follows:

```
*USER SUBROUTINE
SUBROUTINE DFLUX(FLUX,TEMP,KSTEP,KINC,TIME,NOEL,NPT,COORDS,JLTY)
include 'aba_param.inc'
DIMENSION FLUX(2),TIME(2),COORDS(3)

REAL*8 QMAX, K, V
REAL*8 R1,X1
C
C simple heat input function
C
C QMAX = heat flux intensity (cal/in^2)
C K = concentration coefficient (1/in^2)
C v = travel speed (in/sec)
C
C
QMAX=80.0
V=0.1323
R1=(COORDS(3)-V*TIME(2))
K=12.3565
X1=COORDS(1)
FLUX(1)=QMAX*DEXP(-K*R1*R1-K*X1*X1)
RETURN
END
**
```

If the laser beam moves along a circular path, the user subroutine is given as follows:

```
*USER SUBROUTINE
SUBROUTINE DFLUX(FLUX,TEMP,KSTEP,KINC,TIME,NOEL,NPT,COORDS,JLTY)
include 'aba_param.inc'
DIMENSION FLUX(2),TIME(2),COORDS(3)

REAL*8 R1,X1,Z1
REAL*8 RADIUS
C
C laser beam moves along a circular path of radius 0.5"
```

```

C      angular velocity = 18 degree /sec
C
C
      RADIUS=0.5
      IF ( TIME(2) .LE. 36.1 ) THEN
      X1=(COORDS(1)-RADIUS*COS(0.31416*TIME(2)))
      Z1=(COORDS(3)-RADIUS*SIN(0.31416*TIME(2)))
      R1=X1*X1+Z1*Z1+COORDS(2)*COORDS(2)
      FLUX(1)=8.0*DEXP(-12.3565*R1)
      ENDIF
      RETURN
      END
**
**

```

In addition to DFULX subroutine, the element set subjected to heat loads must be specified in STEP session.

```

*DFLUX, OP=NEW
UP, S2NU

```

- *UP is the name of element set that is subjected to surface heat flux.*
- *S2NU indicates that the surface heat flux acts on the top surface of the C3D20 element.*

If the surface of the plate melts, the heat is coming from melt element. The command in next line should be used to indicate a body heat flux within an element.

```

*DFLUX, OP=NEW
UP, BFNU

```

Convection and radiation is the other forms of heat load. Ambient temperature, convection coefficient, radiation constant, and applied surface are necessarily given to model the types of the heat load. If those parameters are temperature-dependent or time-dependent, ABAQUS provides a user subroutine FILM to model them. If those

parameters are constant, ABAQUS/Pre can easily set up them by typing these values in the Convection submenu of the Load/BC menu. ABAQUS/Pre can easily model the applied surfaces subjected to the convection by picking the surfaces in graphic interface. If the surfaces of the plate are not subjected to any heat-load, it means that the surface is adiabatic. In other words, there is no heat flow across the surfaces.

```

**
*FILM, OP=NEW
**
  1,  F6,  70.,  3.3975E-5
  5,  F6,  70.,  3.3975E-5

```

- *Element number*
- *Distributed film type*
- *ambient temperature*
- *Convection coefficient*

## A.6 Initial Condition

The initial nodal temperature of each node needs to be specified; otherwise, ABAQUS assumes that the initial nodal temperature is zero.

```

*INITIAL CONDITIONS, TYPE=TEMPERATURE
NALL, 70.

```

- *The initial temperature of the nodes in Node Set, NALL, is seventy.*

As the laser beam scans the surface of the plate several times, the effects of previous scans must be considered. Therefore, the plate with residual stress needs to be modeled. However, ABAQUS version 5.5 can not define the initial stress in the solid.

## A.7 Boundary Conditions

The boundary condition has been explained in Chapter 6. The most convenient way to set up the constraints of the nodes is using ABAQUS/Pre graphic interface. An example is given as follows:

```
*BOUNDARY, OP=NEW
  2642, 1,, 0.
  2642, 3,, 0.
  2651, 3,, 0.
```

## A.8 Definition of Procedure

This definition of the procedure controls the analysis type, initial criterion, and terminated criterion of the program. The part of definition of procedure in heat transfer analysis is given as follows:

```
*STEP, AMPLITUDE=STEP, INC=1200
*HEAT TRANSFER, END=PERIOD, DELTMX=50.
  0.001, 1000., 0.001, 50.
**
```

- *Total increment during this step is 1200.*
- *The maximum temperature change during one increment is 50. In the heating and cooling stages, temperature changes quickly. The parameter is very important in controlling the time increment of the program.*
- *Initial time increment is 0.001. The value depends on the material properties and mesh size.*
- *The simulation time is 1000 seconds.*

- *The minimum temperature change during each increment is 0.001. At the starting of heating, this value needs to be very small.*
- *The error of temperature measurement in the experiment is 50. Therefore, the maximum temperature change during each increment is 50.*

The part of definition of procedure in thermal stress analysis is given as follows:

```
*STEP, AMPLITUDE=RAMP, INC=1000
*STATIC
    0.001,          600.,          0.001,          50.
**
** read temperatures from .fil file
**
*TEMPERATURE, FILE=filename
NALL
**
```

- *The nodal temperature is read from filename.fil before starting thermal stress analysis.*

If large deformation and strain occur, the configuration of nonlinear geometry is considered. In command line of STEP, NLGEOM option needs to be added.

## **A.9 Execute ABAQUS Input File**

The ABAQUS input files for heat transfer analysis and thermal stress analysis are respectively in Appendix B and C. With ABAQUS input files, ABAQUS/Standard can start analyzing by typing the commands in next time under UNIX system prompt.

```
>abaqus job=filename.inp int
```



ABAQUS/Standard reads the input files, compiles the input file into an executive file, and runs this executive file. If there is any error during compilation or run-time, error message are stored in filename.dat and filename.msg. The results of analyses are stored in filename.dat, filename.res, and filename.fil. The important information of the analysis is saved in this filename.dat file. Numerical procedures, control of tolerance of solution, memory usage, and the outputs of the variables should be referred to this file. Convergence control, iteration details, solver message, and trouble-shooting information are saved in the filename.msg file. The status of the running program can be checked with filename.sta. Filename.dat, filename.sta and filename.msg are readable text files. Filename.res is a binary file that can be processed by ABAQUS/Post. If the program is interrupted by insufficient storage space, the program can continue running with filename.fil after restoring enough space.

## **A.10 Examination of Results**

In order to compare with experimental results, the approaches of extracting the analytical results from ABAQUS are introduced. The examination of FEM results is discussed.

ABAQUS/Post is used to process the results of FEM analysis. Type the commands in next line under UNIX system prompt to run ABAQUS/Post.

```
>abaqus post restart=filename
```

(1) After finishing heat transfer analysis, read the filename.res. Use the ABAQUS/Post commands to show the contour of temperature:

```
>set,fill=on
```

```
>cont,var=nt11
```

- Check if the contour is smooth enough across the element boundary. If the contour is discontinuous, it means that the mesh is too coarse.
- Check if the shape of the contour is similar to theoretical prediction. If the shape is not correct, it means that heat input function or material properties in ABAQUS input file are incorrect.

(2) In the experiment, transient temperature and out-of-plane displacement are measured in specific points. The corresponding points in FEM model need to be determined. Change the view of the plates by using the mouse. Use the commands REPORT NODE and REPROT ELEMENT:

```
>report node  
>report element
```

Click the corresponding points of model on the screen. ABAQUS/Post returns the coordinates, node number, and element number of picking points.

Use the commands Read Curve, and Display to show the time history of temperature of the corresponding points:

```
>read curve, var=nt11, name=curvename, node=nodenum  
>display, all curve  
>display, curve  
>curvename
```

The curve is shown on the screen.

- Check if the model has the same peak temperature as the specimen dose.

The commands in ABAQUS/Post can be written in a text file. ABAQUS/Post can import the text file and execute the commands. The repetitive typing the same commands can be avoided.

```
>read, file=filename
```

- (3) After finishing thermal stresses analysis, read filename.res. Use ABAQUS/Post command:

```
>draw, displaced
```

The original and deformed meshes are shown on the screen.

- Check if the bending direction of the model is the same as that of the specimen. If the deformed shape of the model is different from that of specimen, this inconsistency is involved with many sources of errors: material properties, boundary conditions, and inaccuracy of numerical solution.
- Check if any element is over-distorted. This may lead to inaccuracy of stress.

- (4) Use the commands Read Curve, and Display to show the time history of out-of-plane displacement of the corresponding points:

```
>read curve, var=u2, name=curvename, node=nodenumber  
>display, all curve  
>display, curve  
>curvename
```

The curve can be compared with the curve from the measurement of transient out-of-plane displacement in the experiment. The values of data points of the curve can be exported to a text file by the commands:

```
>set, file=filename  
>report curve, name=curvename
```

- Check if the model has the same transient behavior as the specimen. The model should bend away from heating during heating stage and bend toward heating line during cooling stage.

(5) Calculating transient angular distortion from the out-of-plane displacement of two nodes. Because the bending angle is symmetric about the heating line, total angular distortion is expressed as follows:

$$\theta = 2 \tan^{-1} \left( \frac{y_2 - y_1}{x_2 - x_1} \right)$$

where

$y_1$  = vertical displacement of first node,

$y_2$  = vertical displacement of second node,

$x_1$  = coordinate of first node,

$x_2$  = coordinate of second node.

(6) Investigate the effective plastic strain of the element to understand the mechanism of laser forming.

```
>read curve, var=peeq, name=curvename, element=elementumber
```

(7) Plot temperature curve, displacement curve, and effective plastic strain curve in the same figure to understand the mechanism of laser forming.

## Appendix B: ABAQUS Input File for Heat Transfer Analysis

```

*HEADING
ABAQUS job created on 01-Dec-96 at 10:57:25
*PREPRINT, MODEL=NO, HISTORY=NO, ECHO=NO
**
*RESTART, WRITE, FREQUENCY=20
**
*NODE, NSET=NALL
    1,      0.,      0.
    2,      0.,     -0.00625
    3,      0.,     -0.0125
    4,      0.,     -0.01875
    5,      0.,     -0.025
   67,      0.,     -0.0125,      0.05
   68,      0.,     -0.025,      0.05
   69,      0.,    -0.0375003,      0.05
   70,      0.,     -0.05,      0.05
   71,     0.05,      0.,      0.05
   72,     0.05,     -0.0125,      0.05
   73,     0.05,     -0.025,      0.05
   74,     0.05,    -0.0375003,      0.05
   75,     0.05,     -0.05,      0.05

....

*ELEMENT, TYPE=DC3D20, ELSET=UP
1,      1,      3,      17,      15,      91,      93,      107,
105,     2,     11,     16,     10,     92,     101,     106,
100,     66,     67,     72,     71
    2,     3,     5,     19,     17,     93,     95,
109,
107,     4,     12,     18,     11,     94,     102,
108,
101,     67,     68,     73,     72

....

*ELEMENT, TYPE=DC3D20, ELSET=DOWN
161,     9,     968,     994,     23,     99,     1134,
1160,    113,     967,     984,     993,     14,     1133,     1150,
1159,    104,     70,     1088,     1097,     75
    162,     968,     970,     996,     994,     1134,     1136,
1162,    1160,     969,     985,     995,     984,     1135,     1151,
1161,    1150,     1088,     1089,     1098,     1097

.....

**UP
**

```

```

*SOLID SECTION, ELSET=UP, MATERIAL=INCONEL6
    1.,
**
** down
**
*SOLID SECTION, ELSET=DOWN, MATERIAL=INCONEL6
    1.,
**
** Inconel625
** Date: 01-Dec-96           Time: 10:50:23
**
*MATERIAL, NAME=INCONEL6
**
*DENSITY
    0.325,
**
*SPECIFIC HEAT
    0.098,
**
*CONDUCTIVITY

*INITIAL CONDITIONS, TYPE=TEMPERATURE
NALL, 70.
**
*USER SUBROUTINE
    SUBROUTINE DFLUX (FLUX, TEMP, KSTEP, KINC, TIME, NOEL, NPT, COORDS, JLTYP)
    include 'aba_param.inc'
    DIMENSION FLUX(2), TIME(2), COORDS(3)

    REAL*8 R1, X1
C
C     simple heat input function

    R1=(COORDS(3)-0.1323*TIME(2))
    X1=COORDS(1)
    FLUX(1)=80.0*DEXP(-12.3565*R1*R1-12.3565*X1*X1)
    RETURN
    END
**
**
** step 1, case1
**
*STEP, AMPLITUDE=STEP, INC=1200
*HEAT TRANSFER, END=PERIOD, DELTMX=50.
    0.001,      1000.,      0.001,      50.
**
** conv
**

```

```

*FILM, OP=NEW
**
      1, F6,      70.,    3.3975E-5
      5, F6,      70.,    3.3975E-5
      9, F6,      70.,    3.3975E-5
     13, F6,      70.,    3.3975E-5
     17, F6,      70.,    3.3975E-5
     21, F6,      70.,    3.3975E-5
     25, F6,      70.,    3.3975E-5
*BOUNDARY, OP=NEW
*CFLUX, OP=NEW
*DFLUX, OP=NEW
UP,BFNU
**
*NODE PRINT, FREQ=50
NT
*NODE FILE, FREQ=50
NT
**
*EL PRINT, POSITION=INTEGRATION POINT, FREQ=0
**
*EL FILE, POSITION=INTEGRATION POINT, FREQ=0
**
*EL PRINT, POSITION=NODES, FREQ=0
**
*EL FILE, POSITION=NODES, FREQ=0
**
*EL PRINT, POSITION=CENTROIDAL, FREQ=0
**
*EL FILE, POSITION=CENTROIDAL, FREQ=0
**
*EL PRINT, POSITION=AVERAGED AT NODES, FREQ=0
**
*EL FILE, POSITION=AVERAGED AT NODES, FREQ=0
**
*MODAL PRINT, FREQ=99999
**
*MODAL FILE, FREQ=99999
**
*PRINT, FREQ=50
**
*END STEP

```



## Appendix C: ABAQUS Input File for Structural Analysis

```
*HEADING
ABAQUS job created on 01-Dec-96 at 10:57:25
*PREPRINT, MODEL=NO, HISTORY=NO, ECHO=NO
**
*RESTART, WRITE, FREQUENCY=10
**
*NODE, NSET=NALL
    1,      0.,      0.
    2,      0.,    -0.00625
...
**
*ELEMENT, TYPE=C3D20, ELSET=UP
    1,      1,      3,      17,      15,      91,      93,      107,
  105,      2,      11,      16,      10,      92,      101,      106,
  100,      66,      67,      72,      71
    2,      3,      5,      19,      17,      93,      95,      109,
  107,      4,      12,      18,      11,      94,      102,      108,
  101,      67,      68,      73,      72
...
**
*ELEMENT, TYPE=C3D20, ELSET=DOWN
  161,      9,      968,      994,      23,      99,      1134,      1160,
  113,      967,      984,      993,      14,      1133,      1150,      1159,
  104,      70,      1088,      1097,      75
  162,      968,      970,      996,      994,      1134,      1136,      1162,
  1160,      969,      985,      995,      984,      1135,      1151,      1161,
  1150,      1088,      1089,      1098,      1097
...
**
** UP
**
*SOLID SECTION, ELSET=UP, MATERIAL=INCONEL6
    1.,
**
** down
**
*SOLID SECTION, ELSET=DOWN, MATERIAL=INCONEL6
    1.,
**
** Inconel625
** Date: 01-Dec-96          Time: 10:50:23
**
*MATERIAL, NAME=INCOL625
**
**
*DENSITY
    0.325,
```

```

**
*ELASTIC, TYPE=ISOTROPIC
.299E+08, .304, 0.
.292E+08, .305, 200.
.284E+08, .308, 400.
.275E+08, .308, 600.
.265E+08, .310, 800.
.255E+08, .320, 1000.
.244E+08, .325, 1200.
.233E+08, .335, 1400.
.195E+08, .370, 2000.
*EXPANSION, TYPE=ISO, ZERO=70.
0.71E-5, 200.
0.78E-5, 1000.
0.88E-5, 1600.
*PLASTIC, HARDENING=KINEMATIC
51000., .0, 70.
80000., .01, 70.
34000., .0, 1000.
60000., .01, 1000.
**
**
*INITIAL CONDITIONS, TYPE=TEMPERATURE
NALL, 70.0
**
** step 1, Default
**
*STEP, AMPLITUDE=RAMP, INC=1000
*STATIC
0.001, 600., 0.001, 50.
**
2639, 1,, 0.
2640, 1,, 0.
2641, 1,, 0.
**
** rollerz
**
*BOUNDARY, OP=NEW
2642, 1,, 0.
2642, 3,, 0.
2651, 3,, 0.
2668, 3,, 0.
2677, 3,, 0.
2694, 3,, 0.
2703, 3,, 0.
2720, 3,, 0.
2729, 3,, 0.
2746, 3,, 0.
5397, 3,, 0.
5414, 3,, 0.

```

```

5423, 3,, 0.
5440, 3,, 0.
5449, 3,, 0.
5466, 3,, 0.
5475, 3,, 0.
5492, 2,, 0.
5492, 3,, 0.
**
** rollery
**
*BOUNDARY, OP=NEW
3832, 2,, 0.
3877, 2,, 0.
3998, 2,, 0.
4043, 2,, 0.
4164, 2,, 0.
4209, 2,, 0.
4330, 2,, 0.
4375, 2,, 0.
4496, 2,, 0.
4541, 2,, 0.
4662, 2,, 0.
4707, 2,, 0.
4828, 2,, 0.
4873, 2,, 0.
4994, 2,, 0.
5039, 2,, 0.
5160, 2,, 0.
5205, 2,, 0.
5326, 2,, 0.
5371, 2,, 0.
** read temperatures from .fil file
**
*TEMPERATURE, FILE=t1
NALL
**
**
*NODE PRINT, FREQ=10
U
*NODE FILE, FREQ=10
U
**
*EL PRINT, POSITION=INTEGRATION POINT, FREQ=10
S
E
*EL FILE, POSITION=INTEGRATION POINT, FREQ=10
S
E
**
*EL PRINT, POSITION=NODES, FREQ=10

```

```
PE
*EL FILE, POSITION=NODES, FREQ=10
PE
**
*EL PRINT, POSITION=CENTROIDAL, FREQ=0
**
*EL FILE, POSITION=CENTROIDAL, FREQ=0
**
*EL PRINT, POSITION=AVERAGED AT NODES, FREQ=0
**
*EL FILE, POSITION=AVERAGED AT NODES, FREQ=0
**
*MODAL PRINT, FREQ=99999
**
*MODAL FILE, FREQ=99999
**
*ENERGY PRINT, FREQ=0
**
*ENERGY FILE, FREQ=0
**
*PRINT, FREQ=10
**
*END STEP
```